NOVA SCHOOL OF SCIENCE & TECHNOLOGY

DEPARTMENT OF PHYSICS

GUILHERME LOURENÇO CORREIA

Bachelor of Science in Biomedical Engineering

BRAIN WEARABLES: OPTIMIZING THE EVALUATION OF EAR-EEG DEVICES

MASTER IN BIOMEDICAL ENGINEERING

NOVA University Lisbon
September, 2023

NOVA SCHOOL OF
SCIENCE & TECHNOLOGY

DEPARTMENT OF
PHYSICS

BRAIN WEARABLES:
OPTIMIZING THE EVALUATION OF EAR-EEG DEVICES

GUILHERME LOURENÇO CORREIA

Bachelor of Science in Biomedical Engineering

Adviser: Alejandro Lopez Valdes
Assistant Professor, Trinity College Dublin

Co-adviser: Carla Maria Quintão Pereira
Assistant Professor, NOVA University Lisbon

MASTER IN BIOMEDICAL ENGINEERING

NOVA University Lisbon
September, 2023

Brain Wearables: Optimizing the Evaluation of Ear-EEG Devices

This document was created with the (pdf/Xe/Lua)LaTeX processor and the NOVAthesis template (v6.10.17) [1].

To my family, for their unwavering support.

Acknowledgements

After five long but also quick passing years since I first stepped foot in FCT, I can finally feel like a chapter is about to close. This work represents the last (for the time being) milestone in my journey as a student, and for the better or the worse, it is a work I'm proud of. Right now, I can only thank and express my gratitude to everyone present for me during this challenging but enjoyable experience.

I will start by thanking both Prof. Richard Reilly and Prof. Alejandro Lopez Valdes from Trinity College, who, about one year ago, opened the door for me to take on a project at this institution. Especially to Prof. Alejandro, as my main advisor, I thank you for the opportunity to embark on this project, the guidance, resources, and, above everything, the trust deposited in me and the excellent disposition that you always brought into the lab. I want to thank Trinity College for the time I spent there; more specifically, I want to express my gratitude to all members of the Lopez Valdes Lab, from the students whom I have met in the months spent in the lab complaining about our hardships; to Eugene, who always made himself available to assist me during my project.

In FCT, I want to give a special thanks to Prof. Carla Quintão, my co-advisor, that I have to thank for her diligence in assisting me in starting this journey one year ago and, more importantly than that, for being a staple academic coordinator of the Biomedical Engineering Integrated Masters for the majority of the time I have been in FCT, whom I'm sure my fellow MIEB colleagues also cherish.

On a more personal level, I want to start by thanking all members of the *Grupo de Estudo Moderado* (translated as "Group of Moderate Study"), Daniel, Inês, Lucas, and Catarina. It wasn't easy being far away from you guys during my time in Ireland; if there is something I genuinely thank FCT for, it is the chance to know and call you all friends. I must say I'm curious to see where life takes each one of us from this point forward, but I know that wherever we end up, we will always cherish the moments we spent together, our jokes, Mag8's, and the many lunches at D.Gracinda.

I also want to thank Maria "Drunken Fist" Neutel, my one and only *Praxis* ward, who regularly checked on me during my stay in Ireland. Not every day we encounter such a kind-hearted and thoughtful person in life. I have no doubts you will go far (and take *Achocálhamos* with you)!

Onto my family, whom I will always keep close to my heart, I want to start by thanking my grandparents Maria and Manel, who always looked after me and my brothers, even to this day. Wherever we are, we always look forward to coming back to Lardosa.

I thank Aunt Luzita and Uncle Zé, whom I consider my second parents, for their support in providing me and my brothers with a place we know we can always call home in Lisbon, with you around.

To my mother, Aida, and my younger brother, Eduardo, whom I missed so much both during the time I studied in Lisbon and even more while I was in Ireland, I thank you for being the biggest reason that makes me push forward in whatever I'm trying to achieve. I wish I could be around to help more than I did, but I hope I can do so in the future.

Lastly, I especially thank my Big Brother Julio, who, besides being the best elder brother I could ask for, helped me push through the most stressful times of this project. Without you and Sophie, none of this would even have been possible in the first place. Thank you for having me stay with you during this time. Hopefully, I will be back soon so we can finish that damn Dungeons & Dragons campaign!

”

“I learned this, at least, by my experiment: that if one advances confidently in the direction of his dreams, and endeavors to live the life which he has imagined, he will meet with a success unexpected in common hours.”

— Henry David Thoreau, in **Walden**

Abstract

Electroencephalography (EEG) enabled earbuds represent a promising frontier in evaluating brain activity beyond traditional laboratory settings. However, these innovative devices need more comprehensive characterization before widespread health related usage. In response to this challenge, the present research project has developed a toolbox to facilitate and expand the assessment of ear-EEG devices.

The first component of the toolbox is a user-friendly desktop application ("EaR-P Lab") that integrates essential EEG validation paradigms, including Auditory Steady-State Responses (ASSR), Steady-State Visually Evoked Potentials (SSVEP), auditory and visual Event-Related Potentials (ERP) stimuli as well as Electrooculography (EOG) related tests. This application is designed to be used with EEG amplifiers compatible with the Lab Streaming Layer (LSL), streamlining the validation process of EEG devices.

The second element of the toolbox introduces an adaptation of the phantom testing concept, originally applied to traditional scalp EEG, to the unique domain of ear-EEG by using 3D ear scans of specific tested individuals. This innovation facilitates a more rigorous and objective testing of custom form-fit ear-EEG devices.

The EEG paradigms were validated with a control group of five subjects using a commercially available 12 electrode EEG system following research standards for EEG acquisition. For testing, data was acquired from five subjects with custom-fitted ear-EEG electrodes under wet and dry conditions. Conventional ERP waveform data from within-ear references were not observed, but frequency-based responses were present.

Further analysis of one set of ear-EEG electrodes with the ear-EEG phantom developed in this project highlighted performance differences within the electrodes on the earpiece. Factoring this knowledge to select an optimal electrode reference resulted in increased response power on the ASSR.

The utilization of this toolbox provided a better opportunity for the assessment of ear-EEG devices at the hardware and signal level by offering a readily available and expanded characterization process.

Keywords: Wearable EEG, Ear-EEG, Phantom, Characterization Toolbox

Resumo

A aquisição de sinais eletroencefalográficos (EEG) através de dispositivos semelhantes a aparelhos auditivos é uma opção promissora para aceder à atividade cerebral, fora de um contexto laboratorial. No entanto, estes dispositivos carecem de validação e caracterização antes de poderem ser aplicado num contexto médico. Face a este desafio, neste projeto foi desenvolvido um conjunto de duas ferramentas que visam facilitar e expandir esta caracterização.

A primeira componente é uma aplicação (EaR-P Lab) que integra testes essenciais na validação de sistemas EEG, incluindo respostas a estímulos baseados na sua frequência, respostas obtidas enquanto Potenciais Evocados (PE), e testes para aquisição de sinal electrooculográfico (EOG). Esta aplicação é usada com amplificadores de sinal compatíveis com o protocolo Lab Streaming Layer (LSL).

Noutra vertente, o conceito de fantoma, foi aplicado ao nível do ouvido. Esta inovação permite uma caracterização mais objetiva de dispositivos auriculares personalizados.

Os paradigmas foram validados num grupo de controlo de cinco sujeitos com um sistema de EEG de 12 elétrodos. Aquisições de EEG através do ouvido foram realizadas em grupos de cinco sujeitos (com e sem pasta condutora), validando os aparelhos personalizados. As respostas convencionais para PEs não foram observadas quando o sinal foi referenciado ao ouvido, mas respostas baseadas na frequência verificaram-se presentes.

Análise posterior de um conjunto de aparelhos de EEG baseado no ouvido com o fantoma desenvolvido neste projeto destacaram diferenças de performance entre os elétrodos do aparelho. Utilizando este conhecimento para estabelecer uma melhor referência no ouvido, resultou numa melhoria da resposta auditiva em frequência.

A implementação destas ferramentas promete ser um catalisador no futuro da validação e caracterização de dispositivos EEG baseados no ouvido, ao nível do aparelho físico e do sinal obtido através do mesmo.

Palavras-chave: "Wearable" EEG, EEG baseado no ouvido, Fantoma, Ferramentas de Caracterização

Contents

List of Figures

List of Tables

Abbreviations

ABS Acrylonitrile Butadiene Styrene
ADC Analog-Digital Converter
AEP Auditory Evoked Potential
ASSR Auditory Steady-State Response

BCI Brain-Computer Interface
BG Ballistic Gelatin

CAD Computer Aided Design
CF Carbon Fiber

DAC Digital-Analog Converter

ECG Electrocardiogram
EEG Electroencephalography
EIS Electrochemical Impedance Spectroscopy
EMG Electromyography
EOG Electrooculography
ERP Event Related Potential

FFF Fused Filament Fabrication

GFP Global Field Power
GUI Graphical User Interface

ISI Inter-stimulus Interval

LSL Lab Streaming Layer

mbt mBrainTrain
MMN Mismatch Negativity
MRI Magnetic Resonance Imaging

PET Positron Emission Tomography
PETG Polyethylene Terephthalate Glycol
PLA Polylactic Acid

RMS Root Mean Square

SLA Stereolithography
SNR Signal-to-Noise Ratio
SSVEP Steady State-Visual Evoked Response

VEP Visual Evoked Potential

1 Introduction

1.1 Context and problem description

Conventional Electroencephalography (EEG) is an invaluable tool for assessing neurological disorders, with measurements performed in controlled clinical environments, utilizing full cap systems over the scalp with wet electrodes that provide low impedance for quality measurements with high temporal resolution. However, clinicians have been interested in measuring this biosignal outside of the laboratory for better assessing disorders [2].

As an alternative to bringing conventional EEG out of the clinical environment, the first instances of ambulatory EEG traceback to the '70s, when obtrusive apparel containing recording gear enabled the recording of more extensive data needed, for instance in seizure diagnosis [3], while still representing a high degree of impracticality associated with the large dimensions of this category of systems.

The development of technology has led to the evolution of ambulatory EEG, resulting in research on smaller EEG measurement options. This has given rise to a new category of wearable EEG devices that are wireless, have aesthetic designs limited to only the area around the head, and use dry electrodes. The convenience of these devices enables individuals to incorporate EEG measurement into their everyday lives, making it easier to assess certain medical conditions such as epilepsy and sleep disorders and allowing for Brain-Computer Interface (BCI) applications outside of a laboratory environment. While these types of devices are commercially available and their capabilities acceptable for some current applications, the overall design of these wearables still constitutes a barrier to daily usage, being uncomfortable over long periods of time and making it obvious when a person is utilizing such an EEG apparatus [4, 5].

Quoting Looney et al., the next generation of wearable devices must be "discreet, unobtrusive, robust, user friendly and feasible". An in-ear-EEG approach checks all these boxes, trading spatial resolution across the scalp due to a limited number of electrodes with an inconspicuous EEG recording ability [6]. This ability to acquire reliable brain recordings from inside the human ear is critical to accelerating the development of next-generation

EEG-enabled earbuds. While ear-EEG is one of the best candidates for consumer brain-computer interfaces, being referred to as "beyond wearable" [4], such real-world brain recordings are affected by multiple environmental factors that are not present in the laboratory. A systematic, well-established characterization of in-ear-EEG signal quality is crucial to understanding the limitations and applications of this technology.

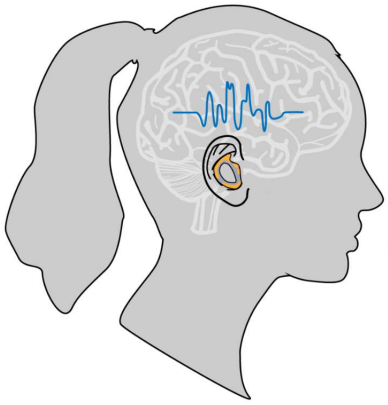

Figure 1.1: Ear-EEG concept, adapted from Kaveh et al. [7]

1.2 Goals and contributions

This dissertation aims to develop an easy-to-use test bench that enables a reliable characterization and comparison of different unobtrusive ear-based EEG acquisition systems. To achieve this goal, two specific objectives must be accomplished:

1. The creation of a suitable test battery (in the form of a user-friendly, well documented framework), comprising the EEG paradigms that are analyzed in Section 3.1, enabling the characterization of ear-EEG devices to be used in real-world situations.

2. The design and prototyping of an ear-EEG suitable physical phantom for systematic characterization of in-ear sensors that would allow to compare the performance of both generic and custom fit form factors for ear-EEG acquisition.

Achieving both objectives will allow for a more reliable future assessment of out-of-the-box ear-EEG devices by providing proper benchmarking tools for comparing systems.

The research work described in this dissertation was carried out in accordance with the norms established in the ethics code of *Universidade Nova de Lisboa*. The work described and the material presented in this dissertation, with the exceptions clearly indicated, constitute original work carried out by the author.

2

Theoretical Concepts

2.1 The human ear - functioning and outer ear description

The human ear has the purpose of transforming sound waves into electric signals to be interpreted in the auditory cortex and comprises three parts: the outer (or external), middle, and inner ear [8].

The outer ear can be divided into two main structures: the auricle or pinna (commonly called "ear") and the external auditory canal, or the outer ear canal. The auricle is the visible part of the ear located on the side of the head over the temporal lobe, capturing the vibrational waves that reach it and transmitting these to the outer ear canal for amplification. The waves progress through the eardrum and middle ear into the inner ear, where the cochlea (which contains a fluid sensible to vibrations) transduces the vibrations into electrical signals sent by the cochlear nerve to the brain [9]. The full ear anatomy and different structures of the auricle are shown in Figure 2.1.

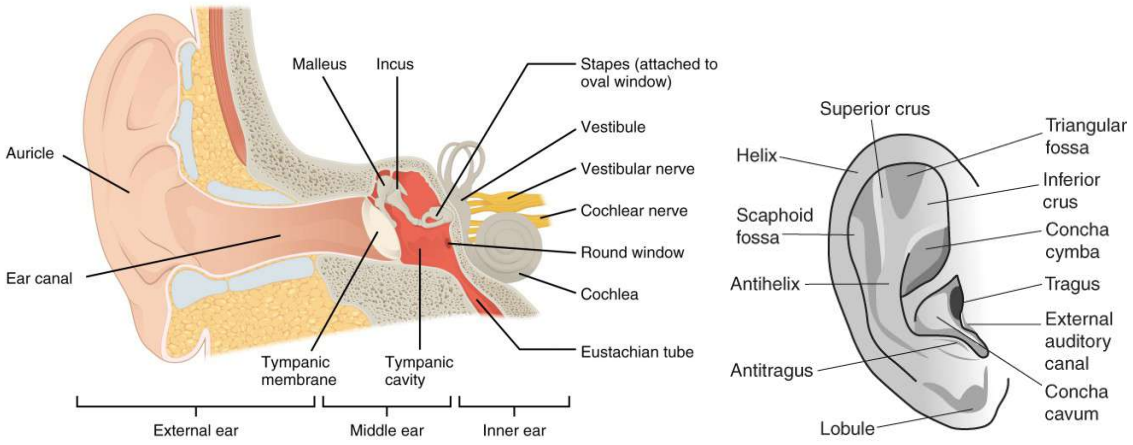

Figure 2.1: **Left -** Cross-section of the ear [10] **Right -** Structures of the auricle [11]

The external auditory canal is a tube-like structure that starts at the auricle and ends at the eardrum. The human ear canal is shaped like a "soft sigmoid", with an average length of about 2.5cm and an average diameter of 8mm at the outer opening and narrowing to

about 5mm at the eardrum, with these measurements varying between individuals. The external ear canal also contains glands that secrete cerumen, a waxy substance that helps keep the ear moist [8]. The first third of the ear canal is surrounded by cartilage, while the remaining two-thirds are surrounded by bone [12].

2.2 EEG validation paradigms

EEG is a non-invasive technique that measures the brain's electrical activity with high temporal resolution. These signals are generated by the activity of neurons in the brain and travel along their axons, which are specialized structures that transmit electrical signals from one neuron to another. When many coordinated neurons are activated, the combined electrical activity is enough to detect a potential by electrodes placed on the scalp [13].

A novel EEG system can be validated through analysis and comparison of obtained responses to well studied paradigms:

2.2.1 Alpha block

Brain waves can be divided into intervals by their frequency in Hertz (Hz) [14]:

- Delta Waves (0.5-4 Hz): Predominant in deep sleep
- Theta Waves (4-8 Hz): Predominant in light sleep and drowsiness
- Alpha Waves (8-12 Hz): Predominant in a relaxed, awake state with eyes closed
- Beta Waves (12-30 Hz): Predominant in states of alertness and attention
- Gamma Waves (30-100 Hz): Predominant in cognitive processing and consciousness

Alpha waves in the 8–12 Hz range are particularly predominant in individuals who are awake and relaxed with their eyes closed [15]. The term alpha block describes the suppression or reduction of alpha rhythm when attention is paid to auditory, visual, or other kind of stimuli [16]. This decrease in alpha frequencies is best seen in the occipital area, where visual information is integrated [17].

2.2.2 Auditory steady-state response

An Auditory Steady-State Response (ASSR) is a paradigm in EEG where the subject is presented with a repetitive amplitude-modulated tone contained in a higher frequency envelope as a carrier frequency. The response from this stimulus is evoked from an auditory cortical origin at the same frequency as the perceived modulated tone [18]. This response can be evaluated on a power spectrum analysis, and while it can be evoked from an interval of frequencies, the ASSR has been shown to be clearer for a frequency of 40Hz in adults, a value commonly used among studies [19].

2.2.3 Visual steady-state response

Homologous to the prior Subsection, a visual steady-state response, which can also be referred to as Steady State-Visual Evoked Response (SSVEP), measures the brain's response in frequency when in the presence of a repetitive visual stimulus, e.g., a low-frequency modulated light [20]. The SSVEP is attributed to the occipital zone, although it is not exclusive to this lobe [21]. While this response can be evoked from an amplitude of low frequencies, it has been shown that the sensitivity of the response is better for a 10Hz frequency, although also dependent on the intensity of the light used [22].

2.2.4 Transient responses

Transient responses are tied to the onset time of a particular stimulus – an event. So, while both steady states and transient response can be categorized as an Event Related Potential (ERP), they differ in the way the paradigm is executed and in the way the response is measured [23]. Since the amplitude of such events is relatively smaller when compared to always present spontaneous EEG waves, most times, time domain averaging over several trials is needed to reveal the waveforms of this stimuli [13].

The N100 (negative deflection around 100ms latency from event onset) Auditory Evoked Potential (AEP), for example, is typically used to assess auditory registration of stimulus, although it can also be elicited from visual events [24]. For Visual Evoked Potential (VEP)s, the obtained waveform can have a variety of prominent reproducible peaks depending on the type of stimuli used (flashes, pattern-reversal, pattern onset-offset) and the stimuli frequency rate [25].

Another existing assessment is to look for the Mismatch Negativity (MMN) passive potential [26]. This response is elicited from an oddball paradigm, where, at random, in a sequence of frequent target stimuli, an oddball stimulus is presented, e.g., in an auditory paradigm, this can be a stimulus of a different frequency. The MMN response is best seen when subtracting the evoked responses from the oddball stimulus from the standard ones and is characterized by a PNP complex with an abrupt negative deflection in the 50 to 250 milliseconds after stimulus onset, signalizing that a stimulus has been detected at auditory level [26].

The P300 (positive deflection around 300ms latency from event onset) component, for instance, like the MMN, is linked to higher processes of the brain but is elicited by an active response of subjects to deviant cues amidst standard ones (reacting to a certain stimulus and not only its passive distinction) and is thoroughly researched as the amplitude of this component is suitable for BCI applications [27].

While not neural in origin, Electrooculography (EOG) saccades can be tied to an event like ERPs in a "follow-the-dot" paradigm that involves presenting a moving dot on a computer screen and asking the participant to follow it with their gaze. This eye movement (the saccade) generates electrical signals that can be measured by EOG electrodes placed near the eye, also being captured at scalp electrodes [28].

2.3 EEG Phantoms

In many areas of research and instrumentation, phantoms are utilized for testing, validating, and calibrating acquisition systems, namely in medical imaging like Positron Emission Tomography (PET) and Magnetic Resonance Imaging (MRI) scans where standardized phantoms are available [29, 30]. In EEG, a state-of-the-art phantom does not exist, although many prototypes from different materials and designs have been prototyped (see Section 3.2). In EEG, the usage of a phantom allows for the playback of a previously recorded known EEG signal through antennas driven inside the phantom. This recognizable signal is referred to as the "ground truth" signal. Then, measurements can be done on the phantom for comparison with this known signal, which constitutes a way of characterizing the acquisition system without the need to account for the inherent variability and lack of repeatability of neural signals present when recording from human subjects, as well as identifying external sources of noise [31, 32]. EEG phantoms also allow for a more controlled analysis of electrode impedance measurements.

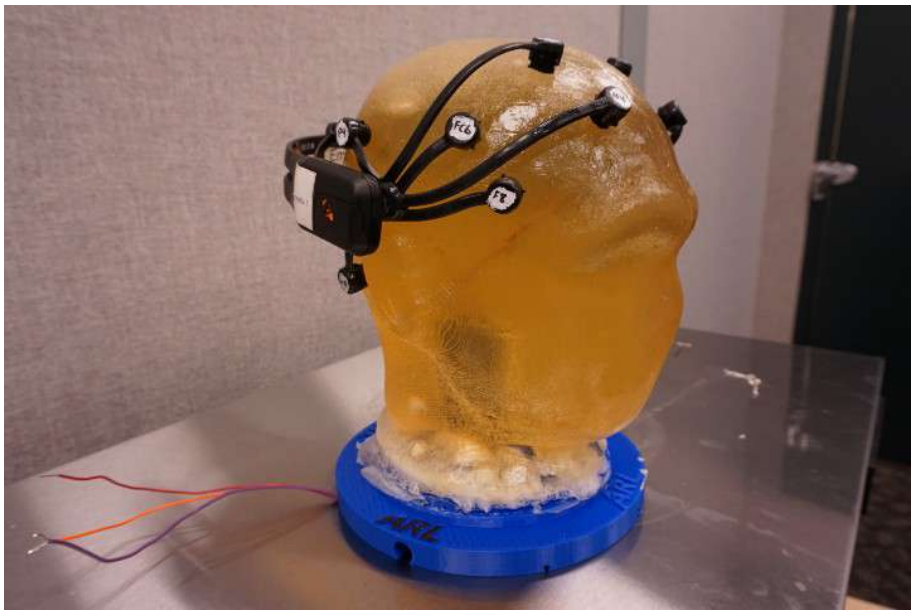

Figure 2.2: EEG scalp device being tested on a standard example of an EEG gelatinous head phantom - the antennas are inserted at the base of the phantom [33]

3

Literature Review

When characterizing a novel EEG system, it is important to assess the system through the obtained responses to validation paradigms in actual EEG recordings (alpha block and ERPs, for instance), as well as the objective capabilities (electrical, mechanical) of the sensors, which can be done by testing in a controlled setting, with a phantom [34].

3.1 Ear-EEG validation

In the current literature concerning ear-EEG devices, it is possible to distinguish between two different kinds of ear-based systems based on the location of the electrodes involved in the measurements: in-ear-EEG, when referring to systems utilizing electrodes inside the outer ear canal and around the concha area; or around-the-ear-EEG, when the electrodes are located on the skin surface of the temporal bones of the skull surrounding the auricular cartilage [35]. The reviewed literature pertains to the first type.

Looney et al. [6] is appointed as the primary source of the idea of in-ear-EEG [36, 37]. A novel approach to measuring EEG signal is proposed in the form of an earpiece (like a hearing aid) embedded with conventional electrodes to record from within the outer ear canal. This prototype was assessed in the alpha block, ASSR and transient visual ERP P300 paradigms, achieving on par results when compared to different scalp electrodes, depending on the paradigm. When compared to the scalp recordings, ear-EEG measurements maintained about the same Signal-to-Noise Ratio (SNR), despite the lower amplitudes obtained, explained by an also lower noise floor in recordings [6]. With the authors suggesting the proposed system required further validation, the positive results obtained by utilizing electrodes within the ear motivated research featuring different types of earpieces and electrode configurations.

On the alpha block paradigm, studies have consistently achieved a clear distinction between a relaxed state with the eyes closed where the alpha waves flare and an open eyes situation, with lower amplitudes when compared to occipital or temporal scalp electrodes [38, 39]. It has been shown that the alpha response is best measured in electrodes either on the anterior part of the first bend of the outer ear canal or on the top part of it [37, 38]. From

recent studies, the best alpha modulation ratio has been obtained by a generic earpiece with dry electrodes, however, only achieving half the modulation ratio of scalp recordings, which is explained by the distance between the ear and the alpha wave sources, in the occipital area [7].

ASSR is a very prevalent paradigm across literature, where peak amplitudes are at most 15dB lower compared to temporal electrodes [40], with a "truly in-ear" ground and reference configuration, a concept introduced in [41]. While amplitudes are about one order of magnitude lower when compared to conventional recordings, SNR in this paradigm has been maintained with an exception in [39], where it was 6 to 8dB lower on a dry electrode earpiece. The performance of this paradigm for two distinct frequencies in ear BCI applications has also been assessed in [42].

On SSVEP, studies report weaker but distinguishable peaks at the selected modulation frequency [40, 43]. While for scalp recordings, the response is shown significant across multiple harmonics, the same may not happen for ear measurements, where the SNR is not maintained for later harmonics, still constituting an improvement over temporal measurements [39].

Amplitudes of transient responses are shown an order of amplitude lower (like steady-state-responses) and with decreased SNR, however maintaining an expected waveform for both visual and auditory stimulus [40, 43], well exemplified for the N100 responses reported in [44]. A high correlation to temporal electrodes in an auditory P300 response to oddball stimuli demonstrates that the signal in the temporal area and the ear is effectively the same in [38]. While auditory ERP responses have been measured in the ear, showing the same waveform as on the scalp, on a MMN analysis, this is not the case when using configurations with only ear electrodes, with results being deemed inconclusive or insignificant [38, 39].

The measurement of other biological signals like Electrocardiogram (ECG) and EOG from the ear is also mentioned. For instance, EOG intentional blink amplitudes were utilized for the activation of a BCI application in [42], and better differentiation in eye blink amplitudes measured in the ear has also been shown in [7] when compared to the scalp. ECG signal has been detected for a specific subject pointed out to have strong cardiac pulsations in the ear, with the wave being treated as a detrimental artifact and not a valuable signal [43]. Recently, the usage of generic ear-EEG devices was found capable of obtaining statistically equivalent sleep monitoring metrics as a polysomnography system, with the later measuring metrics based on ECG and EOG as a case study of how ear-EEG can be used to access this data [45].

To sum up this section, the studies have confirmed the plausibility of in-ear measurements, with most concluding that the achieved results are considered on par with or at least show a clear enough response when compared to scalp recordings (especially for auditory paradigms). Regardless of the earpiece design, validation of these novel wearables relies heavily on well-established EEG paradigms, namely ASSRs, SSVEPs, transient auditory and visual evoked responses with well-known waveforms, and the alpha band

block. While results from different studies are compared to determine the key effects of both dry and wet electrodes, different reference and ground setups, as well as generic and custom fitting to the ear, a more complete and well-rounded assessment of different in-ear-EEG earpieces under the same conditions on a significantly larger pool of subjects is yet to be made.

In Table A.1, a summary with an additional description of the utilized ear-EEG earpieces and the validation paradigms each one underwent within the scope of the reviewed literature is presented.

3.2 EEG phantoms design, materials and testing

Regarding phantoms, different materials and designs are utilized by research groups. For instance, dried gelatin-impregnated human skulls can be used as the phantom foundation to achieve a realistic head shape. To create a realistic conductivity ratio between the primary three biological layers of the head — the brain, skull, and scalp — the skull is then filled with the same gelatin-saline mixture, and a scalp layer consisting of a latex compound may also be added [32, 46].

Using gelatinous compounds, namely Ballistic Gelatin (BG), is a popular choice for phantom making. The doping of ballistic gel (that mechanically resembles biological tissue) with different concentrations of sodium chloride (NaCl) has been shown to be a sure way to tune the impedance of the material, where higher a concentration of NaCl lowers impedance due to a higher amount of free ions, also being a low-cost option [47]. The concentration of this gelatin per mass of the phantom compound also increases the conductivity of the material [48]. Ballistic gel phantoms have been used in both electrode performance assessments regarding recorded noise floor by dry sensors and in studies on the effect of Electromyography (EMG) neck artifacts in EEG data [49, 50]. Separation of motion-induced artifacts from spontaneous EEG has also been achieved with a head phantom made of a mixture of dental plaster, sodium propionate, and water, molded in a hollow mannequin head [51, 52].

Agar-based phantoms, a material that well replicates ion conduction in the head, have been used mixed with salt and water for the study of MRI gradient artifacts in EEG data, with detailed instructions for this mixture present in [53]. Hydrogel coatings doped with low agar concentrations also make good scalp layers [54].

In [55], a hollow phantom made of carbon doped commercially available thermoplastic, which was injection molded by a third party, is presented, and succeeded in replicating human alpha waves at scalp level from the driven electrodes, which constituted an improvement over these author's previous work [56], where this compound was hand mixed. This was accomplished after a calibration process involving algebraic matrix manipulations to effectively generate a desired response, given a specific EEG system [55].

Since the common basis for phantom prototyping is to obtain a mold that resembles the head shape (from digital models based on magnetic resonance imaging (MRI) data,

for example) and fill it with a conductive appropriate material, 3D printing is a suitable method for making the phantom's encasing from common materials like Stereolithography (SLA) resin [57]. Polyethylene Terephthalate Glycol (PETG) printed by Fused Filament Fabrication (FFF) has also been used as a smaller-scale skull material to be filled with agar [58]. Acrylonitrile Butadiene Styrene (ABS) resistivity was shown to be tunable to achieve similar values to those of biological tissue, with the authors suggesting their method can be applied to EEG phantoms [59].

For a known previously recorded signal to be played out of the phantom, electrodes are driven inside it. These can be simple screws, exposed wire tips, or a coaxial cable to create dipoles [52, 55, 58]. For impedance measurements to characterize the material and sensing electrodes, regular silver/silver chloride (Ag/AgCl) electrodes are embedded in the phantom, which is not required to have the shape of a head [48]. The driven antennae are either attached to the interior side of the scalp layer in hollow-shaped phantoms or are put in place during a phase of assembly where the constitution of the filling material allows for this procedure [48, 55].

Concerning the revised literature on this topic, it is possible to conclude that the advantages these tools bring to the table as means to test and validate EEG systems and novel electrodes are recognized, allowing for the characterization of different devices under controlled and known conditions, regarding measured impedance, noise floor values and simulation with artificial input signals. However, it is important to highlight the lack of literature both in applying an EEG phantom to the characterization of in-ear-EEG devices (with the structures of the outer ear canal and auricular cartilage being neglected) and mainly, the nonexistence of an appropriate EEG phantom for this purpose.

Table A.2 presents a summary with an additional description of the phantom prototypes' characteristics and testing usage within the scope of the reviewed literature.

4

Ear-EEG Validation Toolbox

4.1 EaR-P Lab - custom stimuli presentation

4.1.1 General structure and functioning overview

A custom desktop application with the appropriate testing paradigms and functionalities was created to meet the first goal listed in Section 1.2.

This application was written in the **Python** programming language and consists of a collection of local scripts, pre-synthesized stimuli, and other auxiliary different files, folder organized, and wrapped up in a usable Graphical User Interface (GUI), based on the **Tkinter** Python package. The app's stimuli delivery and precise experiment timings are handled by various functions of the **PsychoPy** Python open-source library [60].

The program was dubbed **EaR-P Lab** from the combination of the words "ear" and "ERP" since one of the motivations for this project is to streamline measuring ERPs from within the ear. The main functionalities of **EaR-P Lab** are depicted in Figure 4.1.

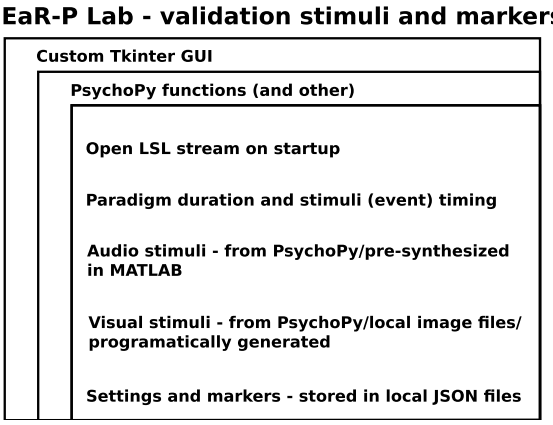

Figure 4.1: **EaR-P Lab** - structure and main functions

EaR-P Lab provides a GUI to present the necessary stimuli and inserts the relevant markers that delimit the paradigms or indicate the start of a given stimulus in the programmed validation test battery. The marker's timestamps are joined with the EEG data through the Lab Streaming Layer (LSL) protocol that handles the synchronization between

these two in EEG acquisitions, making both streams available on the local network [61]. The marker and EEG data streams can then be recorded with **LabRecorder** into a single *.xdf* file on the hard disk to be later analyzed, as illustrated in Figure 4.2.

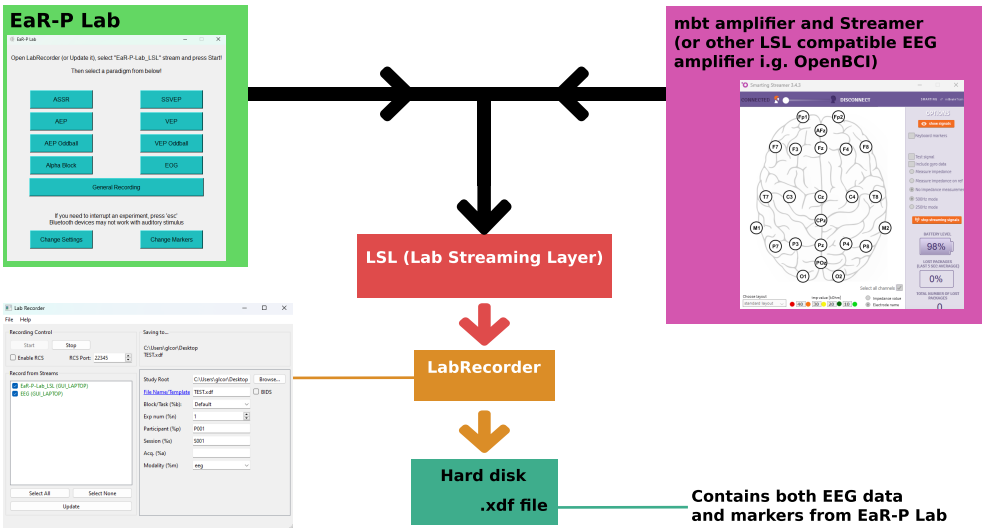

Figure 4.2: Functioning framework of **EaR-P Lab**

4.1.2 GUI - Main Menu

When **EaR-P Lab** is launched, the **Main Menu** in Figure 4.3 appears. This menu gives the user access to various coded validation tests, with the app automatically opening the LSL marker stream using the **pylsl** *StreamOutlet* function at startup. Eleven buttons are presented: nine that direct to the different paradigms and two (**Change Settings** and **Change Markers**) that allow users to alter related variables to these. Some disclaimer information on how **EaR-P Lab** operates is also presented.

Refer to Appendix B for an overview of the features and functions of each button.

4.1.3 Latency testing and issues

To accurately evaluate ERPs, good synchronization between data and markers sent at stimulus onset (triggering) is crucial [62]. The PsychoPy library allows sounds to be pre-scheduled with the high precision PTB settings and *callOnFlip* method to start visual stimuli promptly, both used in **EaR-P Lab** [63, 64]. However, unavoidable latency and jitter issues related to screen refresh rates and monitor syncing still exist [65].

During the early testing phase, we observed a crescent cascading effect on the latency delay when recording blocks of transient responses within the same *.xdf* file, illustrated in Figure B.10. By trial and error, it was discovered that to "reset" this effect, the data streaming from the mBrainTrain (mbt) software must be restarted between blocks of ERPs, which means transient related paradigms must be recorded in separate *.xdf* files.

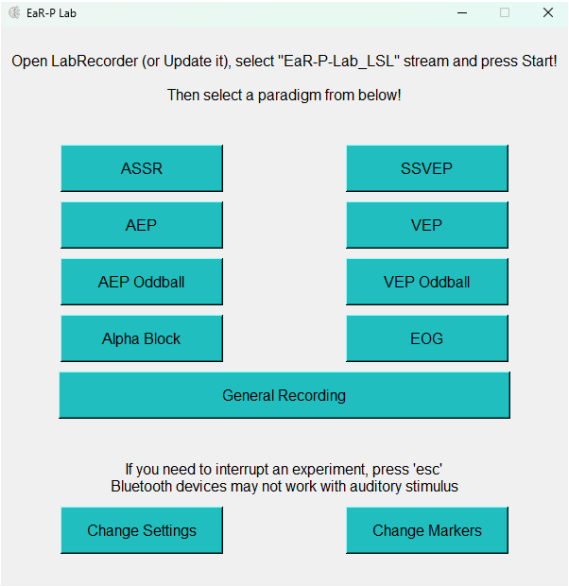

Figure 4.3: **EaR-P Lab** - Main Menu

Within a single *.xdf* file, the latency delay was measured for 1000 trials of both auditory and visual events, showing a mean delay of 0ms (2.2ms std./jitter) and 21ms (2.8ms std./jitter), respectively, rounded to the nearest unit, so the ERP waveforms shown were corrected for these latency values. These values are specific to the used stimuli presenting laptop and may vary between systems, so if possible, they should be tested before data collection, as shown at the end of Appendix B.

4.2 Ear-EEG phantom prototype

To achieve the second goal outlined in Section 1.2, a physical test bench to evaluate ear-EEG devices was developed. The basis for the prototype was similar to the most common type of EEG phantoms: a mold that creates the proper shape and fit for use with an ear-EEG device and that can be filled with a conductive mixture.

In contrast to most common EEG phantoms, this work focused on developing a relatively small design solely focused on the ear anatomy, so the approach to make a complete head-shaped phantom was discarded. It was also deemed advantageous to create a modular ear section for the mold, allowing for testing different ear form factors without having to rebuild an entirely new mold, as well as having a way to secure the signal antennas in place during the setting process of the filling material.

The phantom was designed using the **Fusion 360** Computer Aided Design (CAD) software and then exported as a *.stl* file for 3D printing. The base design is an 18cm cylinder split into two parts along its length, with open ends. The bottom half has two longitudinal railings where the top fits, leaving two round holes centered in the middle for inserting antennas. The cylinder sides can then be closed with lids. The top has two square openings for pouring the conductive mixtures. A 0.1mm gap was used for all

fitting parts to account for the 3D printing resolution. The rendered prototype is shown in Figure 4.4, and the phantom prototype's full dimensions are presented in Appendix C.

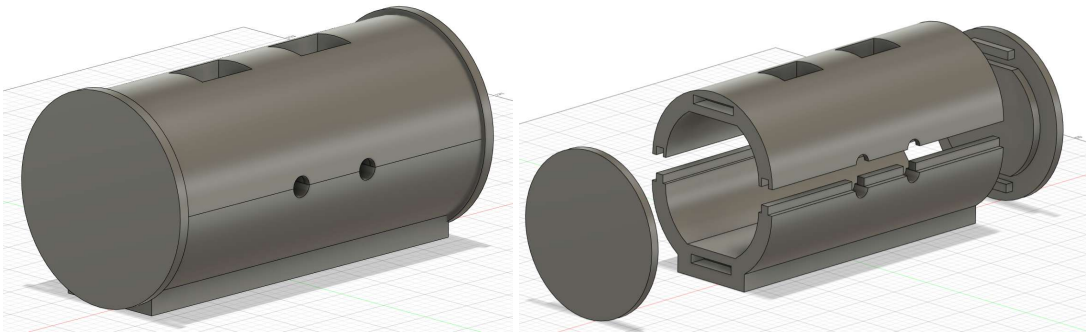

Figure 4.4: **Closed** (left) and **exploded** (right) renders of the ear-EEG phantom prototype

The inside of these lids can then accommodate the outer ear canal and pinna shape to create an imprint on the material inside, where an ear-EEG device can be placed for testing. The current methodology used ear canal scans done by a local audiology practitioner, professionally scanned on-site, and delivered as a *.stl* file (as shown in Figure 4.5), which can be imported as a mesh to Fusion 360 and easily fused with the lid mesh by using the **Mesh Menu - Modify - Combine - Join Operation** in this software.

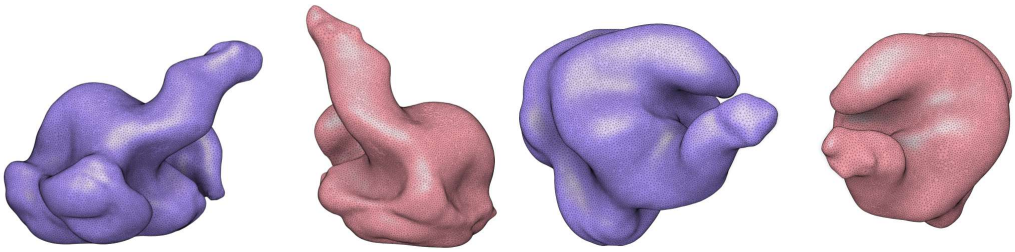

Figure 4.5: Outer ear scans from a subject, received as *.stl* files, shown from two perspectives, obtained by an expert audiologist - **Blue**: Left ear **Red**: Right ear

Ear canal scans were centered on the lid's mesh with the concha symba outline parallel to the mesh's top/bottom. Meshes intersected to a considerate adequate depth as long as the ear canal and pinna structures were visible and protruding, similar to Figure F.1.

The ear-EEG phantom prototype was 3D printed on a Prusa i3 MK3 FFF 3D printer using Polylactic Acid (PLA). PLA was chosen due to its ease of use, fast printing times, affordability, non-warping nature, and lack of post-processing requirements, making it an optimal choice for the project. The printing settings on the Prusa software were set to a *0.15mm QUALITY* printing resolution, using *Prusament PLA* filament with a default structural infill of 15%. The software automatically added necessary support structures *Everywhere* required. The combined printing time of the phantom body and lids was approximately 33 hours. To minimize difficult to remove supports, the cylinder halves were printed vertically. If the phantom's form-fitting factor needs to be changed, printing just another set of lids with the ear impression takes only 6 hours. Figure F.2 shows the different modular parts after printing and support removal.

5

Materials and Methods

5.1 Tested ear-EEG devices

The tested ear-EEG devices utilized were fabricated by a third-party company using a process based on the unique *.stl* of each individual subject, resulting in personalized ear-EEG buds for every participant. Each electrode on the devices is associated with a color-coded wire, and also numbered for easier referencing, according to Figure 5.1.

The earbuds have eight 2mm Ag/AgCl electrodes on the surface. One is located in the concha symba area (1), four around the concha cavum (2-5), one near the antitragus (6), and the last two inside the ear canal (7 and 8), facing the posterior and anterior directions, respectively. The electrodes have wires soldered to them that exit near electrode 6. On the external side, the earbud boasts an earphone insertion vent for sound delivery.

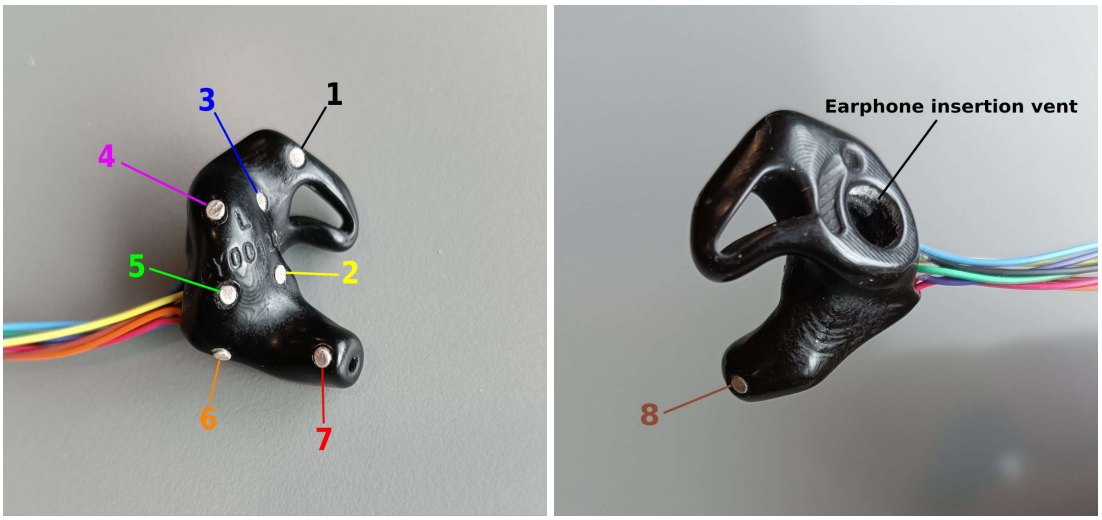

Figure 5.1: **Internal** (left) and **external** (right) sides of an exemplary left ear-EEG earbud provided for testing in the present work

5.2 EEG recording setups and protocol

5.2.1 Acquisition layouts

In this project, three sets of recordings were conducted: a control group with EEG recorded only from the wet scalp for stimuli, platform, and processing pipeline validation, and two groups that combined wet scalp with either dry or wet electrode conditions ear-EEG.

A custom EEG cap with 12 channels was utilized for the EEG control group acquisitions. The cap uses conventional Ag/AgCl electrodes at F3, Fz, F4, T7, C3, Cz, C4, T8, P3, Pz, P4, and Oz positions. The online reference electrode (CMS) and ground (DRL/GND) were situated at FCz and AFz, respectively, as illustrated in Figure 5.2.

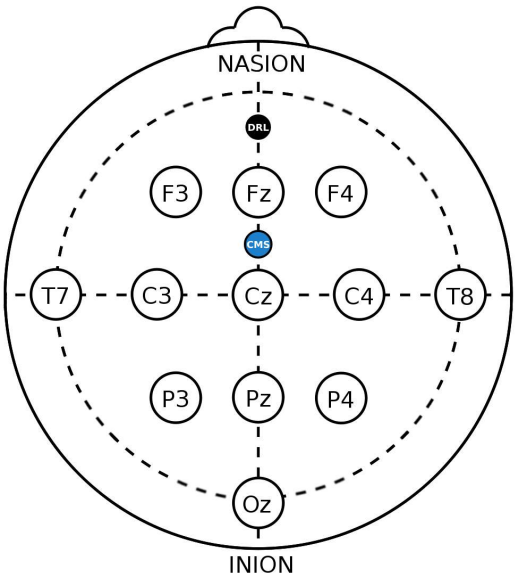

Figure 5.2: EEG control group 12 electrode acquisition scalp only layout

EEG data was collected using the mbt **Smarting mobi** amplifier, capable of high-quality recordings at a sampling rate of 500Hz with wireless data transmission, providing 24 bits of resolution in the Analog-Digital Converter (ADC) [66].

Ear-EEG data was collected simultaneously with conventional EEG from the scalp, using the same amplifier system, to provide a direct reference with an EEG gold standard. However, since this amplifier only supports 24 data channels outside the CMS and DRL, four scalp channels (F3, F4, P3, and P4) from the control group were disconnected to make room for all ear-EEG electrodes on the amplifier connector. In Figure 5.3, the ear-EEG recording layout is illustrated, with the full referencing scheme used in this work.

5.2.2 Recording setup

A laptop (ASUS VivoBook 15, Windows 11 OS, Intel Core i7-10750H Processor, NVIDIA GeForce GTX 1650 Ti Graphics Card, 12GB RAM) ran the essential recording software (**mbt Streamer and LabRecorder**) and stimulus presentation (**EaR-P Lab**). Data was transmitted via Bluetooth from the amplifier at the back of the subject's head to a USB

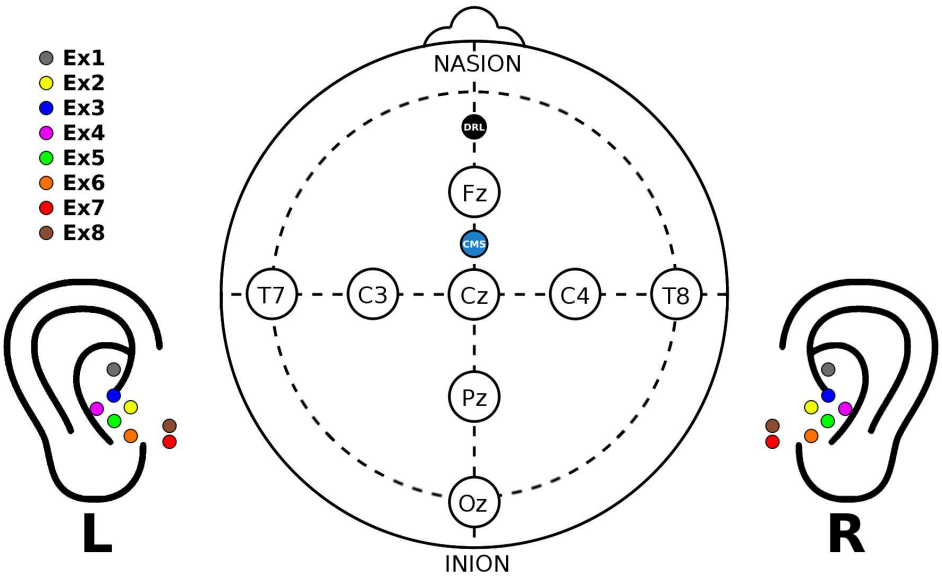

Figure 5.3: Ear-EEG scalp and ears acquisition configuration showing the approximate position of ear electrodes, with colors and numbers matching those in Figure 5.1 - referencing for ear electrodes is provided in the legend, for example, "Ex1" is used to label ear electrode 1 (black), where "x" is replaced by **L** or **R** for left or right ear, respectively

dongle connected to the laptop. Research-grade earphones, shielded with copper tape to reduce interference, delivered sound stimulus to the subjects. To ensure audible stimuli without distortion, an external sound card and Digital-Analog Converter (DAC) were used (see Figure F.3). Laptop and digital-analog converter volumes were set to maximum, with adjustments made on the sound card only. Earphones were fitted with foam ear tips for the control group or connected via the vent on the outer side of the earbuds for ear-EEG recordings (see Figure 5.1). Laptop brightness settings were maximized for visual stimuli.

The earphones were strapped to the participant's back and shoulders. The wiring was taped to the cap with skin-safe tape and connected to the amplifier, as seen in Figure F.4.

5.2.3 Validation battery protocol and settings

EEG recordings were done in a quiet environment with only the participant and the technician present. The participant was asked to sit in a comfortable chair and relax during the recording. The participant was given a brief explanation of the recording process at the start of the session, with thorough instructions provided before each task.

Conductive gel (SIGNAGEL) was applied on each scalp electrode, generally achieving impedances below 5kohm measured by the mbt streamer. A small amount of conductive electrode paste (Ten20) was used for wet electrode ear recordings. The subjects inserted the earpieces themselves at their comfort. It should be noted that ear electrode impedance was generally too high or immeasurable by the streamer, so it won't be assessed.

The EEG data standard and ordered acquisition protocol and settings for each **EaR-P Lab** paradigm employed were as follows:

1. **General Recording -** 4 minutes of resting state

2. **Alpha Block -** 1 minute per section, 4 minutes total

3. **ASSR -** 4 minutes of continuous 1kHz carrier 40Hz modulated sound wave

4. **SSVEP -** 4 minutes of continuous 10Hz visual stimulation, subject at a distance of 60cm from the middle of the screen, measured from the point in between the eyes, during this paradigm, the room's light was turned off, to maximize the flickering

5. **AEP -** 200 trials of discreet 1kHz sound stimulus, with 200ms of duration and a 10ms ramp up/fall off, Inter-stimulus Interval (ISI) between 1200ms and 1800ms, for total duration of around 7 to 8 minutes

6. **VEP -** 200 trials of onset-offset pattern reversal with the dartboard target being shown for 500ms of duration and a 500ms ISI, taking about 5 minutes to complete

7. **AEP Oddball -** Standard: 440Hz sound wave | Target: 880Hz sound wave - a total of 200 oddball/target events were presented to the subject, with every sound having a duration of 100ms with a 10ms ramp up/fall off and ISI between 1200ms and 1800ms, for a total length of around 15 minutes

8. **VEP Oddball -** Standard: Blue Square | Target: Red Circle - a total of 200 oddball/target events were presented to the subject, stimuli on screen for 500ms, ISI between 600ms and 700ms, subjects were told beforehand to press "SPACE" once the target stimuli appear, for a total length of around 18 minutes

9. **EOG -** 80 trials per saccade, dot moved for 500ms, ISI between 1000ms and 1600ms, subject at a distance of 30cm from the middle of the screen, measured from the point in between the eyes, which translates to 16.2° angle for each saccade, for the follow-the-dot paradigm, the subject's head was stabilized using an adjustable chin rest and the monitor was leveled and centered with the subject's eyes by being placed on a box. This section had a total duration of about 10 minutes

For the control group acquisitions, subjects were allowed to calibrate the volume themselves to the highest volume within their own comfort audible zone. For the ear-EEG recordings, the lowest volume setting from the control group was adopted for all subjects. Each acquisition session took about two hours to complete from start to finish, including setting up the EEG cap and earbuds. The subjects were entitled to short breaks (2 to 5 minutes) at the end of each paradigm after the SSVEP session but were also allowed longer breaks when requested. For some subjects, the protocol's order wasn't strictly followed.

5.3 Preprocessing, processing and statistical analysis

All computing referenced in this Section (as well as the plotting of results) was done recurring to the *MATLAB* language and programming environment (MATLAB. (R2020a). Natick, Massachusetts: The MathWorks Inc.) and necessary supplementary packages for the making of custom scripts.

5.3.1 Datasets, channel discard and referencing configurations

EEG data was collected from eight people with normal or corrected vision/hearing. Five people were in the control scalp only group (age avg. 27.0 ± 4.3 std.), five in the scalp plus ear-EEG group (age avg. 36.2 ± 10.6 std.), with two participating in both.

Channel discard was based on a visual inspection of the individual obtained responses to ASSR and EOG paradigms (first and last on the test battery). For all scalp electrodes, only two electrodes were discarded across subjects. The discard ratios for ear electrodes are summarized in Table D.1. Based on this table, the control group and wet ear-EEG recordings will be assessed for the grand average of the five respective subjects. Due to the high discard ratios across the board for dry ear-EEG recordings, the results shown will only pertain to a single significant subject from that group with the greatest amount of usable ear electrodes. Based on the same discard ratios, the following different references will be explored later on in the next Chapter:

- **Cz**, as a standard scalp reference
- **T8**, as a scalp but closer to the ear reference
- **ER3**, as a **within-ear** (assessing ER8, for example) and **between-ears** reference (assessing EL8, for instance)

5.3.2 Preprocessing and processing

The collected data was first parsed and filtered channel to channel with the *filtfilt* function: first, a highpass filter (*butter* function) was applied, followed by a 50Hz notch filter (*iirnotch* function), and finally, a lowpass filter (*butter* again). Frequency-based paradigms (ASSR, SSVEP, and Alpha block) were filtered between 1 and 100Hz, and transient responses (AEP, VEP, MMN, P300, and EOG saccades) were filtered between 1 and 20Hz. To isolate the EOG blinks in the respective three second window, this data was filtered between 0.2 and 3Hz. The data was then referenced to the channels mentioned in the last subsection. The reference channel was zeroed out and left out of further analysis.

ASSR and SSVEP frequency responses were computed with the *pwelch* function on an 8s window with 50% overlap, and the alpha block spectrograms were obtained with the *spectrogram* function on a 2s window, 50% overlap.

All transient responses were baseline corrected to the 100ms pre-stimulus interval and then averaged across trials. To obtain the MMN and P300 responses, the average standard

cue waveform was subtracted from the average target cue waveform for each subject, with the standard events immediately before the oddballs being considered [67].

5.3.3 Statistical analysis

To statistically assess ASSR responses, the power of the 40Hz frequency of interest is compared with the surrounding frequency bins, according to Equation 5.1 [7]:

$$40\ Hz\ SNR = \frac{P\ (40\ Hz)}{P_{\text{average}}(35-45\ Hz)^{*}}\ ,\ ^{*}excluding\ 40\ Hz \tag{5.1}$$

With the same ratio adapted for the SSVEP 10Hz response as per Equation 5.2:

$$10\ Hz\ SNR = \frac{P\ (10\ Hz)}{P_{\text{average}}(5-15\ Hz)^{*}}\ ,\ ^{*}excluding\ 10\ Hz \tag{5.2}$$

A statistical **f-test** was also conducted on these ratios using the *anova1* function.

From the same reference, Equation 5.3 is used to calculate the power of the alpha block effect between the eyes closed and eyes open by averaging both same condition sections into one and considering the alpha frequencies defined between 8 and 12Hz.

$$R_{AM}\ = \frac{P_{\text{average}}\ (Alpha\ Band_{\text{Eyes Closed}})}{P_{\text{average}}\ (Alpha\ Band_{\text{Eyes Open}})}\ ,\ Alpha\ Band\ (8-12\ Hz) \tag{5.3}$$

The modulation significance was also assessed through a **t-test** using the *ttest* function.

ERP responses (AEP, VEP, and respective oddball counterparts) waveforms will be shown with highlighted components deemed significant through a **t-test** using the *ttest* function between the values of the averaged waveform of each subject (or in the case of a single subject, across all trials), at each time point, and zero [43]. These results are also assessed by computing the Global Field Power (GFP) of the channels, split into scalp and channels from each ear individually, in Appendix D.

EOG saccade profiles will be quantified by the amplitude and polarity of each saccade type. For the EOG blinks, an amplitude factor between the averaged peak-to-peak amplitude of the intentional blinks over the regular blinks will be established [7].

Overall, a statistically significant **p-value of 5% confidence (p < 0.05)** was considered.

5.4 Phantom assembly and bulk materials

To assemble the phantom, the antennas (pair of 3.5mm AUX cables) were adjusted to fit the diameter of the cylinder holes by inserting one side of each cable inside PVC tubing and sealing it with duct tape. The cables are placed on the bottom half, then joined by the top and the lids with ear imprints on the side, holding the prototype together. Three strips of plumbing tape are used on the railing fittings, cables, and the inner circumference of the phantom lids to prevent leaks, as in Figure 5.4. The phantom can then be filled with a conductive substance, like the following selected from Section 3.2.

Figure 5.4: Ear-EEG phantom assembly - antennas and railing fittings are sealed with tape

5.4.1 Agar and ballistic gelatin

Agar is a gelatinous vegan substance derived from certain types of seaweed, making a stable gel structure when cooled down after being boiled. An agar phantom can be created by mixing agar, water, and salt at the recommended weight percentages (% w/w) of 4% and 0.5%, of agar and salt, respectively, as per Equations 5.4, with A being the weight of agar, s the weight of salt and w the weight of water [53].

$$\begin{cases} \frac{A}{A+w+s} = 4.0\% \\ \frac{s}{A+w+s} = 0.5\% \end{cases} \Rightarrow \begin{cases} A = \frac{8}{191}w \\ s = \frac{1}{191}w \end{cases} \tag{5.4}$$

The phantom was overestimated to have a capacity of 700ml (equivalent to 700g of water). By substituting w for that value in the solved equations mentioned above, we get the necessary quantities of 30g of agar (*Hoosier Hill Farm*, 10.20€ for 115g, on Amazon) and 4g of salt, rounded up to the nearest unit. The mixture was prepared as follows:

1. Boil 700ml of regular tap water (or deionized water)
2. Add 30g of agar slowly while stirring the mixture
3. Add 4g of table salt while stirring until no granules are present - keep mixing while letting it cool down at room temperature for 10 minutes
4. Pour the mix into the assembled phantom through the top vents until the liquid reaches half the vent's height, let it sit in a refrigerator until it fully solidifies (minimum 2 hours, preferably overnight), which can be checked through the top

BG is the most common material for phantom making, usually made of cattle/pork gelatin. Various weight percentage combos of both gelatin and NaCl are shown to be an appropriate conductive medium [48]. Due to an accessible lesser amount of acquired gelatin bulk powder (*YouHerbIt* 240 Bloom, around 20€ for 350g of powder, on Amazon), values within the middle range of the above study were used, aiming for a 15% weight

percentage on gelatin and 8% weight percentage of NaCl, with BG meaning the weight of gelatin powder instead of agar, which when solved wield the Equations shown in 5.5.

$$\begin{cases} \frac{BG}{BG+w+s} = 15.0\% \\ \frac{s}{BG+w+s} = 8\% \end{cases} \Rightarrow \begin{cases} BG = \frac{15}{77}w \\ s = \frac{8}{77}w \end{cases} \tag{5.5}$$

The same steps as for agar were followed to prepare the gelatin solution, with 140g of gelatin powder mixed with 70g of salt in 700ml of hot (not boiling) water. Unlike agar, gelatin is better mixed at a lower temperature to prevent the formation of air pockets.

Both agar and BG ear-EEG phantoms are shown in Figure 5.5.

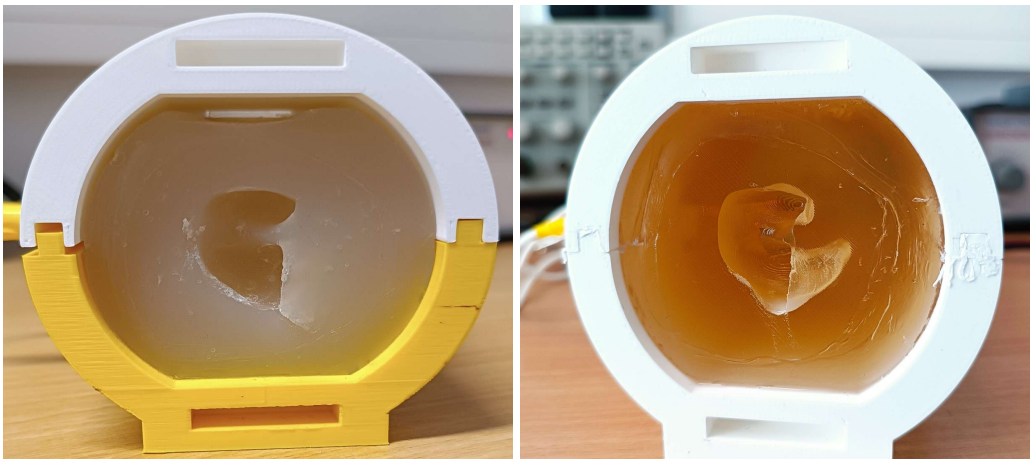

Figure 5.5: **Left -** agar ear-EEG phantom **Right -** BG ear-EEG phantom

5.4.2 Silicone doped with carbon fiber

A non-perishable phantom that can maintain signal integrity indefinitely was also envisioned, as the aforementioned organic materials tend to deteriorate over time.

Conductive fillers have been tested to make silicone rubbers conductive, with Carbon Fiber (CF) found to be the most effective even at a 0.5% weight percentage measuring a 2kohm resistance. Increasing to 1% further lowered resistance to 200ohm, and higher percentages gave similar resistance, indicating that the percolation threshold (filler concentration at what a conductive network is fully established) was reached [68].

A DIY approach in doping the silicone was followed [69], the acquired materials being:

- Chopped carbon fibers, 3mm in length, 30€ for 500g, on Amazon
- Two-part A/B system platinum curable silicone, mixing ratio of 1:1, 23€ for around 630ml, in Amazon (two were acquired for the phantom)

The silicone was estimated to have a density of $1.11 g/cm^3$. Various weight CF percentages were tried according to Equation 5.6 to establish a percolation threshold:

$$\frac{CF}{CF+S} = X\% \ (where \ X = 0.5, 1.0, 1.5, 2.0 \ ...) \tag{5.6}$$

With CF being the weight of CF and S the weight of silicone. It was observed that when the weight percentage of CF exceeded 1%, the mixture became too dense and unsuitable for molding with the current mixing methods. Therefore, only 0.5% and 1.0% percentages were considered and prepared according to Equations 5.7:

$$\begin{cases} CF = \frac{S}{199} \ , \ for \ X = 0.5 \\ CF = \frac{S}{99} \ , \ for \ X = 1.0 \end{cases} \tag{5.7}$$

As seen by the results of the material characterization in *Subsection* C.0.1, this non-perishable phantom was ultimately made for a 1% percentage, with 8g of CF (rounded to nearest unit) being used for a total of 700ml of silicone, following the next steps [69]:

1. Measure 8g of CF into a disposable cup (use a mask/gloves when handling CF)
2. Wet the CF with a small amount of rubbing alcohol, spread them around, and let almost entirely evaporate (to release strands of hair that surround the CF)
3. Add the CF to 350ml of part A silicone and mix thoroughly (an electric mixer with a wider spatula attachment was used) until the mix presents a grey/blueish tint
4. Add 350ml of part B silicone and keep mixing for up to 25 minutes to the same tint
5. Pour into the phantom, equally through each vent, and let cure for 6 hours

It should be noted that the employed mixing method didn't achieve a homogeneous distribution of CF in the silicone, creating conductive (darker) and non-conductive (translucid, low or no CF) areas as perceived in Figure 5.6 (right).

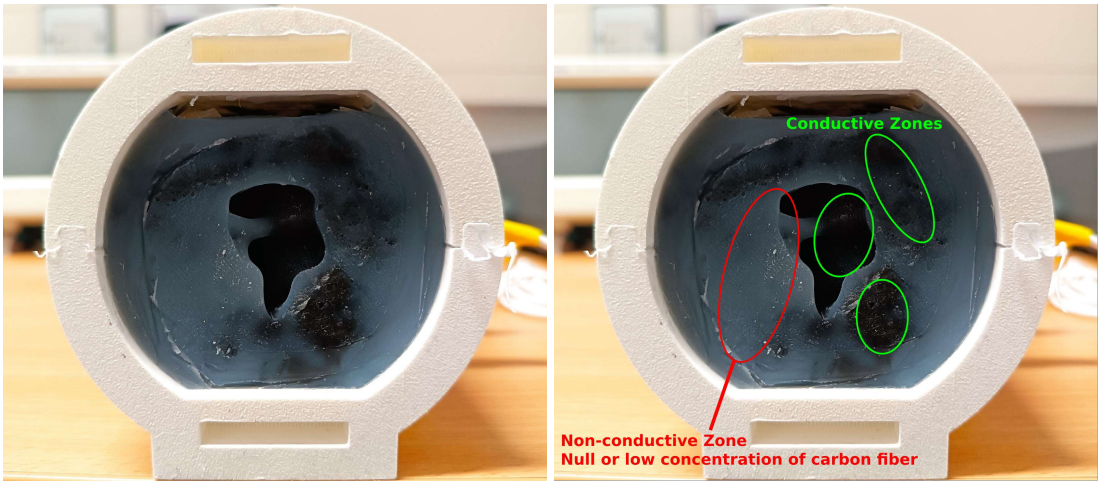

Figure 5.6: Silicone CF ear-EEG phantom - the lack of conductive homogeneity is highlighted on the right, with conductive and non-conductive zones being visible

5.5 Ear-EEG phantom testing protocol and setup

The agar and BG phantoms were tested over eight days, alternating daily, with four sessions each, and refrigerated while not in use (4ºC). Due to time constraints, the silicone CF (1%) phantom was only tested twice, five days apart. All phantoms were made using the ear scans of the same subject, so the same pair of earbuds was used for all testing.

The phantom was firstly weighed without side lids and with the AUX cables stacked on top. The antennas were connected to a signal generator, simulating a **10Hz (alpha band) 100mV square** wave. The oscilloscope probe was jammed in the side of the phantom to measure the signal through the material alone and test for the material's integrity. Both earpieces were inserted, and impedance was measured using an analog impedance meter, which measured discrete impedance values up to 50kohm. The impedance meter's reference electrode was connected to electrode Ex1. The probe was then connected directly to each electrode to visualize the simulated signal, which allowed to test if any electrode wasn't functioning or had a diminished signal amplitude compared to the one measured through the material. To simulate an ear-EEG acquisition, the earbuds were then connected to an **OpenBCI Cyton** amplifier (8 channels, 250Hz sampling rate, 24 bits ADC) and connected per the recommended settings EEG acquisitions [70, 71]. Ex1 was assigned to the bottom SRB2 pin (reference), and Ex2 was assigned to the bottom BIAS pin (noise-canceling), *a priori*. The remaining electrodes were connected in ascending order to the bottom N1P to N6P analog input pins (Ex3 is N1P, and Ex8 is N6P, on the board). Impedance values were also rechecked through the **OpenBCI** GUI. Then 20 second recordings were obtained through the amplifier on each ear, with a gain of 24: a recording with the simulated wave and an acquisition with no signal to assess the recorded noise floor at each electrode, both offline filtered between 0.3 and 100Hz.

The protocol was repeated after applying conductive paste (Ten20) to each ear electrode. The testing setup is illustrated in Figure 5.7.

Noise floor Root Mean Square (RMS) values were obtained with the *rms* function and the alpha simulation SNR **(at 1% confidence)** was calculated as per Equation 5.2.

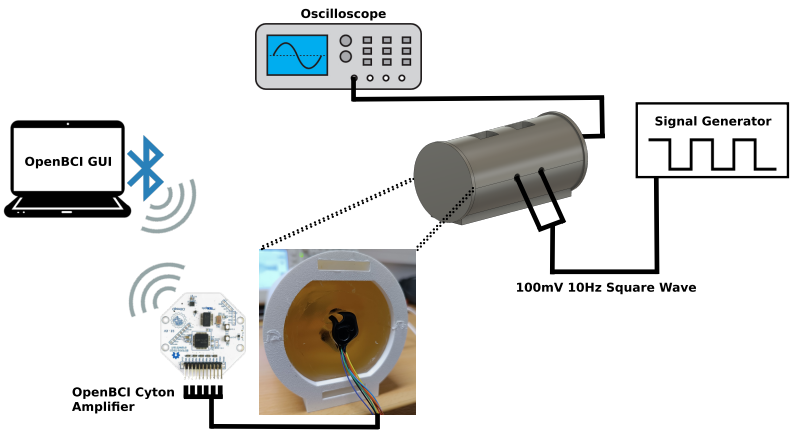

Figure 5.7: Schematic testing setup of the proposed ear-EEG phantom

6

Results and Discussion

6.1 EEG control group - stimuli/pipeline validation

This Section presents scalp EEG grand average (n = 5) results for the control group (Cz referenced), showing the expected responses to validate the used stimuli and processing pipelines. Results will pertain to optimal responses at scalp electrodes and the response at T8, as a near-the-ear electrode, to assess what different paradigms look like at this level.

6.1.1 Alpha block

As seen in Figure 6.1, a distinct effect on alpha wave blocking with the suppression of the 8 to 12Hz band when opening the eyes was achieved with the highest modulation of 6.1dB at Oz, over the occipital lobe. Near the ear at T8, the modulation dropped to 3.7dB.

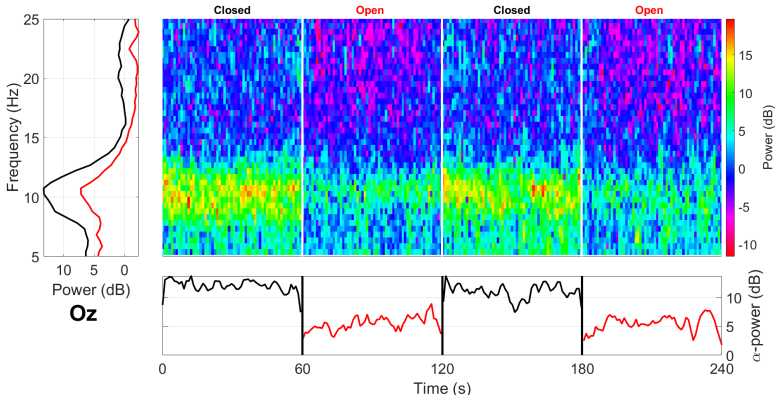

Figure 6.1: Alpha block grand average spectrogram over the control group at Oz (Cz referenced) - the bottom plot shows the alpha power mean power (8 to 12Hz) per section while the left vertical plot shows the frequency response between the two conditions

6.1.2 ASSR

For the ASSR (Figure 6.2), peak frequency responses at the used 40Hz stimulus frequency were obtained, with the highest mean SNR at P4 with 9.9dB, lowering to 4.7dB still significant response at T8.

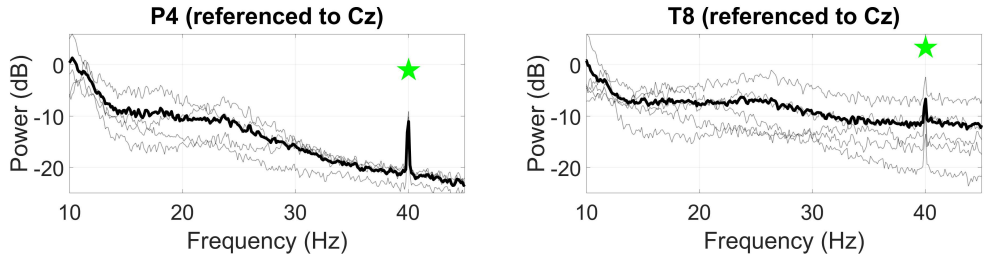

Figure 6.2: Grand average ASSR to a 40Hz stimuli, at P4 (left) and T8 (right) - statistically significant peaks are highlighted by the green star token, based on an f-test ($p < 0.05$)

6.1.3 SSVEP

The SSVEP expected peak frequency of 10Hz response was better at the Oz location with a mean SNR of 11.0dB, as seen in Figure 6.3, where the peaks for several harmonics of 10Hz fundamental frequency are also present, up to the 8th harmonic. At T8, the ratio was lower, with a mean SNR of 7.5db as we are further away from the visual cortex, with harmonic responses only distinguishable up to 40Hz.

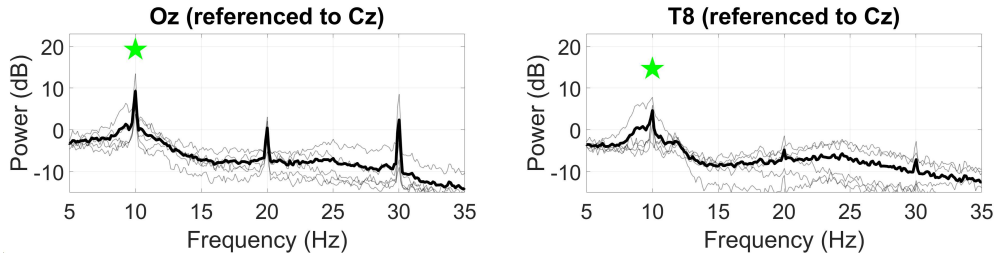

Figure 6.3: Grand average SSVEP to a 10Hz stimuli, at Oz (left) and T8 (right) - statistically significant peaks are highlighted by the green star token, based on an f-test ($p < 0.05$)

6.1.4 AEP (N100)

The response to the auditory 1kHz stimuli is shown in Figure 6.4, presenting three significant components, with the biggest being the expected deflection around 100ms with a 5µV amplitude corresponding to the N100 component (positive due to the Cz reference), resulting in a peak-to-peak amplitude of 8.9µV between the N1 and P2 components.

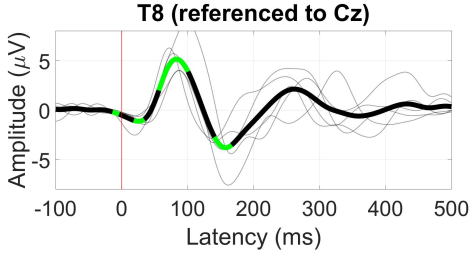

Figure 6.4: Grand average AEP waveform at T8 - statistically significant segments are highlighted in green, based on a t-test ($p < 0.05$)

6.1.5 VEP

The obtained VEP waveform for the onset-offset pattern reversal paradigm is shown in Figure 6.5. In Oz, a significant component is present between 150 and 300ms with a peak amplitude of 15µV at 200ms. In T8 near the ear, the same component isn't deemed significant and, instead, shows two smaller positive deflections at 90 and 300ms of 2 and 3µV, respectively.

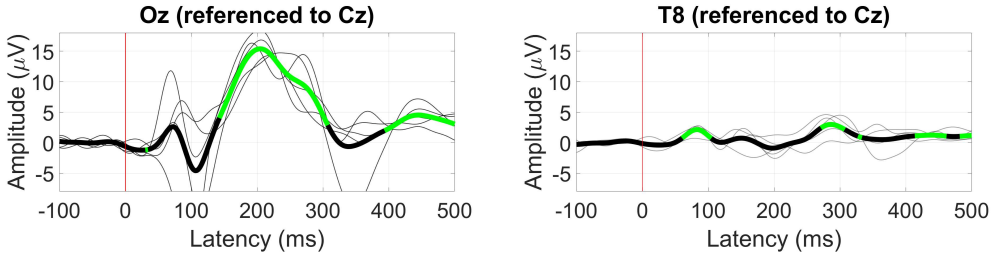

Figure 6.5: Grand average VEP waveform at Oz (left) and T8 (right) - statistically significant segments are highlighted in green, based on a t-test ($p < 0.05$)

6.1.6 Auditory oddballs (MMN)

The MMN response was the strongest at electrode site Pz, shown in Figure 6.6 (left). At 200ms, the expected negative differentiation was observed between the oddball and standard stimuli with an amplitude of 2µV, still present at T8 (Figure 6.6 (right), with the same amplitude, but with the first sensory (100ms) component not being significant.

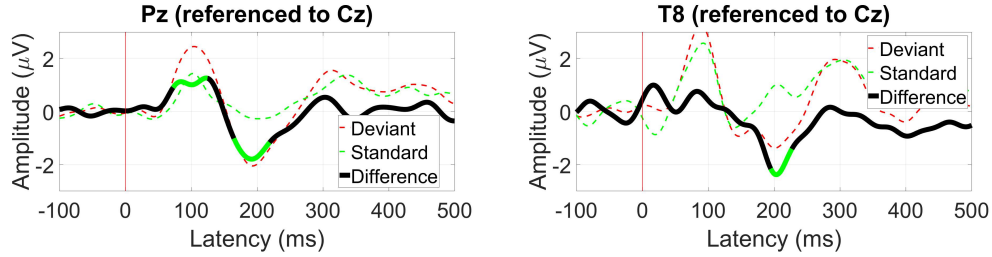

Figure 6.6: Grand average MMN waveform at Pz (left) and T8 (right) - statistically significant segments are highlighted in green, based on a t-test ($p < 0.05$)

6.1.7 Visual oddballs (P300)

The P300 component characteristic of the subject's active response to an oddball stimulus was better observed at P4 between 280ms with a 6µV amplitude, lowering to 4µV at T8 (Figure 6.7) with peak amplitude achieved at around 250ms from the onset.

6.1.8 EOG - blinks and saccades

While not cortical in origin, EOG responses regarding blinking amplitude and saccade profiles are also assessed. The response is naturally better at the scalp level at frontal

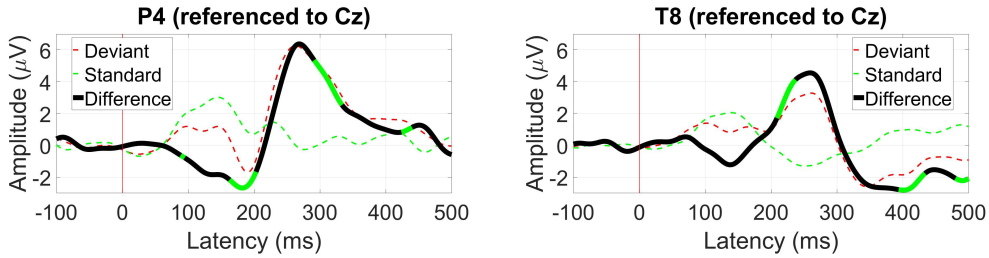

Figure 6.7: Grand average P300 waveform at P4 (left) and T8 (right) - statistically significant segments are highlighted in green, based on a t-test ($p < 0.05$)

electrodes like Fp1 and Fp2, near the eye muscles responsible for these movements. In our setup, we considered F3 and F4 as approximate locations for Fp1 and Fp2.

At F3, in Figure 6.8 (left), for an exemplary subject, the peak-to-peak amplitude difference between hard (8mV) and regular (1.5mV) can be observed, with a lower peak-to-peak amplitude but about the same ratio at T8 (on the right). On the grand average of the five subjects, the ratio between hard and soft blinks was 2.6 at F3 and 2.5 at T8 (higher at 3.7 in T7), as seen in Table D.2.

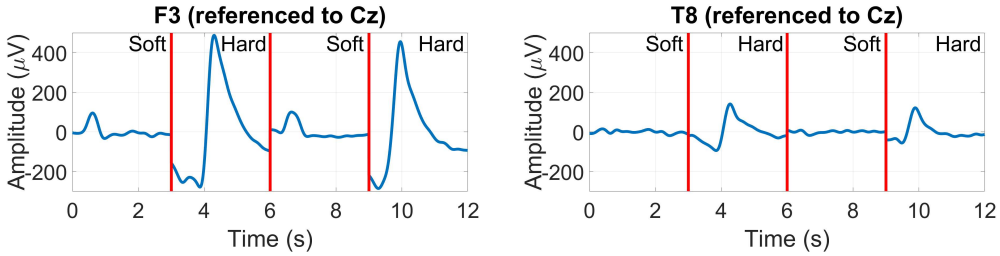

Figure 6.8: Soft/hard blink amplitudes, for an exemplary subject, at F3 (left) and T8 (right)

Figure 6.9 shows the saccade profiles in different directions. The saccades were assessed around 200ms after stimulus onset, where the separation between directions is greater. Between T7 and T8, it is possible to see a 10μV difference between the right (blue line) and left (green line) saccades, with their polarity inverting, depending on the side of the sensing electrode. The vertical-oriented saccades are less differentiated, with only around 2μV amplitude separating their traces.

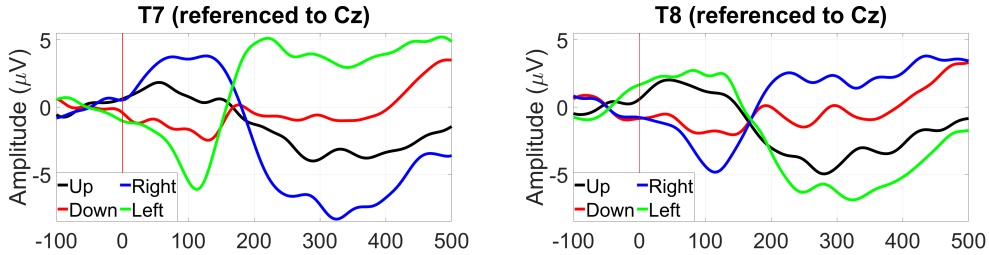

Figure 6.9: Grand average saccade profiles at T7 (left) and T8 (right)

6.1.9 Section overview

Based on the findings in this Section, we can confirm that the anticipated responses are present at the appropriate scalp electrode sites and primarily maintained near the ear at T8 (the VEP waveform changes rather significantly from the Oz response). This validates the **EaR-P Lab** stimuli presentation and processing pipelines utilized. Therefore, our present methods are also suitable for assessing ear-EEG.

6.2 Ear-EEG - wet and dry electrode acquisitions

This Section will present the results of ear-EEG measurements, mainly at the ER8 and EL8 ear electrodes for different referencing schemes on a grand average (n = 5) for the wet ear electrodes setting and for a significant subject (n = 1) for the dry ear electrode conditions, as per Subsection 5.3.1.

6.2.1 Alpha block

Table 6.1 shows the grand average alpha block power at ER8. The modulation was 3.7dB for the scalp Cz reference, about 3dB lower than the control group value at Oz. Referencing to T8, closer to the ear, the modulation decreases to 3.1dB and 2dB for the within-ear reference at ER3, with a lower value for the between-ears assessment. Only the Cz reference was found significant for the dry ears subject, with a value of 1.9dB.

Table 6.1: Grand average Alpha Modulation (dB) at ER8 and EL8 for Cz, T8, and ER3 references - dry ear-EEG results are related to a significant subject - omitted results were statistically not significant, based on a t-test ($p < 0.05$)

	Cz-ER8	**T8-ER8**	**ER3-ER8**	**ER3-EL8**
Wet Ear-EEG	3.7 ± 3.1	3.1 ± 3.0	2.0 ± 2.0	1.8 ± 2.6
Dry Ear-EEG	1.9 ± 2.9	-	-	-

6.2.2 ASSR

The ASSR SNR at ER8 (Table 6.2) for the Cz reference has a value of 7.9dB, a decrease of 1.5dB over the best response in the control group. Comparing the T8 and ER3 references, we can see the SNR is 1.2dB higher for the in-ear ER3 reference over the temporal site. For dry electrodes, the Cz scalp and T8 reference had a better performance (8.2 and 2.6dB, respectively) for the dry conditions subject. However, the in-between ears reference is statistically not significant. The dry ER3 reference has a lower value when measuring at ER8 than wet recordings. However, when measuring at ER4, for instance, the SNR was 3.7dB, showing feasibility for measuring the ASSR response on a dry within-ear setting.

Table 6.2: Grand average ASSR SNR (dB) at ER8 and EL8 for Cz, T8, and ER3 references - dry ear-EEG results are related to a significant subject - omitted results were statistically not significant, based on an f-test ($p < 0.05$)

	Cz-ER8	**T8-ER8**	**ER3-ER8**	**ER3-EL8**
Wet Ear-EEG	7.9 ± 0.8	2.1 ± 0.5	3.3 ± 0.6	1.7 ± 0.4
Dry Ear-EEG	8.2 ± 1.2	2.6 ± 0.8	1.5 ± 0.7	-

6.2.3 SSVEP

Comparing the results from Table 6.3, all measured SNR results were lower when compared to the control group SNR values of 11 and 7.5dB at Oz and T8, respectively. When looking at scalp references (Cz and T8), the SNR at ER8 holds up at 6.4 and 5.9dB. However, the within-ear/between-ears referencing was systematically shown as not significant, even for other electrodes. Only the T8 reference produced a significant response of 5.1dB for the dry ear-EEG subject.

Table 6.3: Grand average SSVEP (dB) at ER8 and EL8 for Cz, T8, and ER3 references - dry ear-EEG results are related to a significant subject - omitted results were statistically not significant, based on an f-test ($p < 0.05$)

	Cz-ER8	**T8-ER8**	**ER3-ER8**	**ER3-EL8**
Wet Ear-EEG	6.4 ± 3.9	5.9 ± 3.1	-	-
Dry Ear-EEG	-	5.1 ± 2.5	-	-

6.2.4 AEP (N100)

When referenced to Cz, the ER8 electrode acquired the N100 component (albeit inverted) at an amplitude of around 6µV for wet and dry recordings. Referenced to T8, the significant component was diminished, with a peak amplitude of around 2µV, as per Figure 6.10.

For the within-ear assessment referencing ER3 (Figure 6.11), only the between-ears configuration measuring at EL8 showed a significant N100 component with a 1µV amplitude, with all dry ear measurements presenting no significant N100 or other components.

6.2.5 VEP

While the VEP waveform seen at Oz for the control group is not maintained near the ear, the resulting waveform is maintained from the Cz to the T8 referencing, with a 2µV drop in amplitude for the latter, as seen in Figures 6.12.

For the ear ER3 reference, only the in-between ears configuration presented statistical significance in the waveform. For the dry setting subject, the early negative deflection at 100ms was maintained at the same amplitude, while for the wet group, a later 200ms component was deemed significant at 1µV.

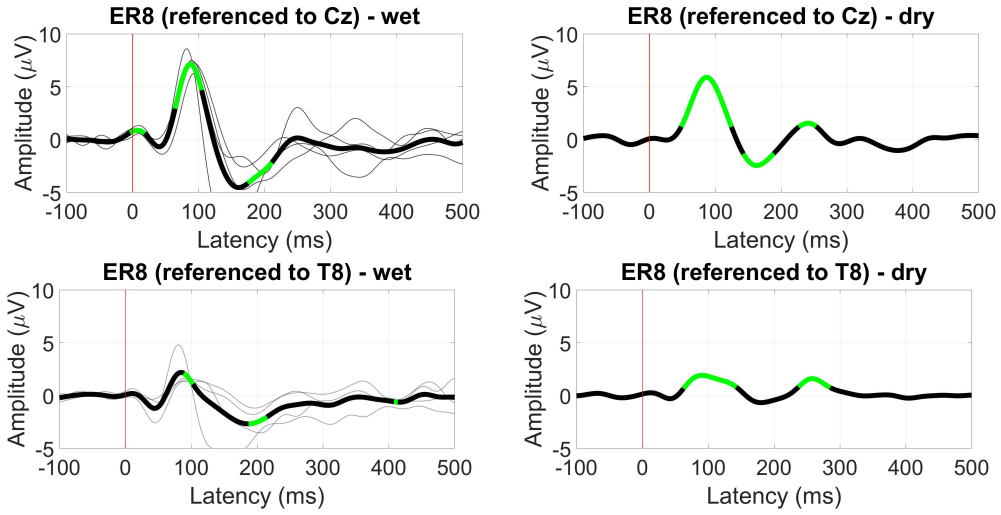

Figure 6.10: Wet grand average (left) and dry conditions single subject (right) ear-EEG AEP waveform at ER8 for Cz (top) and T8 (bottom) references - statistically significant segments are highlighted in green, based on a t-test ($p < 0.05$)

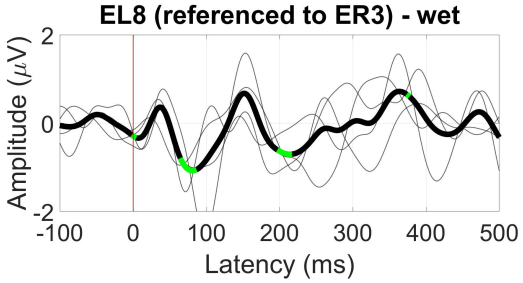

Figure 6.11: Wet grand average ear-EEG AEP waveform at EL8 for an ER3 reference - statistically significant segments are highlighted in green, based on a t-test ($p < 0.05$)

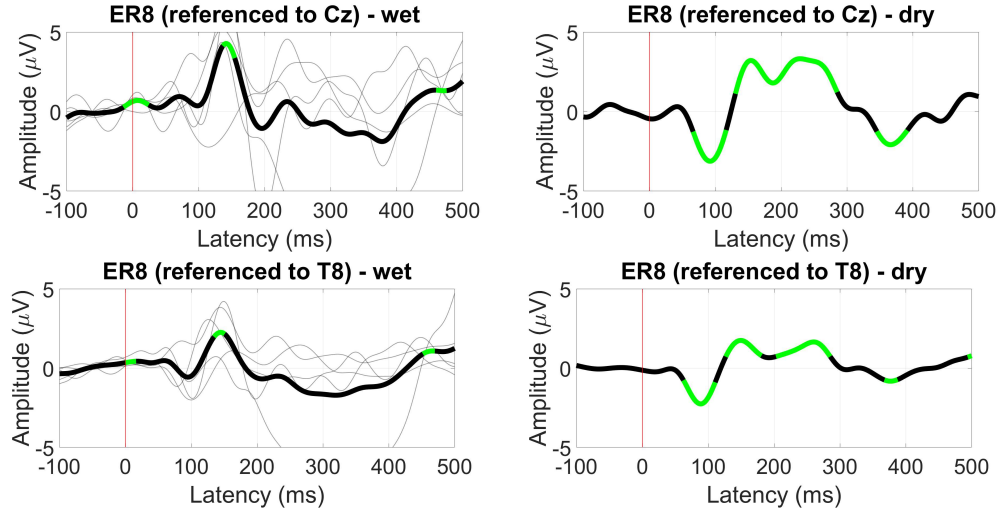

Figure 6.12: Wet grand average (left) and dry conditions single subject (right) ear-EEG VEP waveform at ER8 for Cz (top) and T8 (bottom) references - statistically significant segments are highlighted in green, based on a t-test ($p < 0.05$)

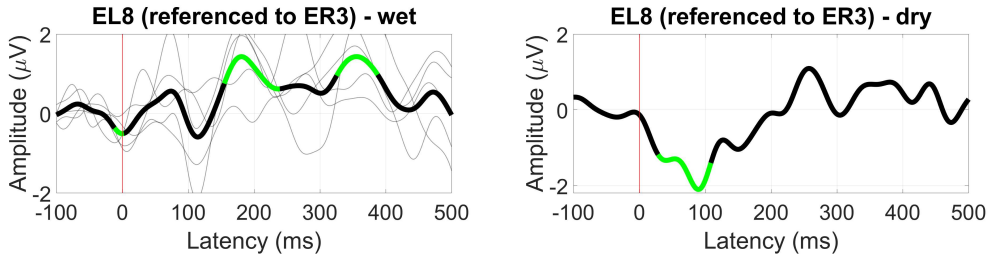

Figure 6.13: Wet grand average (left) and dry conditions single subject (right) ear-EEG VEP waveform at EL8 for an ER3 - statistically significant segments are highlighted in green, based on a t-test ($p < 0.05$)

6.2.6 Auditory oddballs (MMN)

The MMN response referenced from the scalp and T8 is present for ear electrodes for both wet and dry settings as seen in Figure 6.14, showing a 2 to 3μV negative deflection at around 200ms latency, as expected.

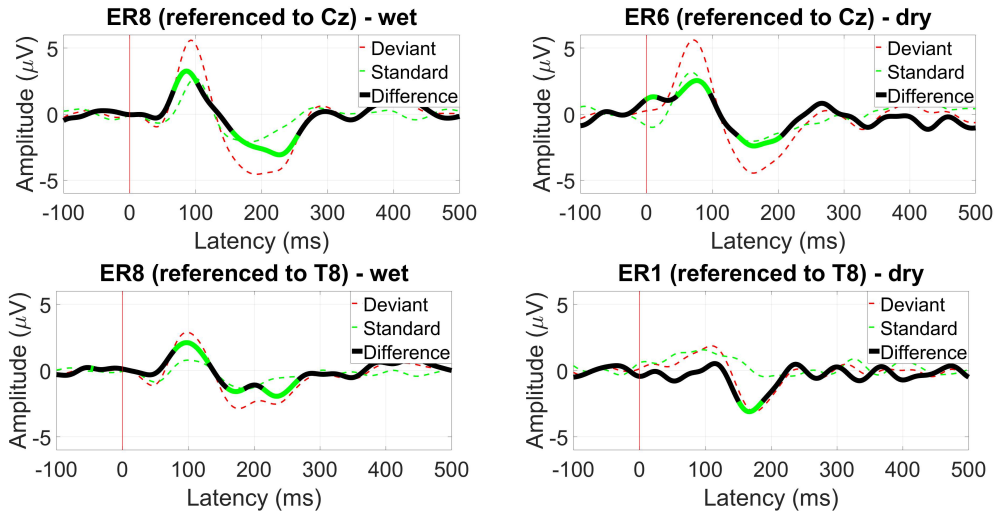

Figure 6.14: Wet grand average (left) and dry conditions single subject (right) ear-EEG MMN waveform at ER8, ER6, and ER1 for Cz (top) and T8 (bottom) references - statistically significant segments are highlighted in green, based on a t-test ($p < 0.05$)

For within-the-ear referencing, no significant components resembling the MMN response in reviewed literature were found, albeit for dry measurements, a constant differentiation (about 1μV from event onset to 200ms, not always significant) between the standard and oddball averaged waveform was observed on some electrodes.

6.2.7 Visual oddballs (P300)

Measured from the scalp to the ear, the greatest observed difference between the oddball and standard stimuli shows a negative deflection around the 350ms latency for both wet and dry assessment, for Cz (5 to 6 μV amplitude) and T8 (1.5 to 2 μV amplitude) referencing as per Figure 6.15, suggesting a later onset for this component than on the scalp.

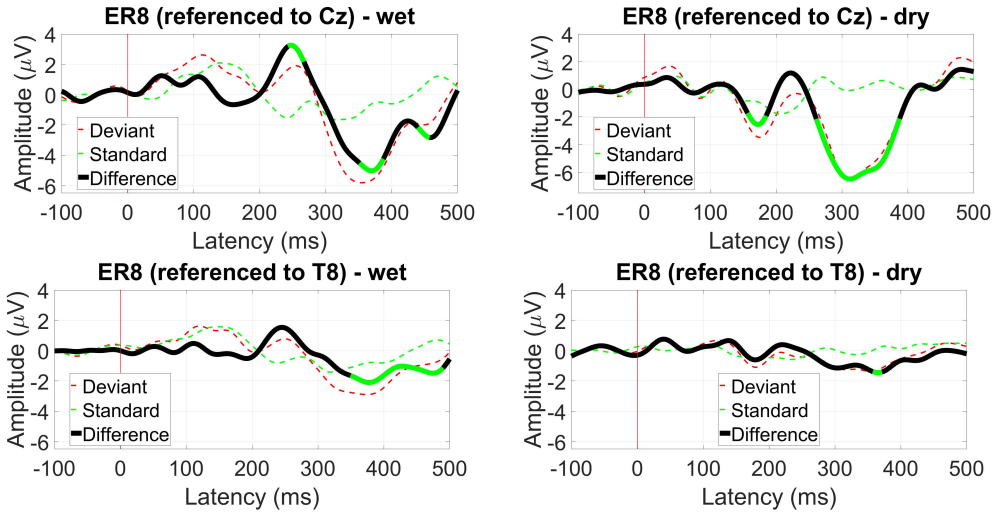

Figure 6.15: Wet grand average (left) and dry conditions single subject (right) ear-EEG P300 waveform at ER8 for Cz (top) and T8 (bottom) references - statistically significant segments are highlighted in green, based on a t-test ($p < 0.05$)

While ear P300 waveforms weren't deemed significant in wet recordings, for the chosen dry subject, significant positive differentiation can be seen at the ear level within (ER4) and across the ear (EL8) at latencies between 300 and 400ms, presented in Figure 6.16.

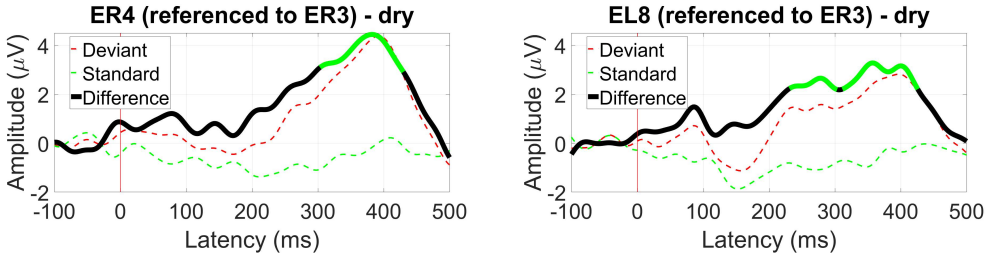

Figure 6.16: Dry conditions single subject ear-EEG P300 waveform at ER4 (left) and EL8 (right) for an ER3 reference - statistically significant segments are highlighted in green, based on a t-test ($p < 0.05$)

6.2.8 EOG - blinks and saccades

Concerning ear EOG blink ratios, from Table 6.4, the ER3 reference for both wet and dry electrodes was about 1.5 times higher than for scalp references near the ear, with diminished results for the between-ears configuration at EL8.

Table 6.4: Grand average hard/soft blink ratios at ER8 and EL8 for Cz, T8, and ER3 references - dry ear-EEG results are related to a significant subject and taken at ER4 instead of the ER8 electrode, as the ratio was consistently higher

	Cz-ER8	**T8-ER8**	**ER3-ER8**	**ER3-EL8**
Wet Ear-EEG	2.0	2.1	3.0	2.4
Dry Ear-EEG	2.7	3.0	4.0	1.5

Measuring at the ER8, saccade profiles were maintained for the different directions, with greater amplitudes for the Cz reference but better differentiation when referencing to T8, with a 10µV difference between up and down saccades, per Figure 6.17.

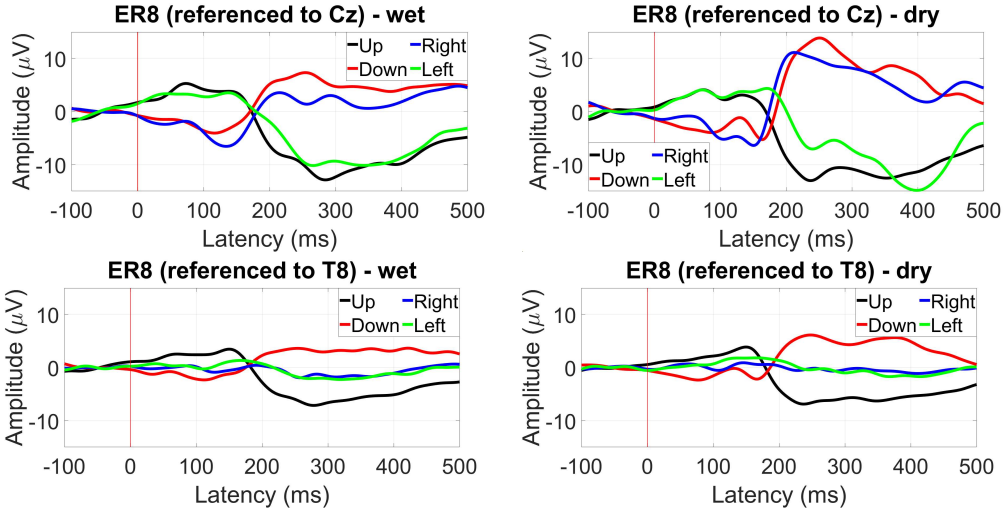

Figure 6.17: Wet grand average (left) and dry conditions single subject (right) ear-EEG saccade profiles waveform at ER8 for Cz (top) and T8 (bottom) references

For within referencing, the vertical saccade plane presents a better differentiation of 3 to 4µV for both wet and dry settings, while recording across the ears shows the best results in amplitude and difference between right and left saccades (the vertical saccades present the same profile), as seen in Figure 6.18.

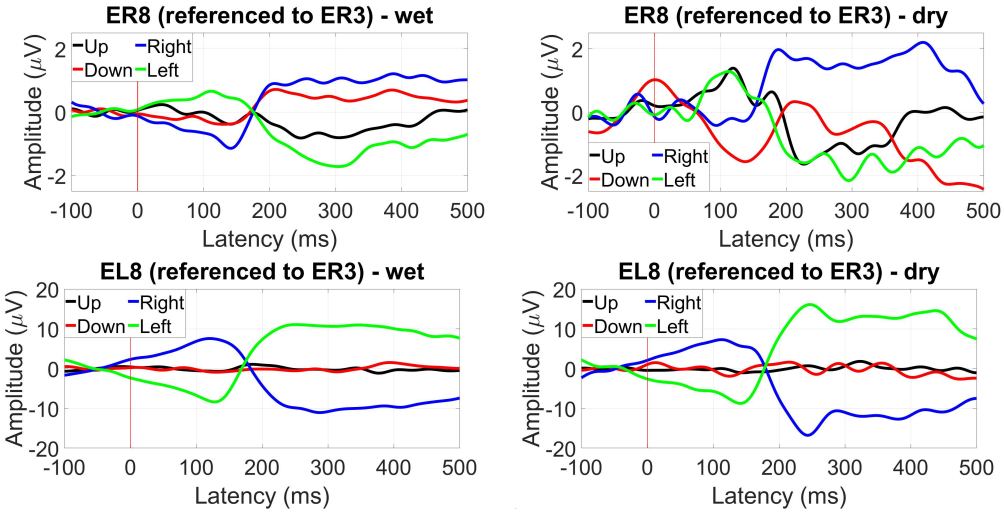

Figure 6.18: Wet grand average (left) and dry conditions single subject (right) ear-EEG saccade profiles at ER8 (top) and EL8 (bottom) for an ER3 reference

6.2.9 Section discussion

Using **EaR-P Lab**, this Section on the first instance shows that results were able to be obtained when measuring EEG through the ear, so the earbuds have the necessary electrical

capabilities to record signals from within the ear, with improved amplitudes and ratios for some paradigms on a Cz reference. On a T8 reference, closer to the ear, most results were seamless to the Cz reference, although with expected lower amplitudes or ratios, which is a primary conclusion that can be taken by the reviewed literature in Section 3.1.

For a within-ear reference at ER3, the measured SNR was lower for frequency responses but still significant, especially for the ASSR paradigm, which performed better for ER3 than the T8 reference. Visual-related paradigms, such as SSVEP, suffered the most within-ear compared to auditory stimuli. Most ERP waveforms were noisier and lost their expected component details compared to scalp responses. Nonetheless, statistical significance was still attributed to amplitudes at relevant latencies from stimulus onset. However, it should be noted that drawing comparisons about these waveforms is challenging because of the present small sample size (five subjects, one for dry) when assessing ear-EEG recordings.

For EOG-related detection, while the prime electrodes in the control setup are not present for ear-EEG recordings, the ear is a more promising location than the scalp to detect eye activity, which could be advantageous for ear-based BCI applications.

6.3 Ear-EEG phantom assessment

6.3.1 Phantom integrity and durability

When measuring the signal through the phantom, it is essential to track the usability of this tool over time. This was achieved by monitoring the net weight of each phantom and measuring the input signal through the medium.

According to the data presented in Table 6.5, we can conclude that during a week-long testing period (by Day 4), the agar and BG phantoms lost no more than 10g in weight (with a higher percentage loss on agar). The reason for this weight loss can be attributed to the evaporation of water in both phantoms. Over five days, the CF phantom lost only 2g in mass, likely due to excess alcohol evaporating.

Table 6.5: Measured mass (g) of each ear-EEG phantom over the testing days

	Day 1	**Day 2**	**Day 3**	**Day 4**
Agar	855	851	850	845
BG	963	959	958	956
CF	921	X	919	X

While the mass measurements may suggest the usability of the phantom even after the testing week period, when measuring the signal integrity over the same time, an amplitude deterioration can be seen in Table 6.6. These measurements were taken visually at the oscilloscope like in Figure F.5.

In the aforementioned Table 6.6, the agar phantom had the more significant amplitude loss, from the initial 100mV, only achieving 44mV on day one, declining to 36mV by the last testing day. The BG phantom started at 80mV and lost half its amplitude throughout

testing due to the phantom material drying up. The CF phantom measured amplitude at the side was maintained constant through testing at 60mV.

Table 6.6: Measured signal amplitude (mV) at the sides of each ear-EEG phantom, directly through the material, as a measure of signal integrity

	Day 1	**Day 2**	**Day 3**	**Day 4**
Agar	44	40	40	36
BG	80	52	52	40
CF	60	X	60	X

6.3.2 Electrode impedance

Impedance measurements (values taken from the OpenBCI GUI and validated with an analog meter) are present in Table 6.7, exemplified for dry and wet agar recordings for the first two days of testing. Impedance measurements show a clear improvement across electrodes when applying conductive paste to the electrodes, reliably bringing the impedance under 10kohm, which is acceptable for EEG data collection (the same effect happened for BG measurements, with overall even lower values than agar). By assessing the presented data, it can be said that the Ex3, EL7, and EL8 electrodes had the most difficulty achieving suitable impedance for dry electrode conditions, with impedance values over 50kohm, indicative of no or very poor contact on the electrodes. This effect was consistent across testing sessions (suggesting ER4 as a better channel than ER3 for dry recordings, at least on this specific subject). However, applying conductive paste brings these electrodes' impedance down to usable levels.

There were instances where the past didn't bring the impedance down for the CF phantom impedance measurements in Table E.1. This is attributed to the more rigid phantom material, aggravating the difficulty of insertion of the earpieces.

Table 6.7: Agar impedances (kohm) for a subset of electrodes in wet and dry recordings for the first two days of testing - values above 50khom are displayed as 50+, meaning very poor or no contact at all

	EL3	**EL4**	**EL7**	**EL8**	**ER3**	**ER4**	**ER7**	**ER8**
Day 1 - Dry	20	7	46	50+	50+	13	9	11
Day 1 - Wet	11	6	13	6	8	9	7	8
Day 2 - Dry	50+	7	50+	50+	50+	13	14	9
Day 2 - Wet	10	6	15	7	8	10	8	8

6.3.3 Noise floor measurements

Like impedance, noise floor measurements (without the input simulated signal) greatly benefit from the usage of paste at each electrode site, bringing the values across all channels close or under 1 µVrms across the board, as seen in Table 6.8 for the first day of testing.

These values tell us that the electrode material and shape are adequate for wet recordings. Comparing the left ear to the right ear results in the same table on a dry setting, we can conclude that the left ear is more prone to have noisier channels (with RMS values in the order of hundreds of µV), when compared to the right side electrodes, suggesting a better performance when assessing the right earpiece on this subject.

For the CF phantom, noise floor values (Table E.2) are much higher than agar and BG, which is related to the tougher nature (harsher insertion of the device) of the material.

Table 6.8: Noise floor measurements (µVrms) for agar and BG on the second day of testing - noise measurements were not executed on the first day for agar and BG

	EL3	**EL4**	**EL7**	**EL8**	**ER3**	**ER4**	**ER7**	**ER8**
Agar - Dry	439.1	43.8	458.4	544.1	24.5	4.9	4.9	5.4
Agar - Wet	1.0	0.4	0.4	0.5	0.9	1.0	1.1	1.1
BG - Dry	58.4	40.8	64.6	36.5	3.3	4.4	4.3	4.4
BG - Wet	1.4	0.2	0.7	0.8	0.7	0.9	1.0	1.0

6.3.4 Alpha wave simulation

When inputting the simulated signal into the phantom through the two antennas, the input frequency (10Hz - within the alpha band) was successfully recorded at all ear electrode sites for the first day of testing in agar and BG, as per Table 6.9. As expected, the modulation SNR value was higher when measured in the ear canal electrodes like ER8 (further away from the within-ear reference at ER1) than, for example, ER3 or ER4, which are closer to the reference. The modulation was overall higher for agar (22.6 and 22.9dB SNR at ER8 for dry and wet recordings, for instance), with some electrodes showing very little difference between wet and dry settings on this frequency-based response.

For subsequent testing days, the left side electrodes on BG were consistently found not significant at a 1% confidence value in the statistical analysis.

Table 6.9: Alpha Modulation SNR (dB) for wet and dry electrode conditions on agar and BG phantom recordings, at electrodes and Ex3, Ex4, Ex8

	EL3	**EL4**	**EL8**	**ER3**	**ER4**	**ER8**
Agar - Dry	17.1 ± 3.4	19.7 ± 4.6	19.7 ± 5.2	4.5 ± 2.7	19.8 ± 3.7	22.6 ± 5.8
Agar - Wet	8.7 ± 2.6	21.2 ± 4.9	21.7 ± 7.0	18.3 ± 3.3	21.9 ± 4.1	22.9 ± 6.1
BG - Dry	12.6 ± 3.4	10.1 ± 2.6	7.2 ± 2.6	10.0 ± 2.6	16.1 ± 3.4	19.2 ± 5.1
BG - Wet	6.0 ± 2.4	10.9 ± 2.4	20.0 ± 4.0	12.3 ± 2.2	20.8 ± 3.9	22.1 ± 5.7

In Figure 6.19, the resulting alpha modulation spectra at ER8 are present, with clear peaks at the 10Hz and 30Hz odd harmonic frequencies that compose the square wave. The noise floor aspect of the spectra resembles what would be expected from an ear-EEG recording, although that was not always the case in the following days of testing when the agar/BG phantom noise floor readings started to increase. Nonetheless, the phantom

antenna signal delivery and materials proved efficient in simulating a given signal, and the present methods regarding this aspect were positively validated.

For the CF ear-EEG phantom, modulation was also achieved, as per Table E.3.

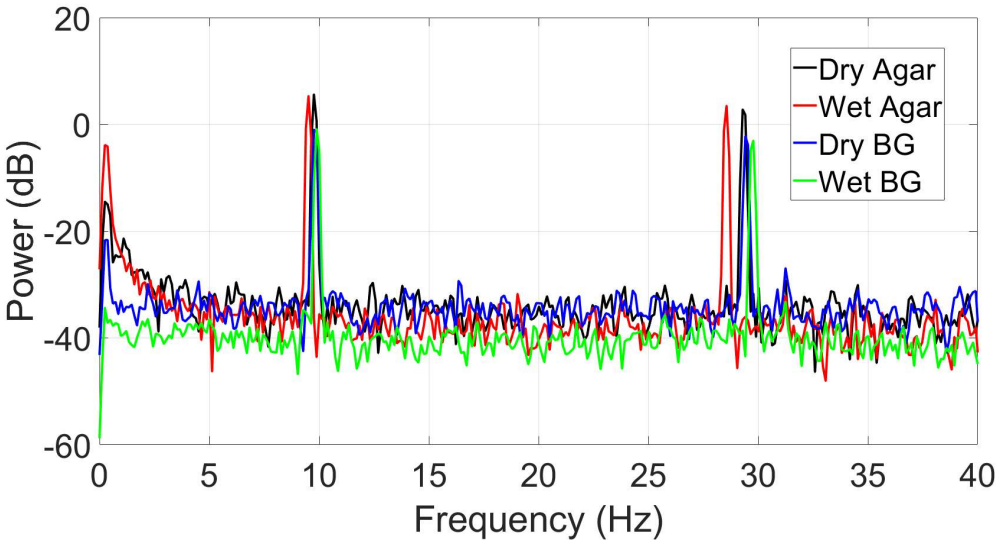

Figure 6.19: Ear-EEG alpha wave (10Hz input) simulation frequency response (dB), for agar and BG, in dry and wet electrode settings

6.3.5 Discussion and reassessment of dry ear-EEG ASSR data

Overall, the usage of either agar or BG (which performed similarly) coupled with the phantom ear 3D imprint of a subject proved to be an efficient methodology for the assessment of ear-EEG devices on their electrode contact impedance, measured noise floor, and acquisition of a known signal.

The tested earbuds in this Section belong to the dry single subject shown in Section 6.2. From the ear-EEG phantom results, it is suggested that the ER4 electrode has better connectivity to the ear than ER3, which was previously selected as a reference, based on the discard ratio from Table D.1. Table 6.10 shows a direct comparison of the ASSR dry data (most viable ear-based paradigm) reanalyzed with ER4 as a reference for this single subject. The suggested electrode ER4 from the phantom improved the SNR at ER8 (and the other electrodes) by about 2.3 dB, exemplifying how the phantom can predict better usability of ear devices without the need to test it on an actual subject.

Table 6.10: Within-ear ASSR SNR (dB) for the single dry electrode conditions subject (tested with the ear-EEG phantom) for an ER3 and ER4 reference, measuring at ER6, ER7, and ER8 - omitted results are deemed not significant, based on an f-test ($p < 0.05$)

	ER6	**ER7**	**ER8**
ER3	-	1.6 ± 0.7	1.5 ± 0.7
ER4	3.7 ± 1.0	3.9 ± 0.9	3.8 ± 0.9

7

Conclusion

7.1 Achieved contributions

This work proposed a toolbox that can facilitate the validation and test benching of ear-EEG devices. An application (**EaR-P Lab**) has been developed and used in this study, allowing ready access to validation-type paradigms for EEG devices. This application has been successfully integrated into a pipeline to measure EEG through the ear canal and concha ear area using customized fit ear-EEG devices. This study, albeit small in scale, aligns with the reviewed literature in that EEG responses can be measured through the ears and that the available earbuds are functional in measuring this signal. When dwelling into within-ear referencing as a means to test if these earbuds could be used in a standalone fashion (without the need for a scalp reference), it was concluded that the earbuds are on par with relevant literature for frequency-based paradigms (ASSR, SSVEP and alpha modulation), as well as showing as an optimal option to acquire EOG data. When it comes to within-ear neural transient waveforms (AEPs, VEPs, and the oddball paradigms), the obtained responses in the ear neither resembled the scalp responses nor showed similar waveforms to the reviewed literature, which were expected to be obtained at least for the auditory AEP and MMN most literature prevalent paradigms [38, 39]. It should be mentioned that more rigorous preprocessing could be done to reveal better waveforms, like removing noisier trials from the average and averaging of ear electrodes, which was done in the above mentioned studies. So, while these responses were shown to be captured for within-ear/between-ears referenced ear-EEG, we cant say the present lack of results at this level is due to the current tested ear sensors. Still, we obtained statistically significant hints about how some evoked responses look at ear referencing.

Additionally, the concept of EEG phantom was successfully integrated into characterizing a pair of ear-EEG buds, establishing a physical test bench with the proposed prototype based on 3D scans of an individual's ear canal. The ear-EEG phantom allowed the assessment of intrinsic characteristics of the earbuds at a hardware level, like the contact impedance between electrodes and the material, and the successful acquisition of simulated known signals that can, for instance, be compared between devices.

On a broader overview, the main objective of this project was achieved as the proposed toolbox, and the necessary framework has been successfully laid out and applied to facilitate a more straightforward, faster, and fuller assessment of different ear-EEG devices.

7.2 Limitations of the present work

This work's main limitation is that no generic earpiece assessment was done, contrary to the initial prospects, as this type of earpiece wasn't ultimately made available. In that line, the control and wet ear-EEG results are only based on a population of five subjects (down to one significant subject for dry electrode recordings), as per the number of available EEG earbuds, which is a small sample size to work with the presented grand average results. Still, it is essential to highlight that the success of this project is not tied to the degree of performance of the ear devices but to the feasibility of the proposed toolbox (EaR-P Lab and the ear-EEG phantom) in enabling an expanded characterizing of said earpieces.

Regarding the phantom filling materials, attempts were made to study their intrinsic properties, but this characterization was incomplete. For example, this data was assessed two weeks after the preparation of the samples due to equipment booking issues, and the samples were evaluated for only one day (testing should be done over several days). Although the BG and agar performed similarly, the silicone CF approach, which is more durable, was also successful in conducting the signal. However, this option was not extensively tested and requires better tools, material testing, and time to be considered a reliable test bench. The mixing method needs significant improvement to provide a more homogeneous medium. Therefore, testing of this material was not highlighted.

7.3 Future work

Future work in line with the outcome of this project should dwell on applying the provided toolbox to a greater extent (more subjects, targeting of specific paradigms) to characterize ear-EEG devices for both custom and generic fit form factors in earpieces. For instance, we have demonstrated some plausibility on how assessing the earpieces through the phantom can help choose optimal within-ear referencing for an individual's ear, suggesting that more research can also be allocated to this purpose.

It is also acknowledged that the proposed tools while working, can also be polished and improved upon. **EaR-P Lab** is, as of now, an application that requires a local Python manual installation, with the efforts in turning it into a standalone executable (with PyInstaller) failing due to both incompatibilities between the PsychoPy library and an inadequate coding structure. The phantom design should also be upgraded to feature more antennas, a generic ear canal to assess this kind of device, or to be turned into an anatomical head featuring the ear structures, using the employed 3D scanning method, that would allow for testing of other phenomena, like how gait affects ear-EEG recordings.

Bibliography

[1] J. M. Lourenço. *The NOVAthesis LaTeX Template User's Manual*. NOVA University Lisbon. 2021. URL: https://github.com/joaomlourenco/novathesis/raw/main/template.pdf.

[2] A. Casson et al. "Wearable Electroencephalography". In: *IEEE Engineering in Medicine and Biology Magazine* 29 (3 2010-05), pp. 44–56. ISSN: 0739-5175. DOI: 10.1109/MEMB.2010.936545. URL: http://ieeexplore.ieee.org/document/5463026/.

[3] E. Waterhouse. "New horizons in ambulatory electroencephalography". In: *IEEE Engineering in Medicine and Biology Magazine* 22 (3 2003-05), pp. 74–80. ISSN: 0739-5175. DOI: 10.1109/MEMB.2003.1213629. URL: http://ieeexplore.ieee.org/document/1213629/.

[4] A. J. Casson. "Wearable EEG and beyond". In: *Biomedical Engineering Letters* 9 (1 2019-02), pp. 53–71. ISSN: 2093-9868. DOI: 10.1007/s13534-018-00093-6. URL: http://link.springer.com/10.1007/s13534-018-00093-6.

[5] M. Soufineyestani, D. Dowling, and A. Khan. "Electroencephalography (EEG) Technology Applications and Available Devices". In: *Applied Sciences* 10 (21 2020-10), p. 7453. ISSN: 2076-3417. DOI: 10.3390/app10217453. URL: https://www.mdpi.com/2076-3417/10/21/7453.

[6] D. Looney et al. "The In-the-Ear Recording Concept: User-Centered and Wearable Brain Monitoring". In: *IEEE Pulse* 3 (6 2012-11), pp. 32–42. ISSN: 2154-2287. DOI: 10.1109/MPUL.2012.2216717. URL: http://ieeexplore.ieee.org/document/6378569/.

[7] R. Kaveh et al. "Wireless User-Generic Ear EEG". In: *IEEE Transactions on Biomedical Circuits and Systems* 14 (4 2020-08), pp. 727–737. ISSN: 1932-4545. DOI: 10.1109/TBCAS.2020.3001265. URL: https://ieeexplore.ieee.org/document/9115876/.

[8] M. Mozaffari, R. Nash, and A. S. Tucker. "Anatomy and Development of the Mammalian External Auditory Canal: Implications for Understanding Canal Disease and Deformity". In: *Frontiers in Cell and Developmental Biology* 8 (2021-01). ISSN: 2296-634X. DOI: 10.3389/fcell.2020.617354. URL: https://www.frontiersin.org/articles/10.3389/fcell.2020.617354/full.

[9] *How the ear works*. Accessed: 2023-09-25. URL: https://www.hopkinsmedicine.org/health/conditions-and-diseases/how-the-ear-works.

[10] L. L. OpenStax. *Anatomy and physiology I*. Accessed: 2023-09-25. URL: https://courses.lumenlearning.com/suny-ap1/chapter/audition-and-somatosensation/.

[11] U. Themes. *Diseases of the external ear*. Accessed: 2023-09-25. 2016-06. URL: https://entokey.com/diseases-of-the-external-ear-2/.

[12] M. M. School. *Ear Anatomy - Outer Ear*. Accessed: 2023-09-25. 2022-08. URL: https://med.uth.edu/orl/online-ear-disease-photo-book/chapter-3-ear-anatomy/ear-anatomy-outer-ear/.

[13] M. Teplan et al. "Fundamentals of EEG measurement". In: *Measurement science review* 2.2 (2002), pp. 1–11.

[14] *The Science of Brainwaves - the language of the brain*. Accessed: 2023-09-25. 2019-12. URL: https://nhahealth.com/brainwaves-the-language/.

[15] C. E. D. Alloway, R. D. Ogilvie, and C. M. Shapiro. "The Alpha Attenuation Test: Assessing Excessive Daytime Sleepiness in Narcolepsy-Cataplexy". In: *Sleep* 20 (4 1997-04), pp. 258–266. ISSN: 1550-9109. DOI: 10.1093/sleep/20.4.258. URL: https://academic.oup.com/sleep/article-lookup/doi/10.1093/sleep/20.4.258.

[16] A. Hartoyo et al. "Inferring a simple mechanism for alpha-blocking by fitting a neural population model to EEG spectra". In: *PLOS Computational Biology* 16.4 (2020-04), pp. 1–19. DOI: 10.1371/journal.pcbi.1007662. URL: https://doi.org/10.1371/journal.pcbi.1007662.

[17] O. Jensen and A. Mazaheri. "Shaping Functional Architecture by Oscillatory Alpha Activity: Gating by Inhibition". In: *Frontiers in Human Neuroscience* 4 (2010). ISSN: 1662-5161. DOI: 10.3389/fnhum.2010.00186. URL: http://journal.frontiersin.org/article/10.3389/fnhum.2010.00186/abstract.

[18] R. Galambos, S. Makeig, and P. J. Talmachoff. "A 40-Hz auditory potential recorded from the human scalp." In: *Proceedings of the National Academy of Sciences* 78 (4 1981-04), pp. 2643–2647. ISSN: 0027-8424. DOI: 10.1073/pnas.78.4.2643. URL: https://pnas.org/doi/full/10.1073/pnas.78.4.2643.

[19] P. Korczak et al. "Auditory steady-state responses". In: *Journal of the American Academy of Audiology* 23.03 (2012), pp. 146–170.

[20] F. D. Russo et al. "Spatiotemporal analysis of the cortical sources of the steady-state visual evoked potential". In: *Human Brain Mapping* 28 (4 2007-04), pp. 323–334. ISSN: 10659471. DOI: 10.1002/hbm.20276. URL: https://onlinelibrary.wiley.com/doi/10.1002/hbm.20276.

[21] F.-B. Vialatte et al. "Steady-state visually evoked potentials: Focus on essential paradigms and future perspectives". In: *Progress in Neurobiology* 90 (4 2010-04), pp. 418–438. ISSN: 03010082. DOI: 10.1016/j.pneurobio.2009.11.005. URL: https://linkinghub.elsevier.com/retrieve/pii/S0301008209001853.

[22] H. de Lange Dzn. "Research into the Dynamic Nature of the Human Fovea→Cortex Systems with Intermittent and Modulated Light I Attenuation Characteristics with White and Colored Light". In: *Journal of the Optical Society of America* 48 (11 1958-11), p. 777. ISSN: 0030-3941. DOI: 10.1364/JOSA.48.000777.

[23] A. Capilla et al. "Steady-State Visual Evoked Potentials Can Be Explained by Temporal Superposition of Transient Event-Related Responses". In: *PLOS ONE* 6.1 (2011-01), pp. 1–15. DOI: 10.1371/journal.pone.0014543. URL: https://doi.org/10.1371/journal.pone.0014543.

[24] F. D. Russo et al. "Cortical sources of the early components of the visual evoked potential". In: *Human Brain Mapping* 15 (2 2002-02), pp. 95–111. ISSN: 10659471. DOI: 10.1002/hbm.10010. URL: https://onlinelibrary.wiley.com/doi/10.1002/hbm.10010.

[25] U. Themes. *Visual evoked potential*. Accessed: 2023-09-25. 2016-07. URL: https://entokey.com/visual-evoked-potential/.

[26] R. Näätänen et al. "The mismatch negativity (MMN) in basic research of central auditory processing: A review". In: *Clinical Neurophysiology* 118 (12 2007-12), pp. 2544–2590. ISSN: 13882457. DOI: 10.1016/j.clinph.2007.04.026. URL: https://linkinghub.elsevier.com/retrieve/pii/S1388245707001939.

[27] M. D. Vos et al. "P300 speller BCI with a mobile EEG system: Comparison to a traditional amplifier". In: *Journal of Neural Engineering* 11 (3 2014). ISSN: 17412552. DOI: 10.1088/1741-2560/11/3/036008.

[28] Y. Jia and C. W. Tyler. "Measurement of saccadic eye movements by electrooculography for simultaneous EEG recording". In: *Behavior Research Methods* 51 (5 2019-10), pp. 2139–2151. ISSN: 15543528. DOI: 10.3758/s13428-019-01280-8.

[29] *What are imaging phantoms?* Accessed: 2023-09-25. 2022-04. URL: https://www.nist.gov/physics/what-are-imaging-phantoms.

[30] *Pet-CT phantom*. Accessed: 2023-09-25. URL: https://capintec.com/product/pet-ct-phantom/.

[31] A. R. Marathe, A. J. Ries, and K. McDowell. "Sliding HDCA: Single-trial eeg classification to overcome and quantify temporal variability". In: *IEEE Transactions on Neural Systems and Rehabilitation Engineering* 22 (2 2014), pp. 201–211. ISSN: 15344320. DOI: 10.1109/TNSRE.2014.2304884.

[32] R. Leahy et al. "A study of dipole localization accuracy for MEG and EEG using a human skull phantom". In: *Electroencephalography and Clinical Neurophysiology* 107 (2 1998-04), pp. 159–173. ISSN: 00134694. DOI: 10.1016/S0013-4694(98)00057-1. URL: https://linkinghub.elsevier.com/retrieve/pii/S0013469498000571.

[33] *Methods for signal validation / EEG "Phantom heads"*. Accessed: 2023-09-25. 2016-02. URL: https://openbci.com/forum/index.php?p=2Fdiscussion2F6372Fmethods-for-signal-validation-eeg-phantom-heads.

[34] S. N. Wyckoff et al. "Validation of a wireless dry electrode system for electroencephalography". In: *Journal of NeuroEngineering and Rehabilitation* 12 (1 2015-12), p. 95. ISSN: 1743-0003. DOI: 10.1186/s12984-015-0089-2. URL: http://www.jneuroengrehab.com/content/12/1/95.

[35] S.-I. Choi and H.-J. Hwang. "Effects of Different Re-referencing Methods on Spontaneously Generated Ear-EEG". In: *Frontiers in Neuroscience* 13 (JUL 2019-08). ISSN: 1662-453X. DOI: 10.3389/fnins.2019.00822. URL: https://www.frontiersin.org/article/10.3389/fnins.2019.00822/full.

[36] N. Kaongoen and S. Jo. "An auditory P300-based brain-computer interface using Ear-EEG". In: vol. 2018-January. IEEE, 2018-01, pp. 1–4. ISBN: 978-1-5386-2574-3. DOI: 10.1109/IWW-BCI.2018.8311519. URL: http://ieeexplore.ieee.org/document/8311519/.

[37] H. Dong, P. M. Matthews, and Y. Guo. "A new soft material based in-the-ear EEG recording technique". In: IEEE, 2016-08, pp. 5709–5712. ISBN: 978-1-4577-0220-4. DOI: 10.1109/EMBC.2016.7592023. URL: http://ieeexplore.ieee.org/document/7592023/.

[38] K. B. Mikkelsen et al. "EEG Recorded from the Ear: Characterizing the Ear-EEG Method". In: *Frontiers in Neuroscience* 9 (NOV 2015-11). ISSN: 1662-453X. DOI: 10.3389/fnins.2015.00438. URL: http://journal.frontiersin.org/Article/10.3389/fnins.2015.00438/abstract.

[39] S. L. Kappel et al. "Dry-Contact Electrode Ear-EEG". In: *IEEE Transactions on Biomedical Engineering* 66 (1 2019-01), pp. 150–158. ISSN: 0018-9294. DOI: 10.1109/TBME.2018.2835778. URL: https://ieeexplore.ieee.org/document/8357918/.

[40] P. Kidmose et al. "A Study of Evoked Potentials From Ear-EEG". In: *IEEE Transactions on Biomedical Engineering* 60 (10 2013-10), pp. 2824–2830. ISSN: 0018-9294. DOI: 10.1109/TBME.2013.2264956. URL: http://ieeexplore.ieee.org/document/6521411/.

[41] P. Kidmose et al. "Ear-EEG from generic earpieces: A feasibility study". In: IEEE, 2013-07, pp. 543–546. ISBN: 978-1-4577-0216-7. DOI: 10.1109/EMBC.2013.6609557. URL: http://ieeexplore.ieee.org/document/6609557/.

[42] J. Lee et al. "A 0.8-V 82.9-μW In-Ear BCI Controller IC With 8.8 PEF EEG Instrumentation Amplifier and Wireless BAN Transceiver". In: *IEEE Journal of Solid-State Circuits* 54 (4 2019-04), pp. 1185–1195. ISSN: 0018-9200. DOI: 10.1109/JSSC.2018.2888845. URL: https://ieeexplore.ieee.org/document/8606233/.

[43] V. Goverdovsky et al. "In-Ear EEG From Viscoelastic Generic Earpieces: Robust and Unobtrusive 24/7 Monitoring". In: *IEEE Sensors Journal* 16 (1 2016-01), pp. 271–277. ISSN: 1530-437X. DOI: 10.1109/JSEN.2015.2471183. URL: http://ieeexplore.ieee.org/document/7217787/.

[44] J. H. Lee et al. "CNT/PDMS-based canal-typed ear electrodes for inconspicuous EEG recording". In: *Journal of Neural Engineering* 11 (4 2014-08), p. 046014. ISSN: 1741-2560. DOI: 10.1088/1741-2560/11/4/046014. URL: https://iopscience.iop.org/article/10.1088/1741-2560/11/4/046014.

[45] Y. R. Tabar et al. "At-home sleep monitoring using generic ear-EEG". In: *Frontiers in Neuroscience* 17 (2023-02). ISSN: 1662453X. DOI: 10.3389/fnins.2023.987578.

[46] S. Baillet et al. *Evaluation of inverse methods and head models for EEG source localization using a human skull phantom*. 2001, pp. 77–96. URL: www.iop.org/Journals/pbPII:S0031-9155.

[47] W. D. Hairston, G. A. Slipher, and A. B. Yu. *Ballistic gelatin as a putative substrate for EEG phantom devices*. 2016. DOI: 10.48550/ARXIV.1609.07691. URL: https://arxiv.org/abs/1609.07691.

[48] A. Y. Owda and A. J. Casson. "Investigating Gelatine Based Head Phantoms for Electroencephalography Compared to Electrical and Ex Vivo Porcine Skin Models". In: *IEEE Access* 9 (2021), pp. 96722–96738. ISSN: 21693536. DOI: 10.1109/ACCESS.2021.3095220.

[49] A. Velcescu et al. "Flexible 3D-printed EEG electrodes". In: *Sensors (Switzerland)* 19 (7 2019-04). ISSN: 14248220. DOI: 10.3390/s19071650.

[50] N. Richer et al. "Adding neck muscle activity to a head phantom device to validate mobile EEG muscle and motion artifact removal". In: *2019 9th International IEEE/EMBS Conference on Neural Engineering (NER)*. 2019, pp. 275–278. DOI: 10.1109/NER.2019.8716959.

[51] A. S. Oliveira et al. "Induction and separation of motion artifacts in EEG data using a mobile phantom head device". In: *Journal of Neural Engineering* 13 (3 2016-05). ISSN: 17412552. DOI: 10.1088/1741-2560/13/3/036014.

[52] A. D. Nordin, W. D. Hairston, and D. P. Ferris. "Dual-electrode motion artifact cancellation for mobile electroencephalography". In: *Journal of Neural Engineering* 15 (5 2018-08). ISSN: 17412552. DOI: 10.1088/1741-2552/aad7d7.

[53] M. E. Chowdhury et al. "Effects of the phantom shape on the gradient artefact of electroencephalography (EEG) data in simultaneous EEG-fMRI". In: *Applied Sciences (Switzerland)* 8 (10 2018-10). ISSN: 20763417. DOI: 10.3390/app8101969.

[54] A. Hunold, R. Machts, and J. Haueisen. "Head phantoms for bioelectromagnetic applications: a material study". In: *BioMedical Engineering Online* 19 (1 2020-12). ISSN: 1475925X. DOI: 10.1186/s12938-020-00830-y.

[55] W. E. Audette and L. V. Allen. *Design and Demonstration of a Head Phantom for Testing of Electroencephalography (EEG) Equipment Hearing Protection View project DPOAE Level and Phase Mapping View project*. DOI: 10.13140/RG.2.2.12078.25920. URL: https://www.researchgate.net/publication/339697951.

[56] T. J. Collier et al. "Creation of a human head phantom for testing of electroencephalography equipment and techniques". In: *IEEE Transactions on Biomedical Engineering* 59 (9 2012), pp. 2628–2634. ISSN: 00189294. DOI: 10.1109/TBME.2012.2207434.

[57] S. Wood, T. Martins, and T. S. Ibrahim. "How to design and construct a 3D-printed human head phantom". In: *Journal of 3D Printing in Medicine* 3 (3 2019-08), pp. 119–125. ISSN: 2059-4755. DOI: 10.2217/3dp-2019-0016.

[58] D. Kuratko et al. "Forward Model of Rat Electroencephalogram: Comparative Study of Numerical Simulations With Measurements on Rat Head Phantoms". In: *IEEE Access* 10 (2022), pp. 92023–92035. ISSN: 21693536. DOI: 10.1109/ACCESS.2022.3202206.

[59] J. Zhang et al. "A novel 3D-printed head phantom with anatomically realistic geometry and continuously varying skull resistivity distribution for electrical impedance tomography". In: *Scientific Reports* 7 (1 2017-12). ISSN: 20452322. DOI: 10.1038/s41598-017-05006-8.

[60] J. W. Peirce. "Generating stimuli for neuroscience using PsychoPy". In: *Frontiers in Neuroinformatics* 2 (JAN 2008-01). ISSN: 16625196. DOI: 10.3389/neuro.11.010.2008. URL: http://journal.frontiersin.org/article/10.3389/neuro.11.010.2008/abstract.

[61] M. R. Ghods et al. "Multimodal-Multisensory Experiments Internal and external mechanisms of task selection View project choice reaching trajectory analysis View project Multimodal-Multisensory Experiments". In: (2020). DOI: 10.20944/preprints202008.0614.v1. URL: https://www.researchgate.net/publication/343927712.

[62] J. Mladenovic. *Event triggering and data synchronization with mobile EEG fully mobile EEG devices*. Accessed: 2023-09-25. 2023-07. URL: https://mbraintrain.com/event-triggering-and-data-synchronization-with-mobile-eeg/.

[63] Bogdan. *Setting up precise sound stimulation with psychopy*. Accessed: 2023-09-25. 2023-07. URL: https://mbraintrain.com/how-to-set-up-precise-sound-stimulation-with-psychopy-and-pylsl.

[64] D. Bridges et al. "The timing mega-study: comparing a range of experiment generators, both lab-based and online". In: *PeerJ* 8 (2020-07), e9414. ISSN: 2167-8359. DOI: 10.7717/peerj.9414. URL: https://peerj.com/articles/9414.

[65] *Can PsychoPy deliver millisecond precision*. Accessed: 2023-09-25. 2023-07. URL: https://www.psychopy.org/general/timing/millisecondPrecision.

[66] *Mobile EEG - smarting mobi*. Accessed: 2023-09-25. 2022-11. URL: https://mbraintrain.com/smarting-mobi/.

[67] D. V. M. Bishop and M. J. Hardiman. "Measurement of mismatch negativity in individuals: A study using single-trial analysis". In: *Psychophysiology* 47 (4 2010-02), pp. 697–705. ISSN: 00485772. DOI: 10.1111/j.1469-8986.2009.00970.x. URL: https://onlinelibrary.wiley.com/doi/10.1111/j.1469-8986.2009.00970.x.

[68] A. Saleem, L. Frormann, and A. Soever. "Fabrication of extrinsically conductive silicone rubbers with high elasticity and analysis of their mechanical and electrical characteristics". In: *Polymers* 2 (3 2010-09), pp. 200–210. ISSN: 20734360. DOI: 10.3390/polym2030200.

[69] Blorgggg and Instructables. *SILC circuits: High performance conductive silicone*. Accessed: 2023-09-25. 2018-04. URL: https://www.instructables.com/Silc-Circuits-High-Performance-Conductive-Silicone/.

[70] *OpenBCI Cyton*. Accessed: 2023-09-25. URL: https://shop.openbci.com/products/cyton-biosensing-board-8-channel.

[71] *OpenBCI EEG Setup*. Accessed: 2023-09-25. 2021-11. URL: https://docs.openbci.com/GettingStarted/Biosensing-Setups/EEGSetup/.

[72] T. Vanderwal et al. "Inscapes : A movie paradigm to improve compliance in functional magnetic resonance imaging". In: *NeuroImage* 122 (2015-11), pp. 222–232. ISSN: 10538119. DOI: 10.1016/j.neuroimage.2015.07.069. URL: https://linkinghub.elsevier.com/retrieve/pii/S1053811915006898.

A

Main Reviewed Literature Summary

Table A.1: Summary of in-ear-EEG articles

	Electrodes	**Fitting**	**Subjects**	**Tested paradigms***	**"Truly in-ear" [41]**
[6]	Wet Ag/AgCl	Custom	2	Alpha Block, ASSR, P300	
[40]	Wet Ag	Custom	8	ASSR, SSVEP(6) AEP(3), VEP(3)	**X**
[44]	Dry CNT/PDMS	Generic	6	Alpha block, ASSR, AEP N100	
[38]	Wet	Custom	13	ASSR, Alpha Block(10), AEP, MMN	
[43]	Silver-plated conductive cloth	Generic	1	ASSR, SSVEP, VEP	
[37]	Dry silvered glass silicone	Generic	2	Alpha Block	
[42]	Dry	Custom	9	ASSR, EOG blinks	**X**
[39]	Dry Ti coated in IrO_2	Custom	12	SSVEP, ASSR, AEP, MMN, Alpha Block	
[7]	Dry Ag	Generic	3	EOG Blinks, Alpha Block, ASSR	

*Numbers between parentheses indicate that certain paradigms were tested for a subpopulation of the total Subjects

Table A.2: Summary of main EEG phantoms articles

	Prototype description	**Signal source**	**Testing**
[4]	Molded full head made of BG and NaCl doped	Two embedded electrodes	Acquisition of artifical pre-recorded EEG data
[48]	Cuboid shaped BG	One embedded Ag/AgCl electrode	Impedance measurements for different NaCl percentages
[49]	Cuboid shaped BG	One embedded Ag/AgCl electrode	Contact impedance measurements and noise floor RMS for novel electrodes
[59]	Four-layered hollow head made of ABS doped with carbon black	N/A	Electrical impedance tomography simulations
[53]	Molded full head made of agar-NaCl mix	N/A	EEG-fMRI induced gradient artifacts
[51]	Molded full head made of dental plaster, sodium propionate and water	Eight exposed wire tips	Study of motion artifacts in simulated EEG data
[55]	Hollow injection molded full head made with doped polypropylene	Eight button-head screws	Acquisition of artificial and pre-recorded EEG data
[58]	Rat head made of agar-NaCl mix	Five coaxial cable dipoles	Acquisition of artificial and pre-recorded EEG data

B

EaR-P Lab - GUI Overview and Paradigm Functioning

An explanation of what is provided by each button will ensue.

General Recording

Shows a white cross centered on the screen (Figure B.1), for the selected duration of time. This option was implemented, for instance, to record resting state EEG or any custom test not readily provided by default in **EaR-P Lab**.

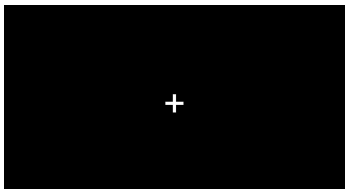

Figure B.1: Focus cross utilized by the "General Recording", "ASSR" and "Alpha Block" paradigms

ASSR

Shows the same focus as Figure B.1, while playing an adequate sound file for an ASSR test. The duration of the experiment is the same as the duration of the sound file.

SSVEP

The "SSVEP" button runs a test where the target in Figure B.2 is shown. The target consists of a radial black and white pattern centered on a black background, with a diameter that is equal to the screen height. The target will flicker at a rate that equals the chosen frequency and is changeable in the **"Settings"** window for a modifiable duration.

Alpha Block

This paradigm starts with onscreen instructions for the subject to press "SPACE" and close its eyes. After a specified amount of time, there is a transition phase where an artificially generated voice will warn the subject to open its eyes and look at the cross for

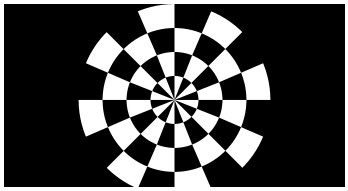

Figure B.2: Target used for the "SSVEP" experiment in **EaR-P Lab**

the same time as before. These instructions repeat one more time so in total there are two phases with eyes closed and two with eyes open, that are alternated between them. At the beginning of each phase, the specific markers seen in Figure B.3 are also sent through LSL to LabRecorder.

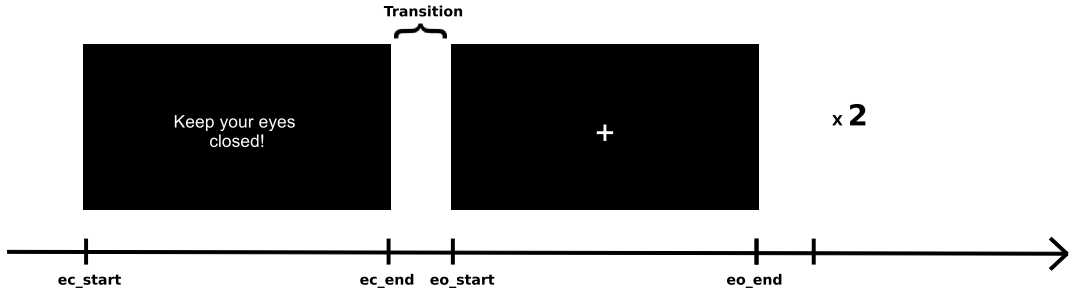

Figure B.3: "Alpha Block" paradigm functioning, with the markers that are sent at the start and end of each phase

AEP

The "AEP" button starts a sequence of discrete auditory stimuli, with the native duration of the respective sound file or a chosen duration if a PsychoPy default sound is used instead. The stimuli are separated by an adjustable ISI, and each time the stimuli start the "aep" marker is sent to LabRecorder. In order to keep the subject engaged (to help avoid drowsiness while the test is running), the *Inscapes* animation is also played in the background, as shown in Figure B.4. This animation was originally crafted to maintain children "engaged while minimizing the certain aspects of cognitive processing" [72]. The original sound was removed from the animation, and it will loop back to the beginning until the test is finished.

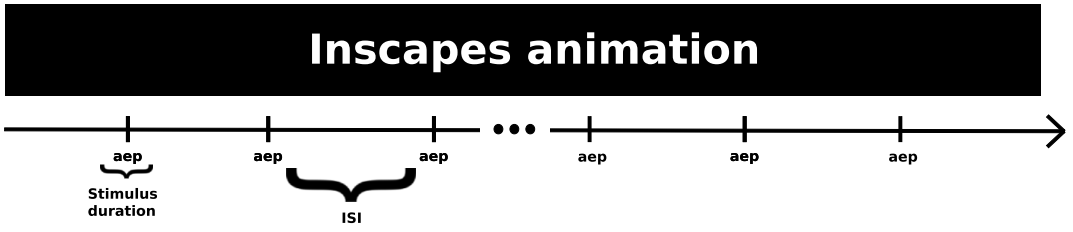

Figure B.4: "AEP" sequence featured in **EaR-P Lab**

VEP

On to the "VEP", the programmed sequence is similar to its auditory counterpart, with the default option of a shape being shown on screen for a certain amount of time and with an interval between them. For this paradigm, some other custom stimuli were added, like the option to do a flash type stimuli, where the screen is black and quickly turns white for the specified duration, and also two kinds of visual tasks with either a checkerboard or a dartboard (as shown in Figure B.5) target that can be used in onset-offset or pattern reversal tasks (if the associated ISI is set to zero). Every time the onscreen stimulus changes to a new one, the "vep" marker is sent to LabRecorder.

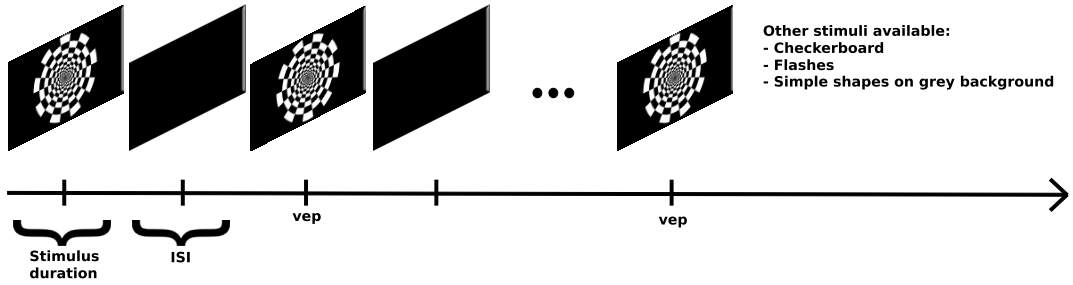

Figure B.5: "VEP" button paradigm structure and options

Oddball Paradigms

Both the "Oddball" buttons start a sequence of twenty standard stimuli, followed by a randomly generated sequence of both standard and oddball events, as portrayed in Figure B.6. The oddball events appear at a **random chance of 20%**, which, for the time being, is hard coded into the platform. For the auditory version of the oddballs, akin to the regular "AEP" sequence, the *Inscapes* movie is played in the background. Additionally, two rules are also implemented during these paradigms, this being that there can't be a succession of two oddballs in a row (so there is always at least one standard stimuli before and after each oddball) and that in the case there is a part of the sequence made up of eight standard events in a row (excluding the first twenty events), the next event is compulsorily an oddball stimulus. The "standard", "target", and "response" markers are utilized in sync with the presented stimulus, with the latter being sent in case the subject presses "SPACE" in response to an oddball event.

EOG

The "EOG" paradigm is split into two parts: eye blinks and saccades. During the eye blinks phase, the subject is prompted to do a total of four eye blinks, alternated between a normal or "soft" blink and an intentional or "hard" blink. For each blink, the subject has a three second window that starts once "SPACE" is pressed, according to the instructions. As shown in Figure B.3, the "soft_blink_start", "soft_blink_end", "hard_blink_start" and "hard_blink_end" static markers are used to limit each blink window.

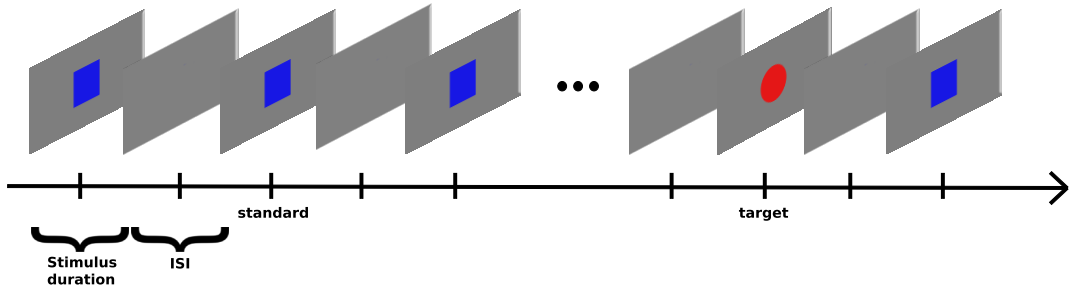

Figure B.6: "Oddball" type paradigms sequence - example of visual oddballs

The next part of this paradigm is a "follow-the-dot"test, shown in Figure B.7. Here, a red dot starting in the center of the screen disappears and reappears at one of the four main cardinal directions for the subject to follow to test for eye saccade amplitudes and profiles. The dot jumps a distance equal to half the screen height for each saccade, is held in that position for a specified duration, and returns to the middle during the ISI period. The appropriate marker stating "top", "right", "left" or "bottom" is sent when the dot moves to the respective location. The static markers "follow_start" and "follow_end" also limit this part of the coded "EOG" paradigm.

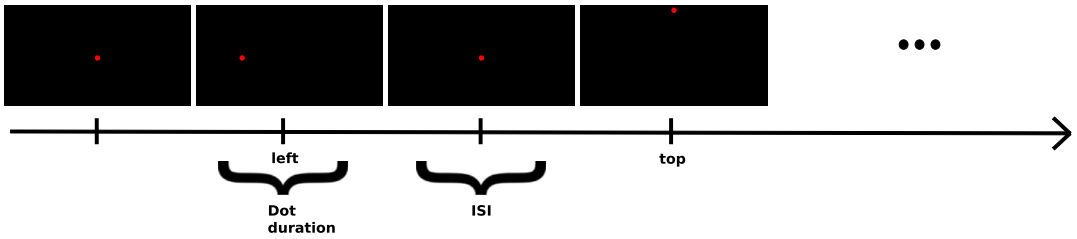

Figure B.7: "Follow-the-dot" phase of the "EOG" paradigm in **EaR-P Lab**

Settings Menu

The "Settings" button opens up a secondary window (Figure B.8) with different boxes and options that control what happens and is shown in each paradigm mentioned above. These settings range from the type of stimuli, frequency of the SSVEP, testing durations, total trial number for the AEP/VEP paradigms, how many oddballs until the oddball type tasks are complete, and how many repetitions for each saccade in the EOG test. Additionally, there is some information about how to proceed to add more stimuli to **EaR-P Lab**, a disclaimer about the ISI for auditory paradigms, and a button to automatically measure the angle of the saccades in the EOG task dependent on the dimensions of the stimuli presentation monitor used and the subject's distance to said screen.

Markers Menu

Like the "Settings" menu, here a secondary window (Figure B.9) is presented with

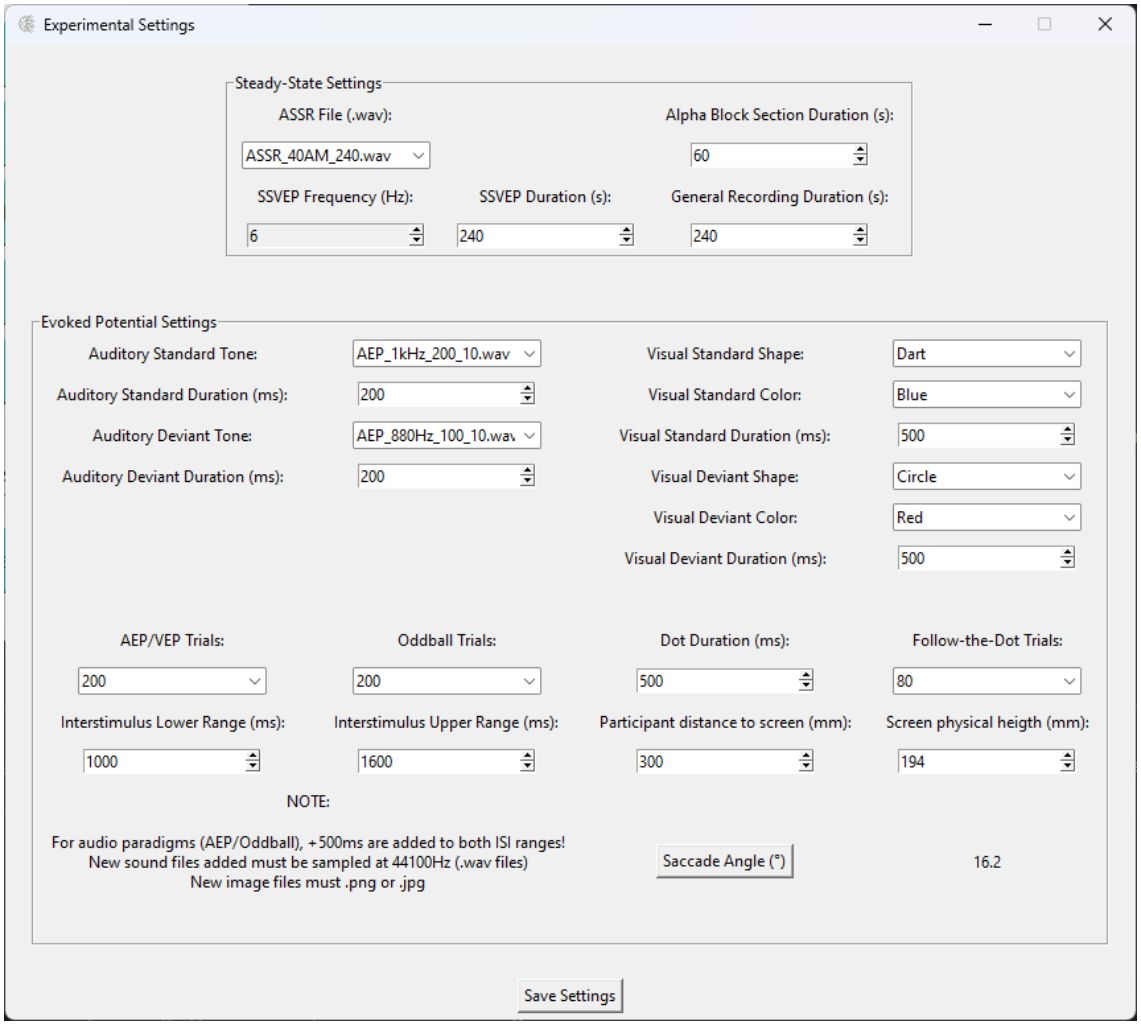

Figure B.8: **EaR-P Lab** - Settings Menu

text boxes about each paradigm so that the user can set its delimiting markers for each experiment. This feature is useful, for instance, to record the same type of paradigm within the same *.xdf* file and to help with accurate data parsing. At the bottom of the window, there is information about the static (meaning non-changeable) markers used by **EaR-P Lab**, as shown in the above paragraphs.

Latency Issues

To the best of our knowledge, when using **EaR-P Lab** with the mbt **Smarting mobi** amplifier at least, recording multiple ERP blocks in the same *.xdf* file with LabRecorder results in a cascading effect and latency deterioration exemplified in Figure B.10. This was checked by using the mbt Delay/Jitter (DJ) box (compatible with the used amplifier), which is a device with an audio input, output, and photodiode sensor that allowed us to test the marker synchronization with the audio and visual stimuli. The device was placed at the latest stage possible in the audio delivery setup, with the photodiode centered and

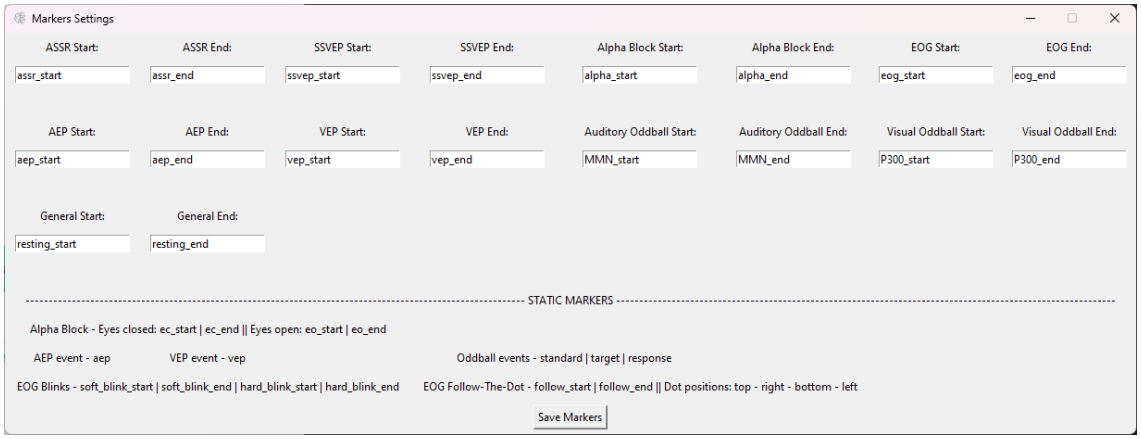

Figure B.9: **EaR-P Lab** - Markers Menu

30cm away pointing to the center of the screen.

The boxplot in Figure B.10 prompted us to recommend having a new separate *.xdf* file for the AEP, VEP, EOG, and oddball type paradigms, as it was discovered through trial and error that resetting the mbt data stream fixed the issue but also made it impossible to record all paradigms (or different subjects), on the same *.xdf* file, concerning ERP related paradigms.

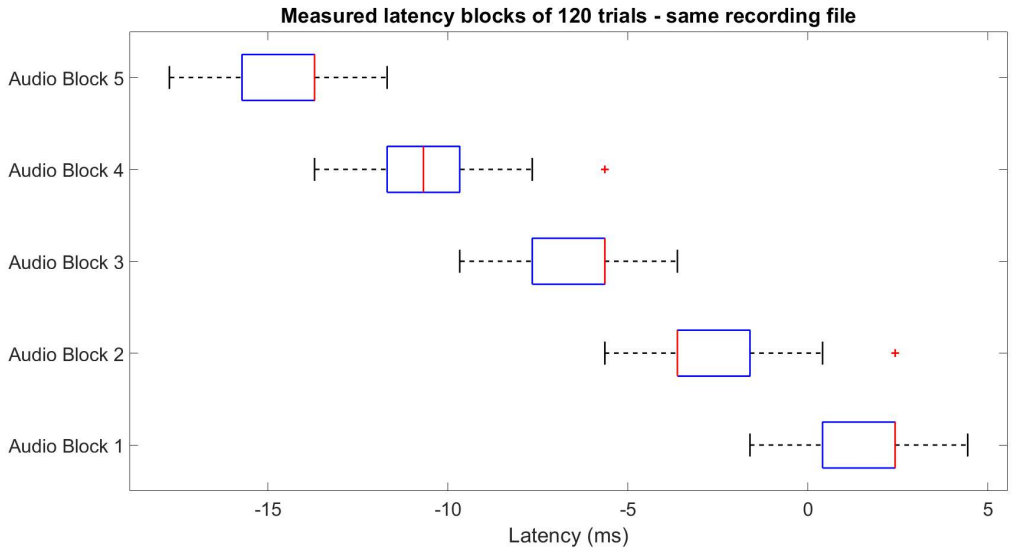

Figure B.10: Escalating latency when recording multiple ERP blocks on the same file, exemplified for auditory stimuli - a similar effect happens for visual stimuli

C

Ear-EEG Phantom Dimensions and Material Characterization

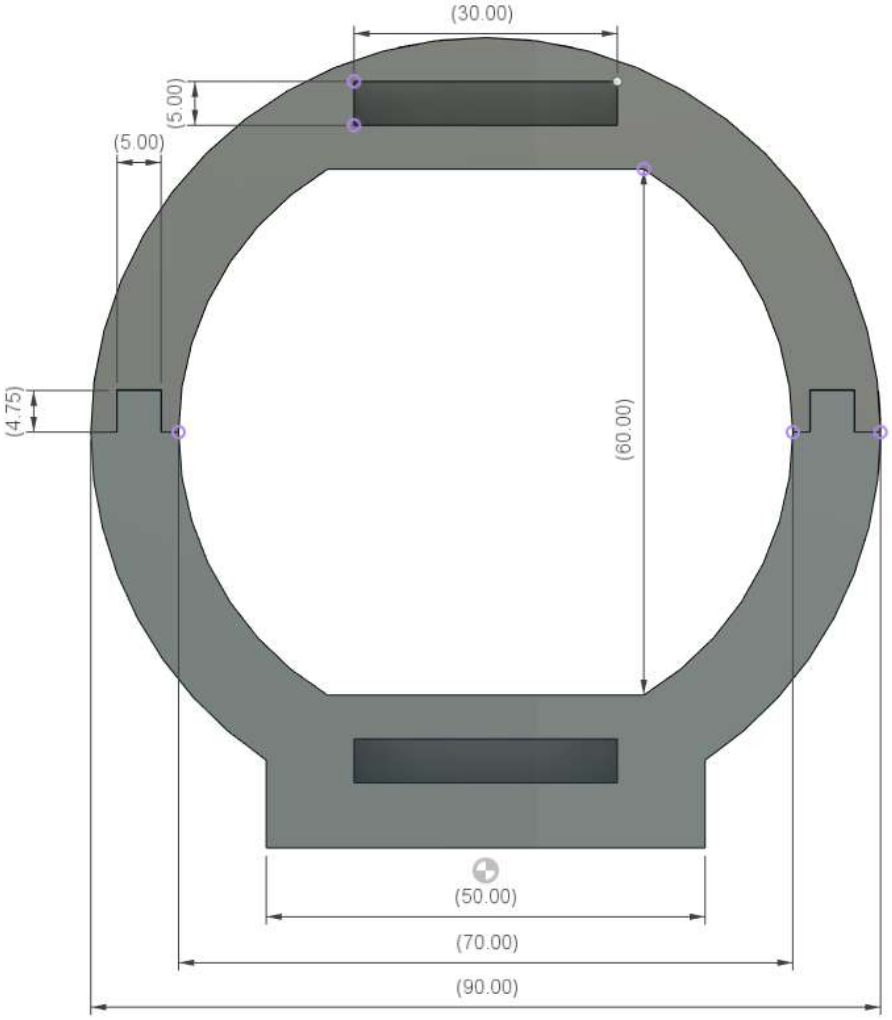

Figure C.1: Proposed Ear-EEG phantom prototype dimensions - Side View

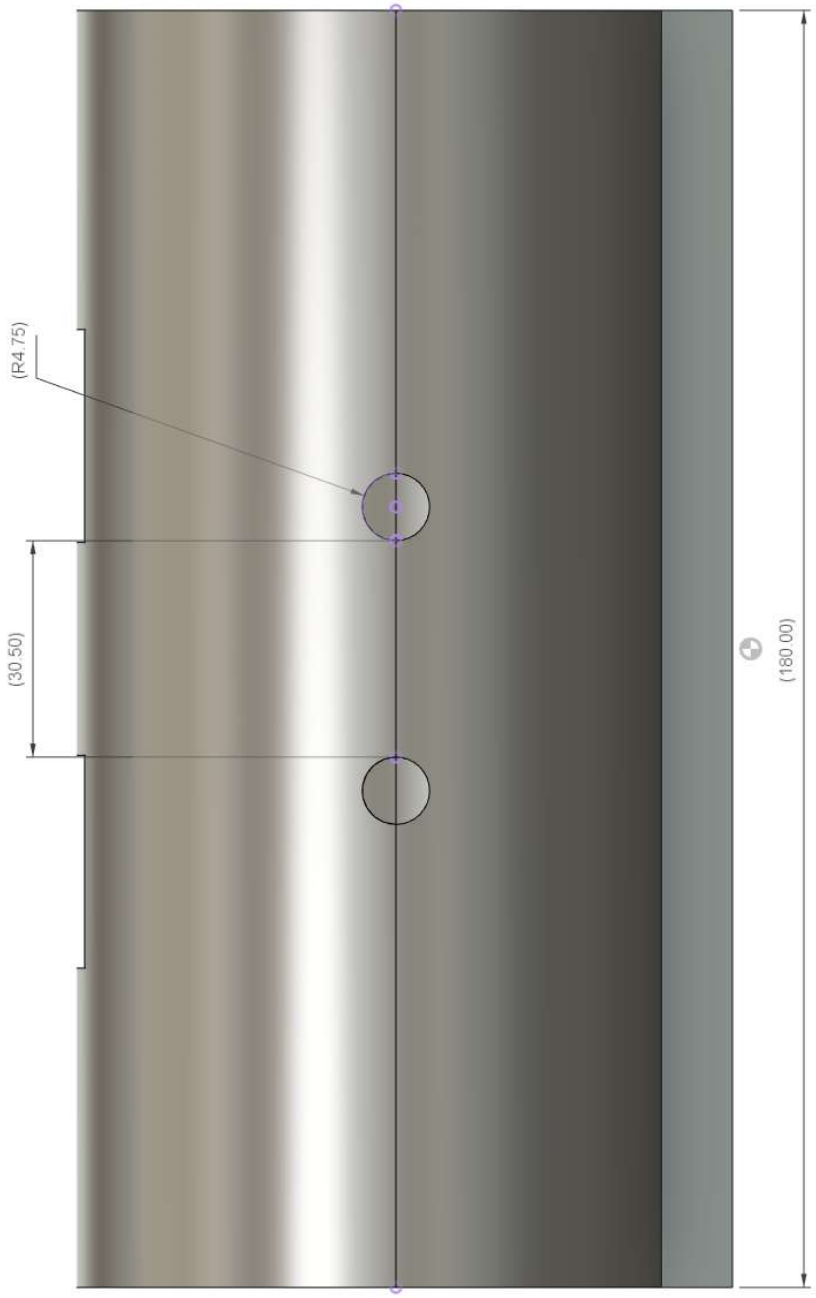

Figure C.2: Proposed Ear-EEG phantom prototype dimensions - Front View

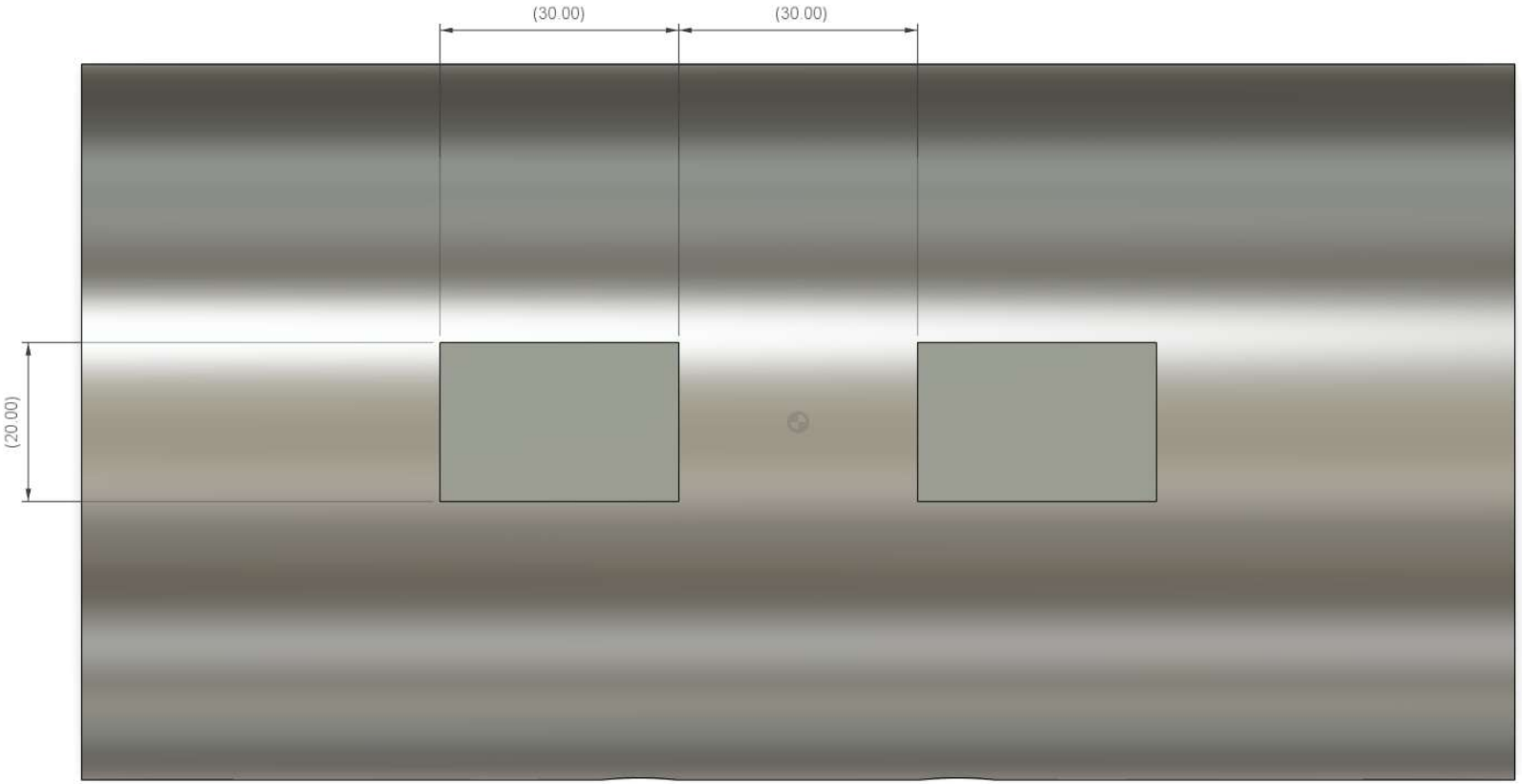

Figure C.3: Proposed Ear-EEG phantom prototype dimensions - Top View

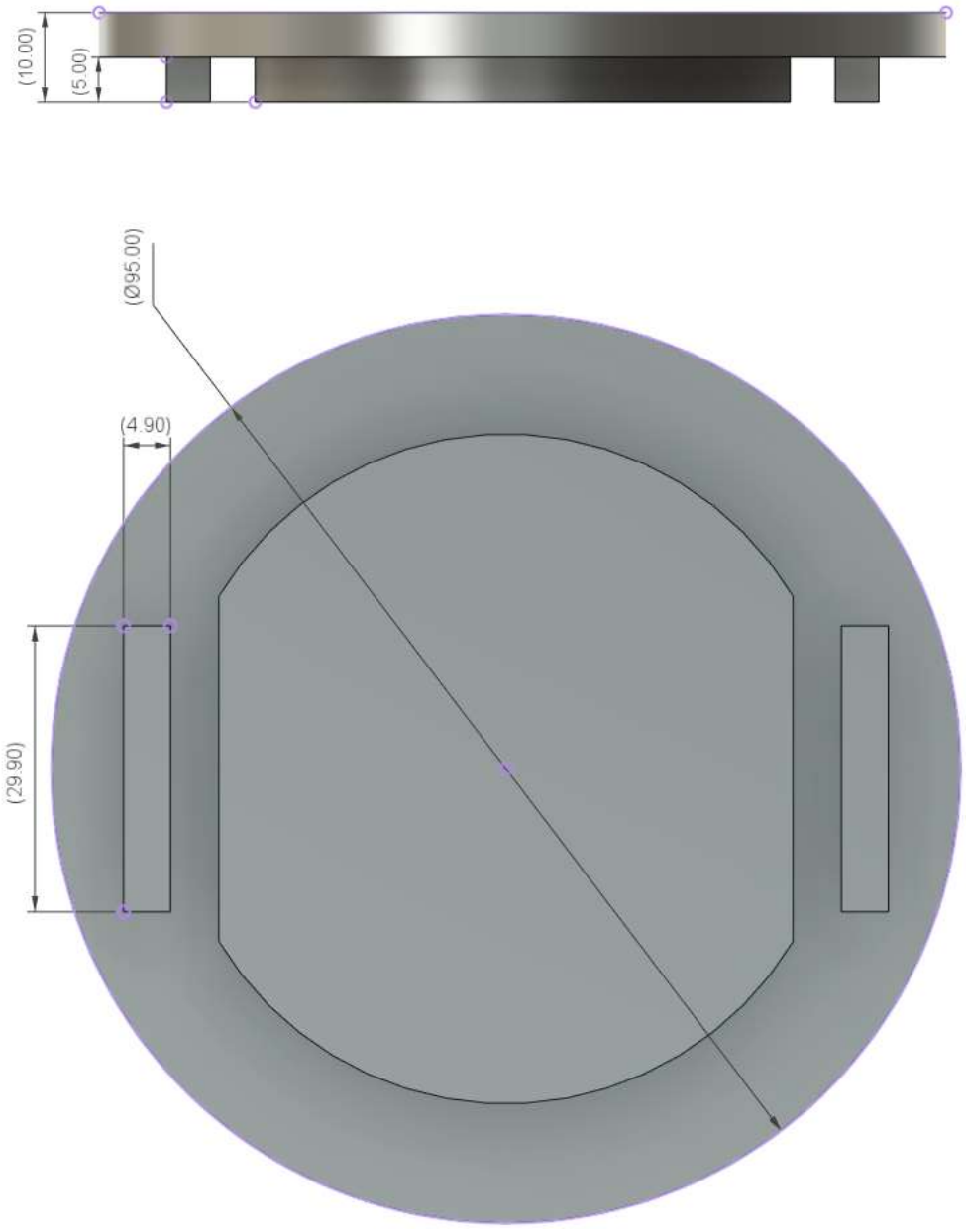

(b) Side View

(a) Front View

Figure C.4: Proposed Ear-EEG phantom prototype dimensions - Lids

C.0.1 Material characterization

For reference, the phantom materials were also characterized by their electrical conductivity and Electrochemical Impedance Spectroscopy (EIS) impedance over frequency measurements. Conductivity was assessed according to Equation C.1.

$$\begin{cases} \rho = R\frac{A}{L} \\ \sigma = \frac{1}{\rho} \end{cases} \Rightarrow \sigma = \frac{L}{R \times A} \tag{C.1}$$

Where ρ is the material resistivity, R is the measured resistance, A is the area of the cross-section of the sample, and L is the sample's length. σ is the material's conductivity as the inverse of resistivity. Fine strips (30x10x2mm) of each material were cut and sent to an external lab within Trinity College. Each strip was painted with silver paint at the edges and remeasured. The traditional two-wire method took the resistance across the sample, once on each side of the strip, taking the average as the resistance. By substitution in Equation C.1, the conductivity values for each material are listed in Table C.1.

Table C.1: Electrical conductivity, in Siemens per meter, for samples of each material proposed for the phantom - no conductivity was obtained from the 0.5% CF sample

	Agar	**BG**	**CF 0.5%**	**CF 1.0%**
Conductivity [S/m]	0.309	0.918	-	14.035

EIS data was taken from samples (30x20x5mm) with a manually embedded electrode that were again outsourced to another lab. The fitting model is unknown, and it should be noted that due to scheduling limitations, the BG sample was taken a significant time after the sample was made, with the agar sample deteriorating while waiting, results for the BG may not be accurate. In Figure C.5, the Bode plots for BG and CF (1%) are shown.

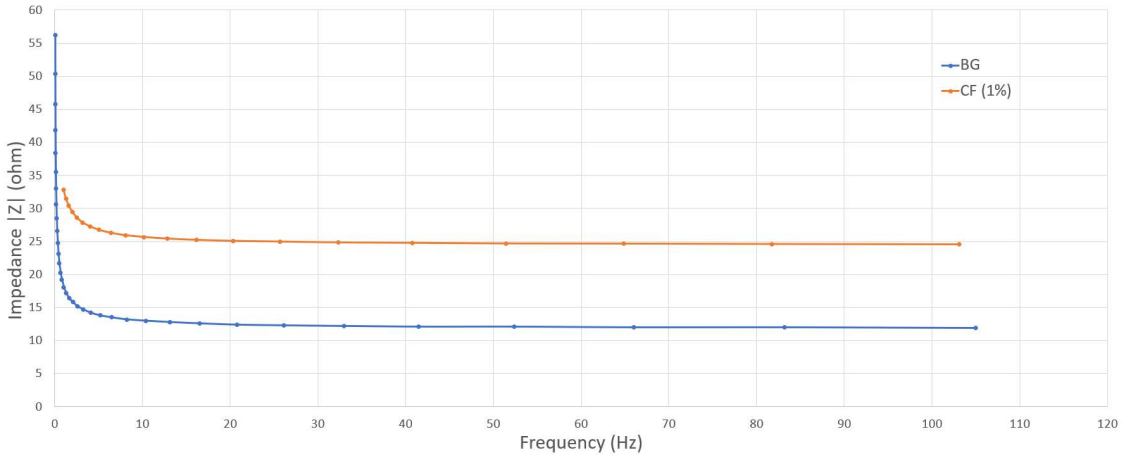

Figure C.5: Bode plots (0-100 Hz) of the BG **(blue)** and CF (1%) **(orange)** samples

D

Control and Ear-EEG Results

Table D.1: Discard ratios (over a total of five subjects) for each ear electrode, based on visual inspection of ASSR and EOG responses - electrodes marked with a * weren't physically present on one of the subject's earpieces

Wet Ear-EEG

EL1	**EL2**	**EL3**	**EL4**	**EL5**	**EL6**	**EL7**	**EL8**
0.2	0.4	0.0	0.2	0.0	0.0	0.0	0.0
ER1	**ER2***	**ER3**	**ER4**	**ER5**	**ER6**	**ER7**	**ER8**
0.2	0.2	0.0	0.0	0.0	0.0	0.0	0.0

Dry Ear-EEG

EL1	**EL2**	**EL3**	**EL4**	**EL5**	**EL6**	**EL7**	**EL8**
0.8	0.8	0.8	0.4	0.6	0.6	0.0	0.0
ER1	**ER2***	**ER3**	**ER4**	**ER5**	**ER6**	**ER7**	**ER8**
0.8	0.6	0.4	0.6	0.6	0.6	0.2	0.0

D.1 Control/validation EEG results

Table D.2: Control Group (n = 5) - Cz referenced - ASSR, SSVEP, Alpha Modulation SNR (dB) and EOG Blinks (hard/soft) ratios - omitted values were deemed not significant

	F3	**F4**	**C3**	**C4**	**P3**	**P4**
ASSR	2.4 ± 0.5	2.4 ± 0.6	2.3 ± 0.7	1.5 ± 0.5	8.7 ± 1.1	9.9 ± 1.4
SSVEP	7.4 ± 3.3	7.5 ± 3.2	5.7 ± 2.9	6.6 ± 3.1	9.4 ± 2.8	9.6 ± 3.0
α Mod.	2.8 ± 2.0	2.6 ± 1.9	2.5 ± 1.8	3.1 ± 2.3	4.5 ± 1.9	5.6 ± 2.4
H/S Blink Ratio	2.6	1.7	1.2	1.1	1.5	1.8

	T7	**T8**	**Fz**	**Pz**	**Oz**
ASSR	2.6 ± 0.5	4.7 ± 0.5	6.6 ± 1.1	9.4 ± 1.3	8.3 ± 1.0
SSVEP	7.0 ± 2.7	7.5 ± 2.8	7.1 ± 2.6	11.3 ± 2.9	11.0 ± 2.5
α Mod.	3.2 ± 1.7	3.7 ± 1.7	3.6 ± 2.1	4.7 ± 2.3	6.1 ± 1.9
H/S Blink Ratio	3.3	2.5	1.8	1.6	1.7

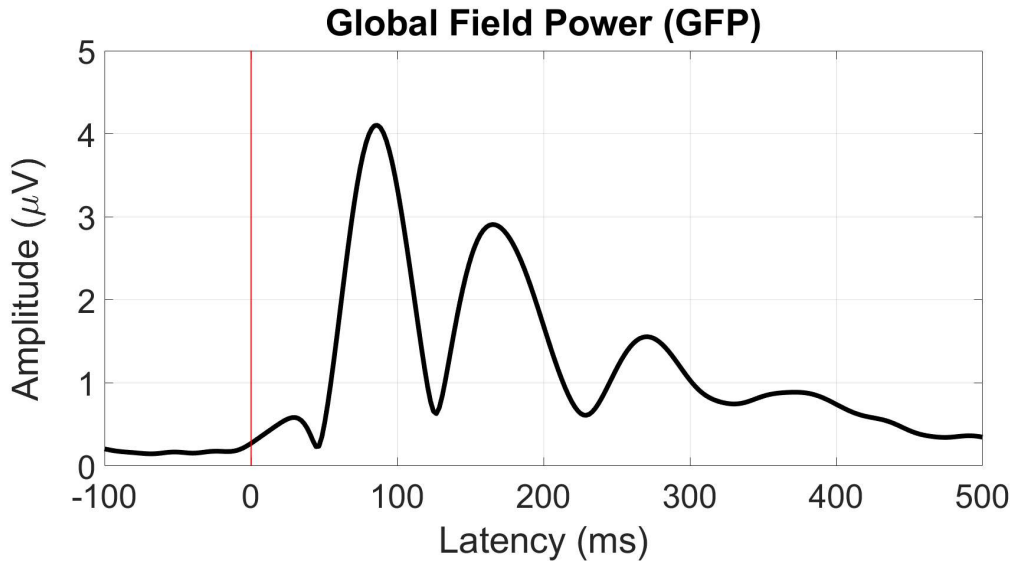

Figure D.1: Global Field Power (GFP) (Cz referenced) for the control AEP paradigm

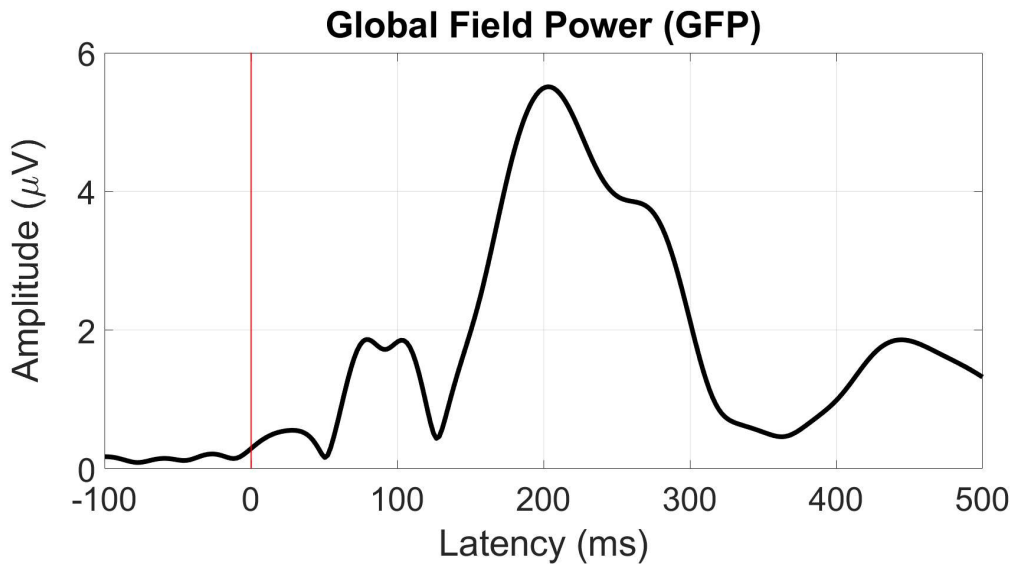

Figure D.2: Global field power (GFP) - Cz referenced for the control (n = 5) VEP paradigm

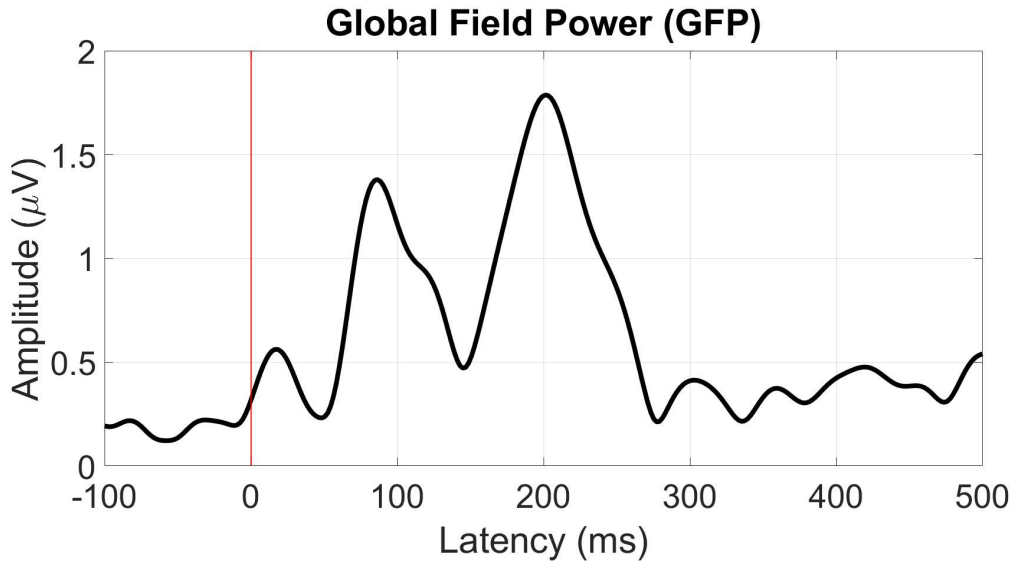

Figure D.3: Global field power (GFP) - Cz referenced for the control (n = 5) MMN paradigm

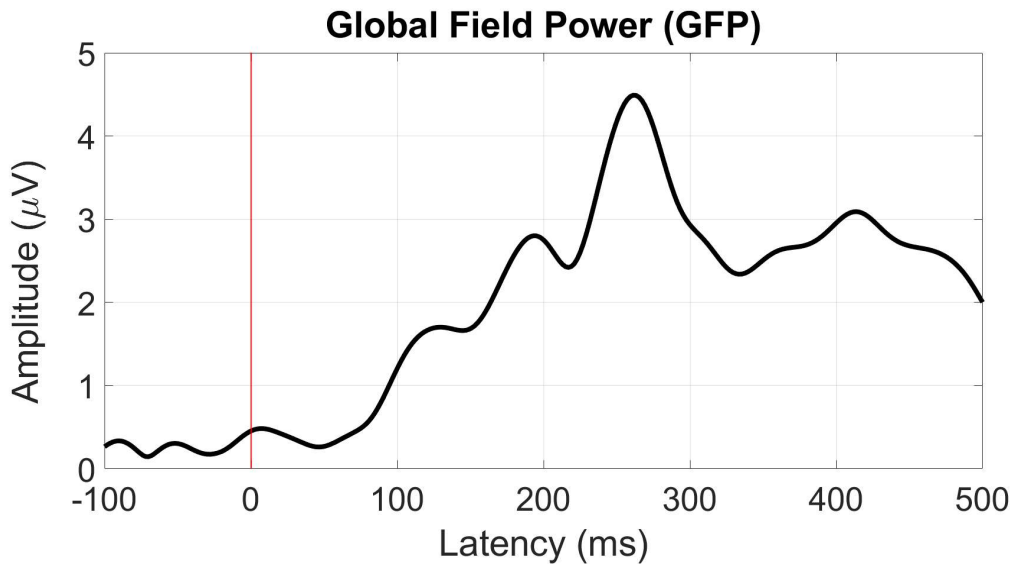

Figure D.4: Global field power (GFP) - Cz referenced for the control (n = 5) P300 paradigm

D.2 Ear-EEG results

Table D.3: Ear-EEG ASSR SNR (dB) for a Cz, T8, and ER3 references across scalp, left ear, and right ear (ordered top to bottom) electrodes for wet (n = 5) and dry (n = 1) electrode settings - omitted values were deemed not significant, based on an f-test ($p < 0.05$)

	C3	**C4**	**T7**	**T8**	**Fz**	**Cz**	**Pz**	**Oz**
					Wet Ear-EEG			
Cz	-	3.4 ± 0.7	1.6 ± 0.4	1.9 ± 0.5	3.9 ± 0.9	X	9.7 ± 1.3	8.8 ± 1.0
					Dry Ear-EEG			
Cz	-	-	3.5 ± 0.8	6.7 ± 1.0	7.8 ± 1.7	X	10.8 ± 1.5	11.2 ± 1.7

	EL1	**EL2**	**EL3**	**EL4**	**EL5**	**EL6**	**EL7**	**EL8**
					Wet Ear-EEG			
Cz	9.3 ± 1.0	8.9 ± 1.0	8.9 ± 1.0	8.6 ± 0.9	8.7 ± 0.9	7.7 ± 0.9	8.4 ± 0.9	8.0 ± 0.9
T8	3.9 ± 0.6	2.4 ± 0.5	3.9 ± 0.6	2.7 ± 0.5	2.5 ± 0.5	2.1 ± 0.5	2.2 ± 0.5	2.1 ± 0.5
ER3	1.1 ± 0.5	1.2 ± 0.5	1.1 ± 0.5	1.1 ± 0.5	1.4 ± 0.4	1.8 ± 0.4	1.8 ± 0.4	1.7 ± 0.4
					Dry Ear			
Cz	X	7.5 ± 1.2	X	6.6 ± 1.0	7.0 ± 1.1	7.4 ± 1.2	7.7 ± 1.2	7.4 ± 1.2
T8	X	3.2 ± 0.8	X	1.9 ± 0.7	2.8 ± 0.7	2.9 ± 0.8	2.8 ± 0.8	2.6 ± 0.8
ER3	X	-	X	-	-	-	-	-

	ER1	**ER2**	**ER3**	**ER4**	**ER5**	**ER6**	**ER7**	**ER8**
					Wet Ear-EEG			
Cz	6.2 ± 0.7	5.9 ± 0.7	6.2 ± 0.7	6.2 ± 0.7	6.6 ± 0.7	7.9 ± 0.8	8.2 ± 0.9	7.9 ± +0.8
T8	3.1 ± 0.5	2.6 ± 0.5	2.9 ± 0.5	2.8 ± 0.5	2.0 ± 0.5	1.9 ± 0.5	2.0 ± 0.5	2.1 ± 0.5
ER3	3.4 ± 0.5	1.2 ± 0.5	X	6.5 ± 0.8	5.1 ± 0.7	3.4 ± 0.6	3.7 ± 0.5	3.3 ± 0.6
					Dry Ear-EEG			
Cz	4.9 ± 1.0	4.7 ± 1.0	6.8 ± 1.1	4.2 ± 1.0	8.2 ± 1.2	8.8 ± 1.3	8.6 ± 1.3	8.2 ± 1.2
T8	3.1 ± 0.8	2.9 ± 0.9	2.3 ± 0.7	3.4 ± 0.9	3.7 ± 0.9	3.5 ± 0.8	2.9 ± 0.8	2.6 ± 0.8
ER3	2.4 ± 0.9	2.6 ± 0. 8	X	3.7 ± 1.0	-	-	1.6 ± 0.7	1.5 ± 0.7

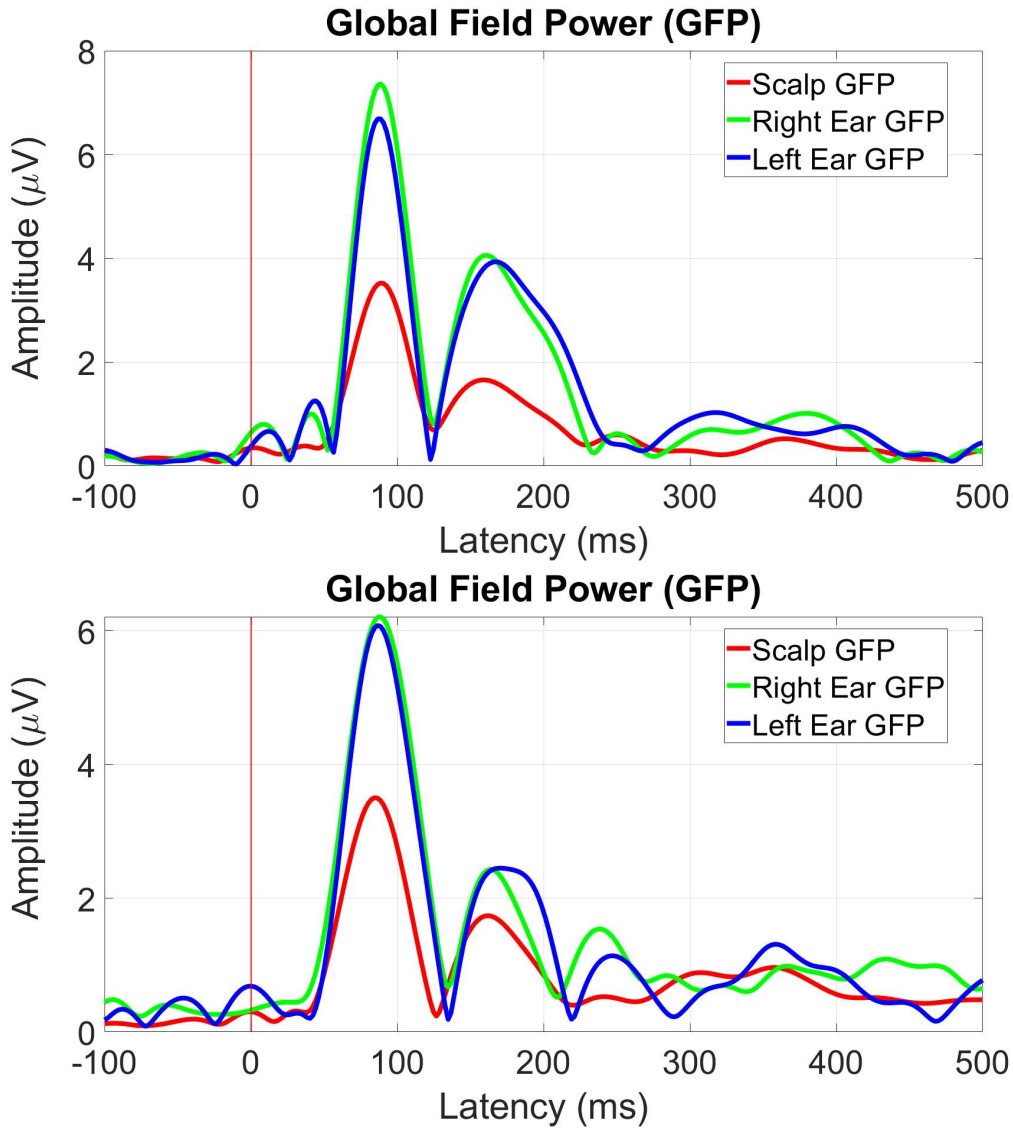

Figure D.5: Global Field Power (GFP) - Cz referenced for the ear-EEG AEP paradigm, split between scalp, left and right ear electrodes for a wet (n = 5) (top) and dry (n = 1) (bottom) electrode settings

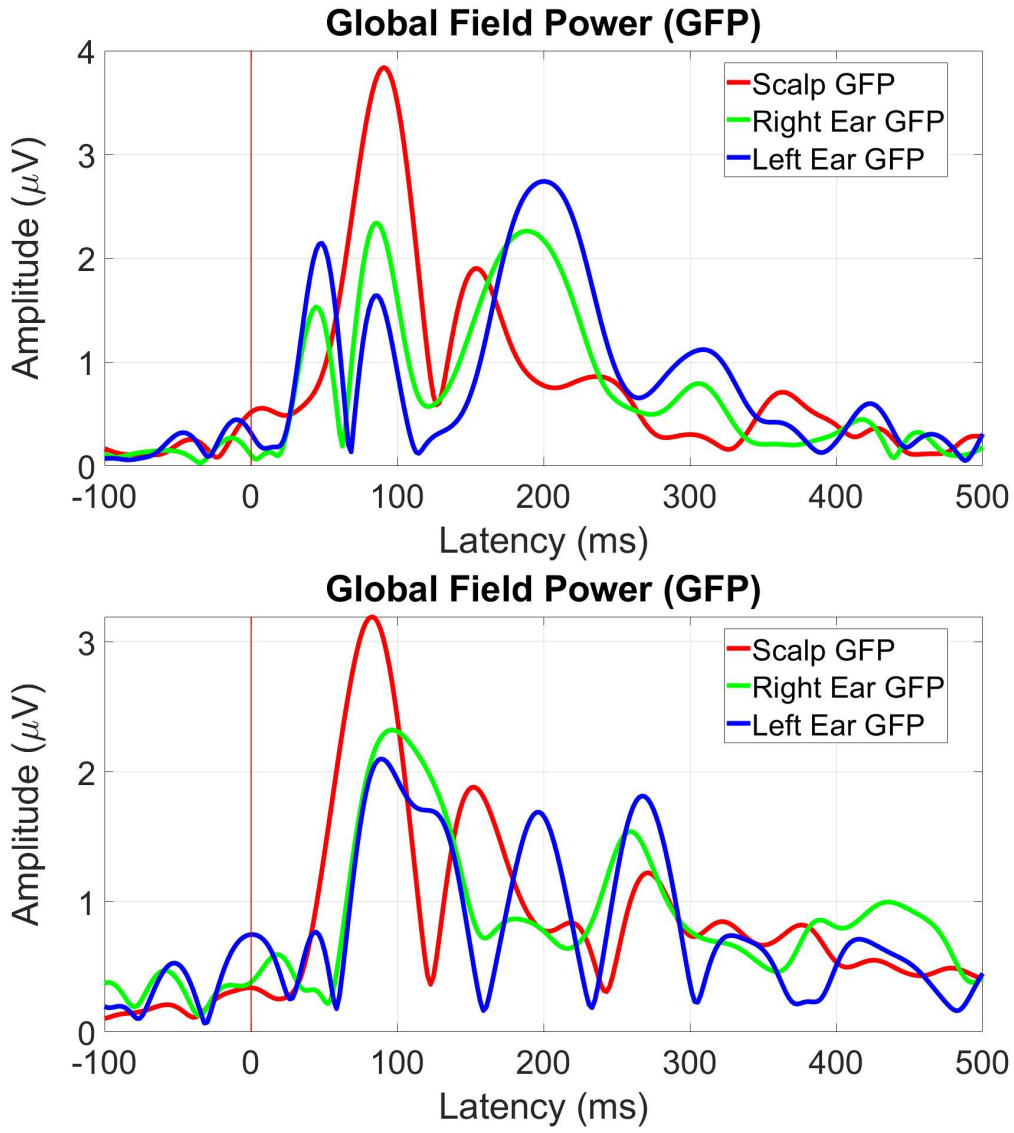

Figure D.6: Global Field Power (GFP) - T8 referenced for the ear-EEG AEP paradigm, split between scalp, left and right ear electrodes for a wet (n = 5) (top) and dry (n = 1) (bottom) electrode settings

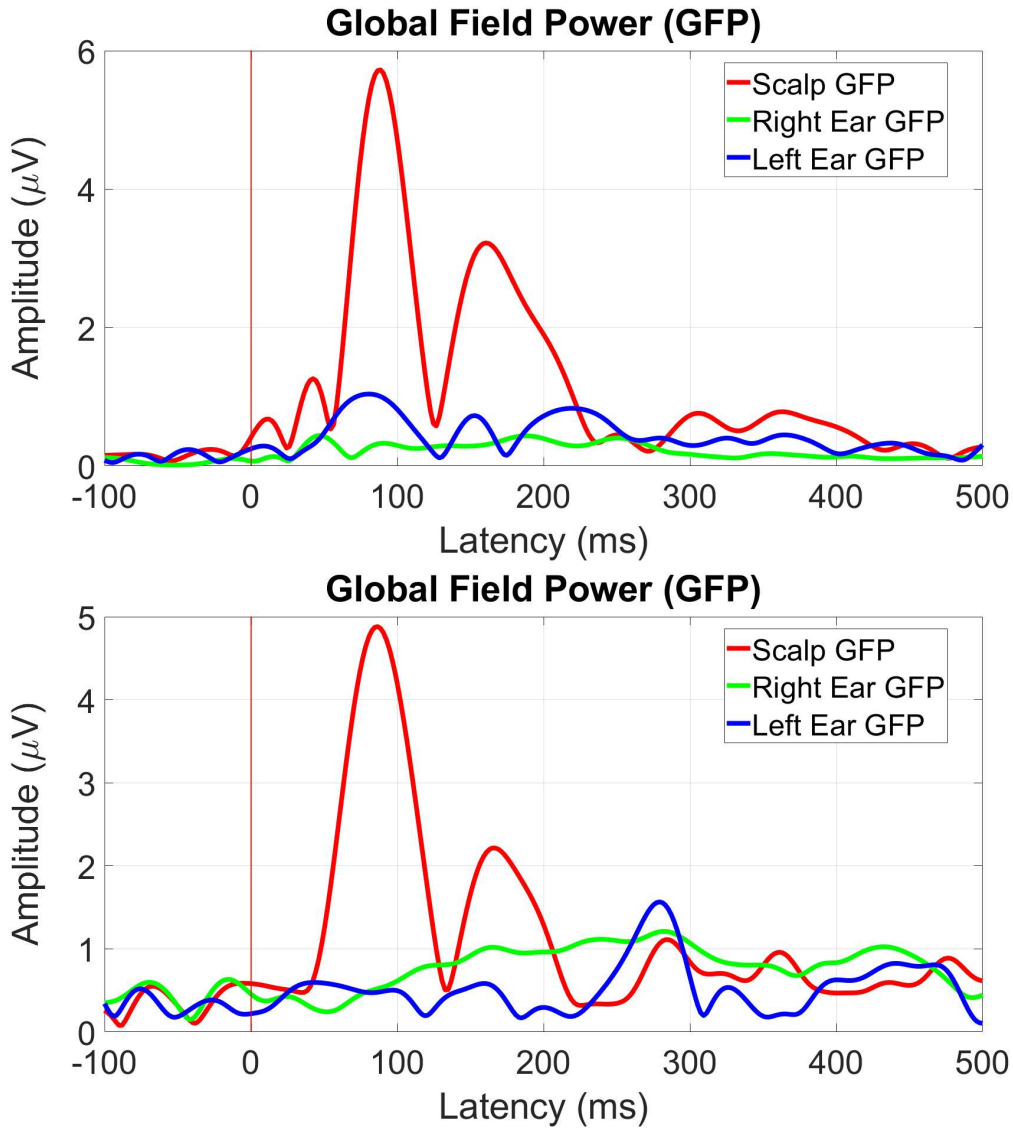

Figure D.7: Global Field Power (GFP) - ER3 referenced for the ear-EEG AEP paradigm, split between scalp, left and right ear electrodes for a wet (n = 5) (top) and dry (n = 1) (bottom) electrode settings

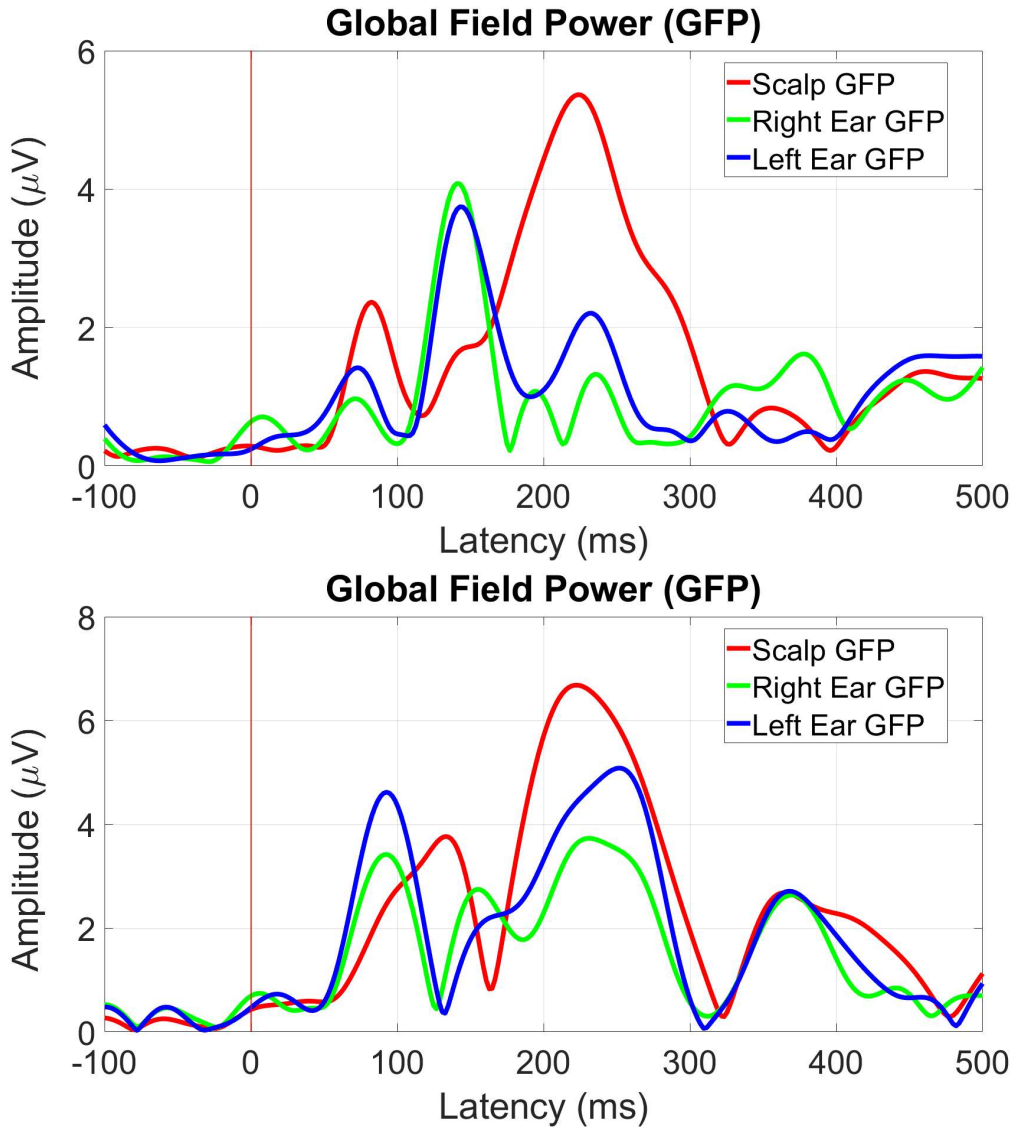

Figure D.8: Global Field Power (GFP) - Cz referenced for the ear-EEG VEP paradigm, split between scalp, left and right ear electrodes for a wet (n = 5) (top) and dry (n = 1) (bottom) electrode settings

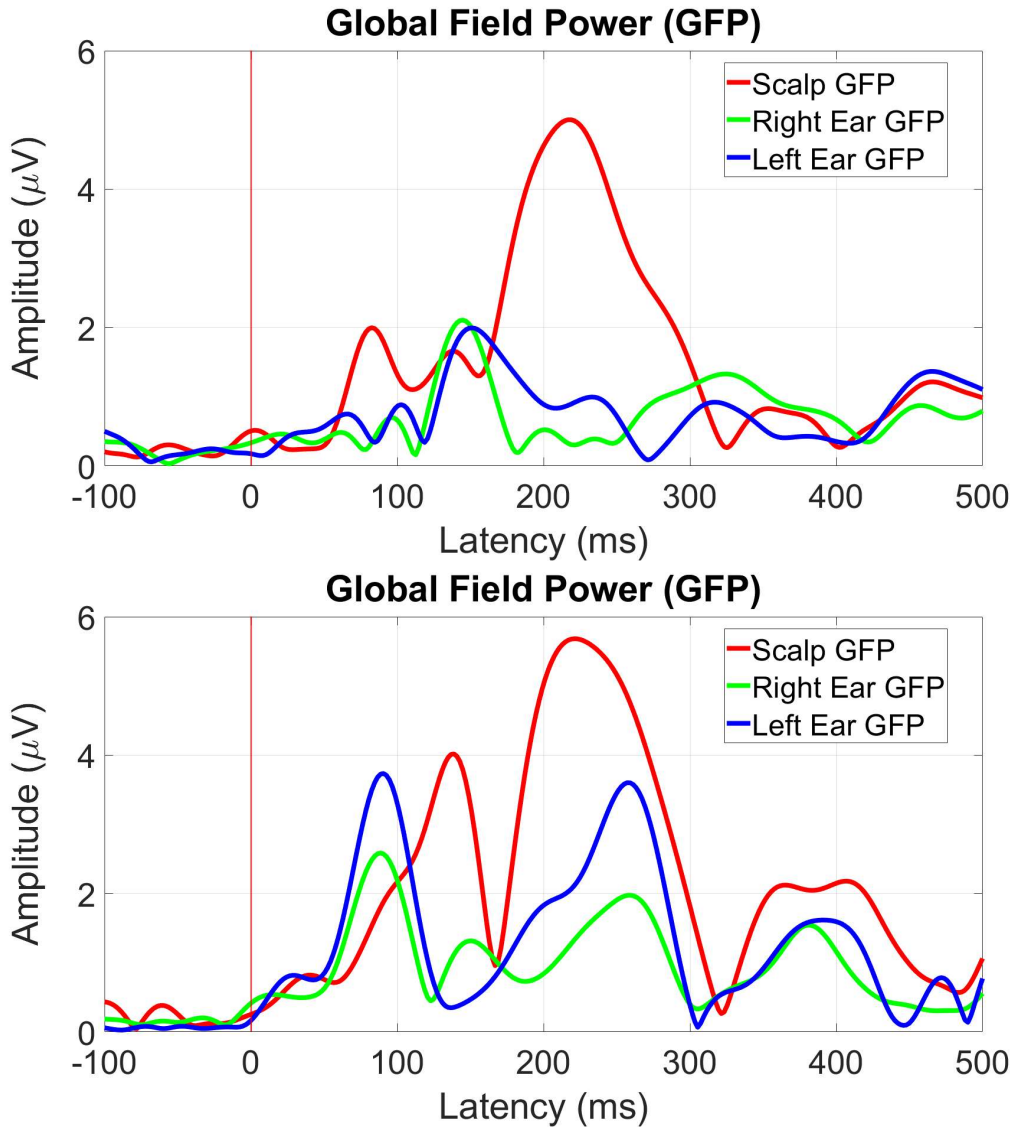

Figure D.9: Global Field Power (GFP) - T8 referenced for the ear-EEG VEP paradigm, split between scalp, left and right ear electrodes for a wet (n = 5) (top) and dry (n = 1) (bottom) electrode settings

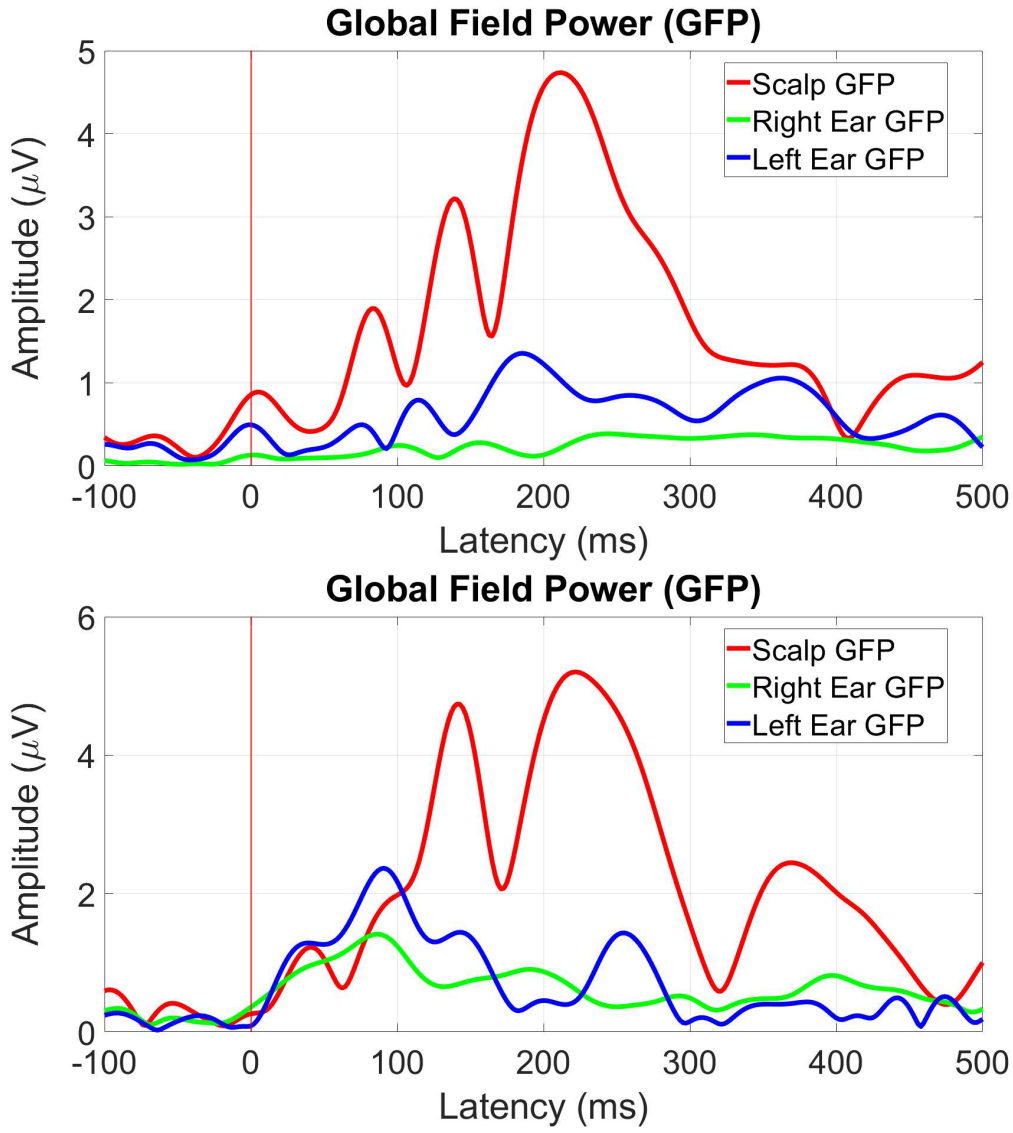

Figure D.10: Global Field Power (GFP) - ER3 referenced for the ear-EEG VEP paradigm, split between scalp, left and right ear electrodes for a wet (n = 5) (top) and dry (n = 1) (bottom) electrode settings

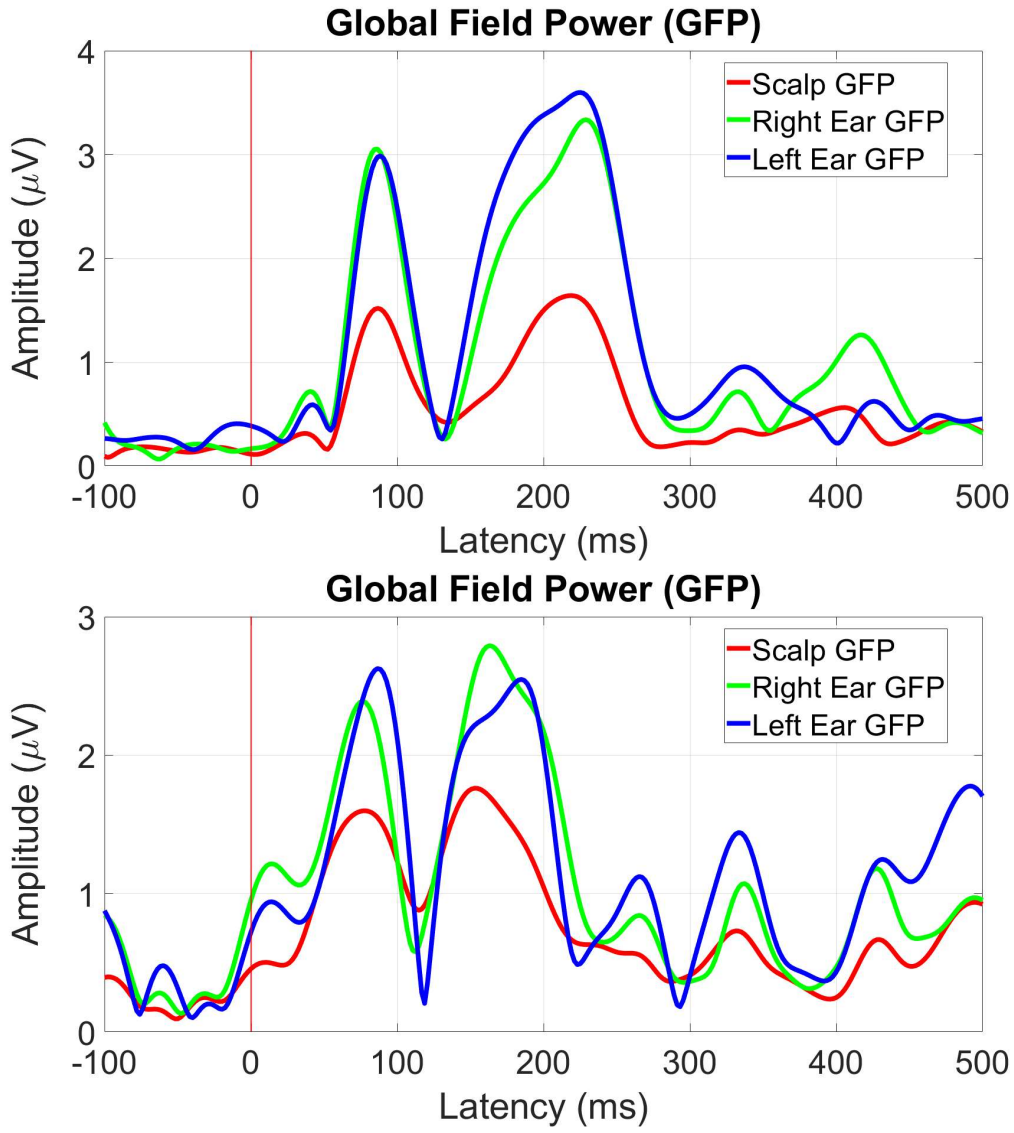

Figure D.11: Global Field Power (GFP) - Cz referenced for the ear-EEG MMN paradigm, split between scalp, left and right ear electrodes for a wet (n = 5) (top) and dry (n = 1) (bottom) electrode settings

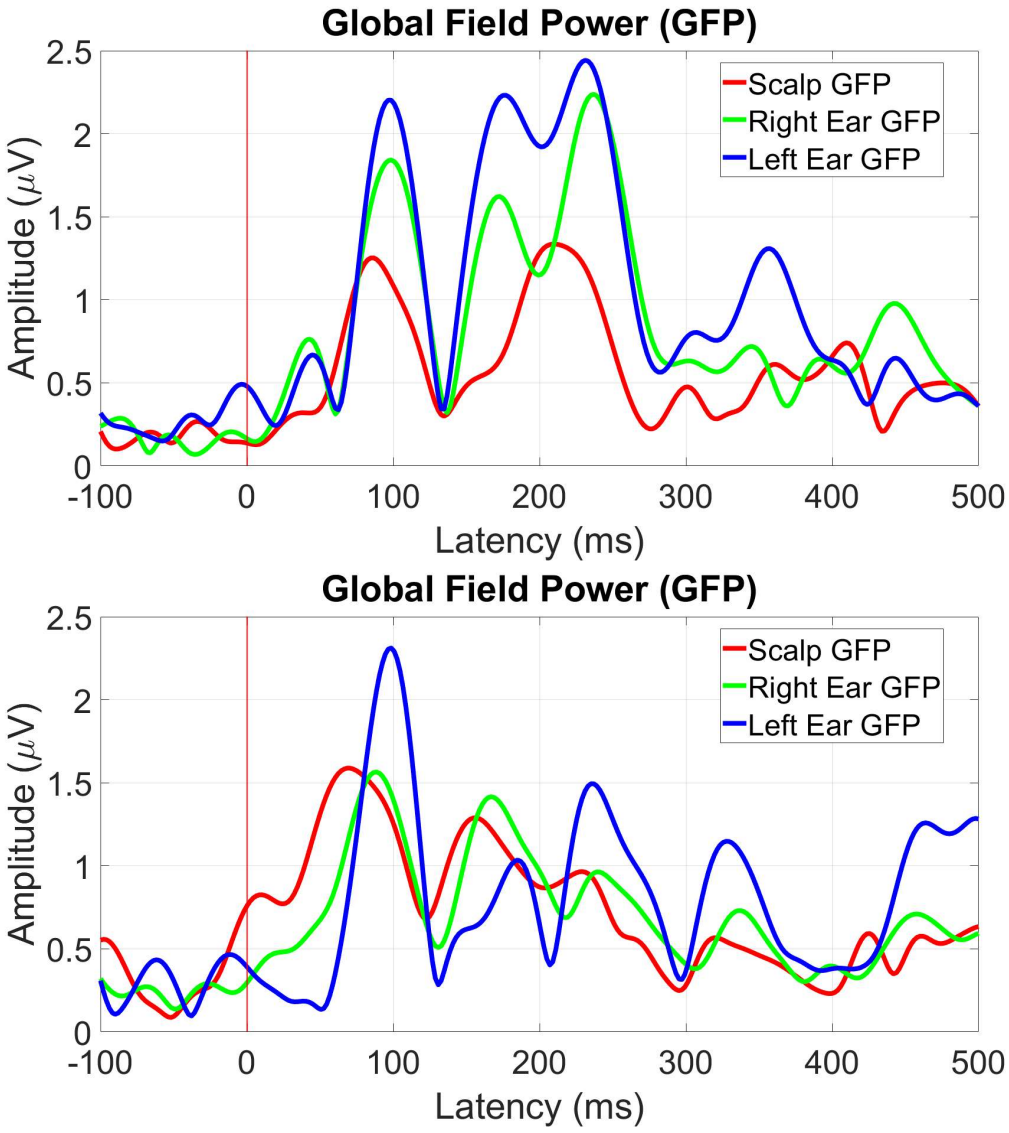

Figure D.12: Global Field Power (GFP) - T8 referenced for the ear-EEG MMN paradigm, split between scalp, left and right ear electrodes for a wet (n = 5) (top) and dry (n = 1) (bottom) electrode settings

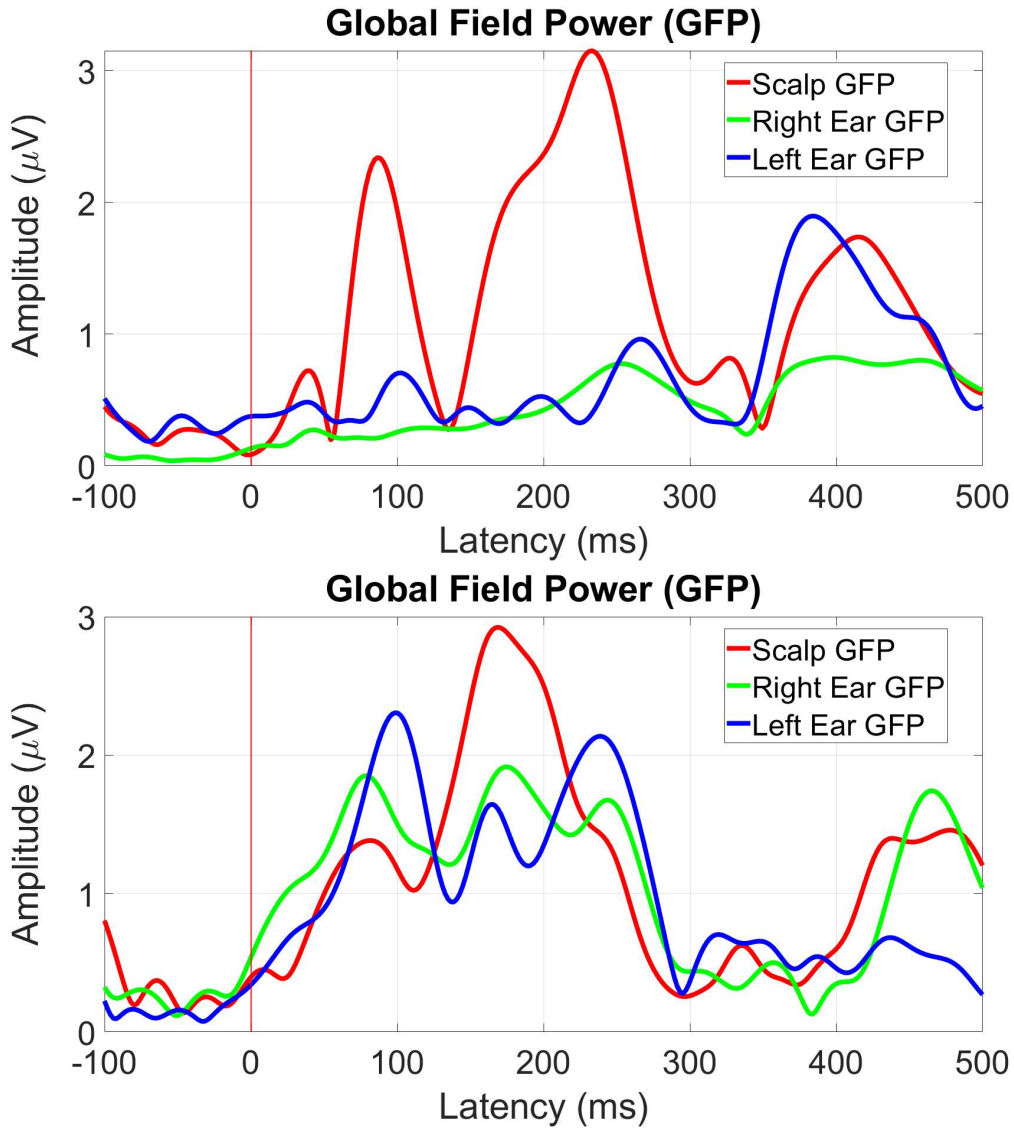

Figure D.13: Global Field Power (GFP) - ER3 referenced for the ear-EEG MMN paradigm, split between scalp, left and right ear electrodes for a wet (n = 5) (top) and dry (n = 1) (bottom) electrode settings

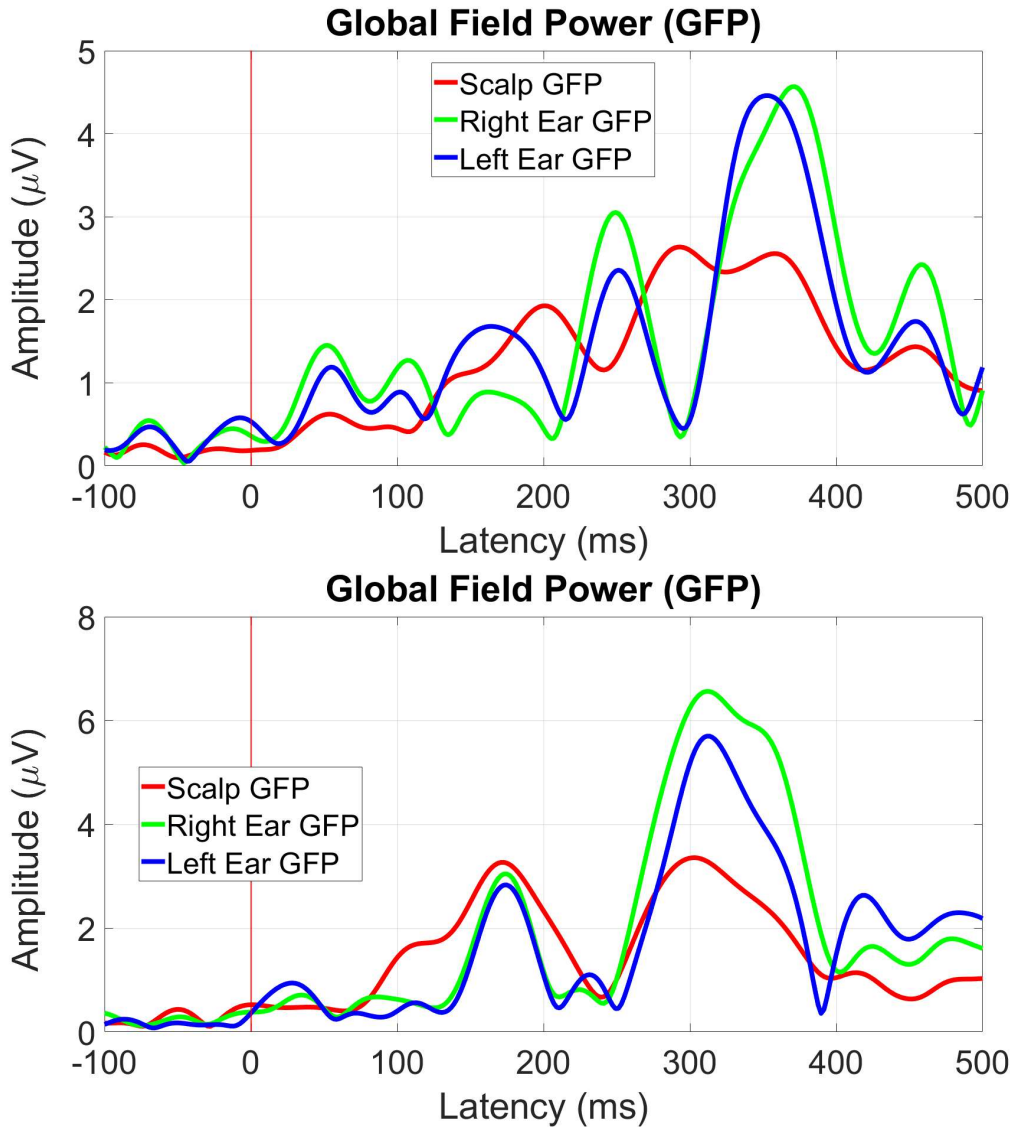

Figure D.14: Global Field Power (GFP) - Cz referenced for the ear-EEG P300 paradigm, split between scalp, left and right ear electrodes for a wet (n = 5) (top) and dry (n = 1) (bottom) electrode settings

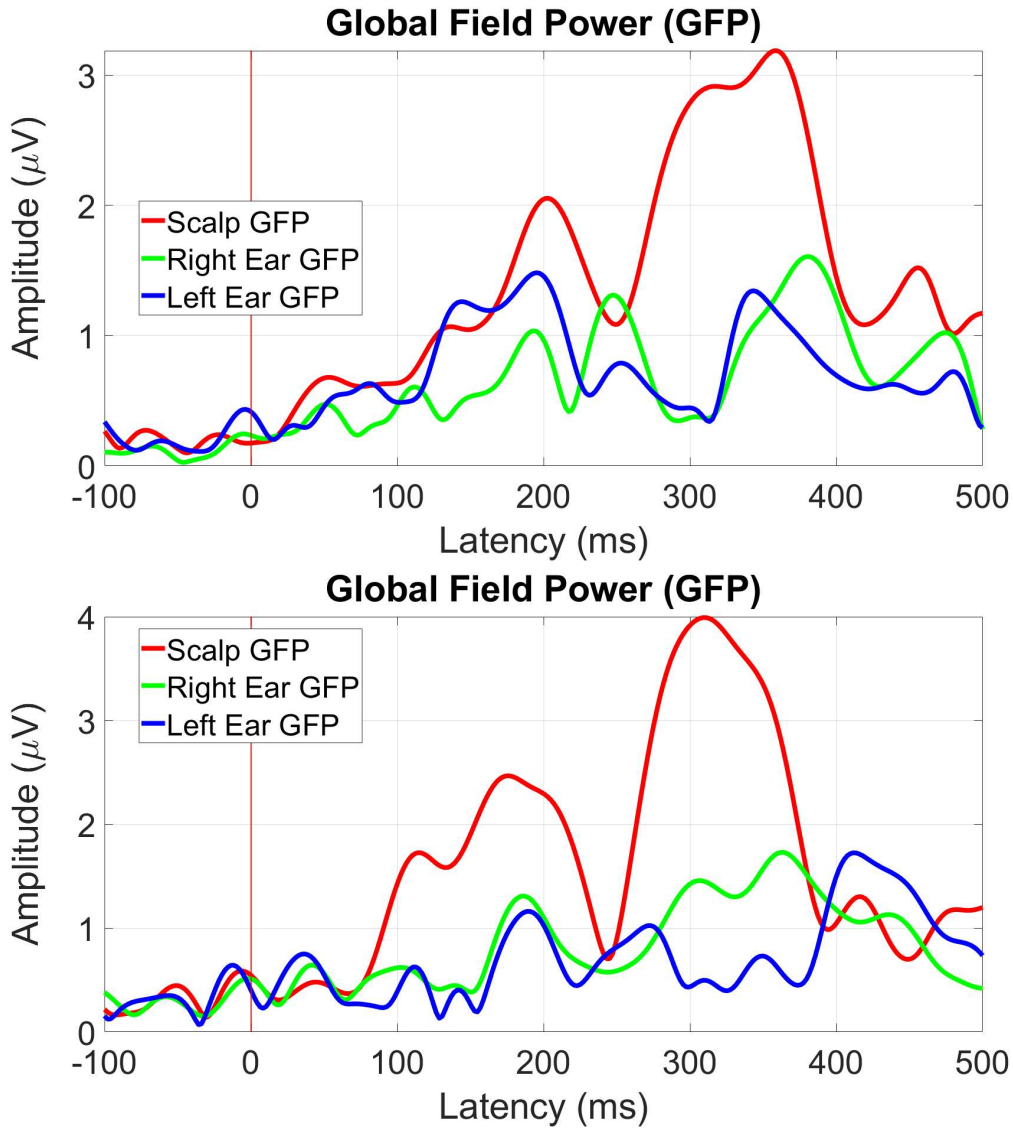

Figure D.15: Global Field Power (GFP) - T8 referenced for the ear-EEG P300 paradigm, split between scalp, left and right ear electrodes for a wet (n = 5) (top) and dry (n = 1) (bottom) electrode setting

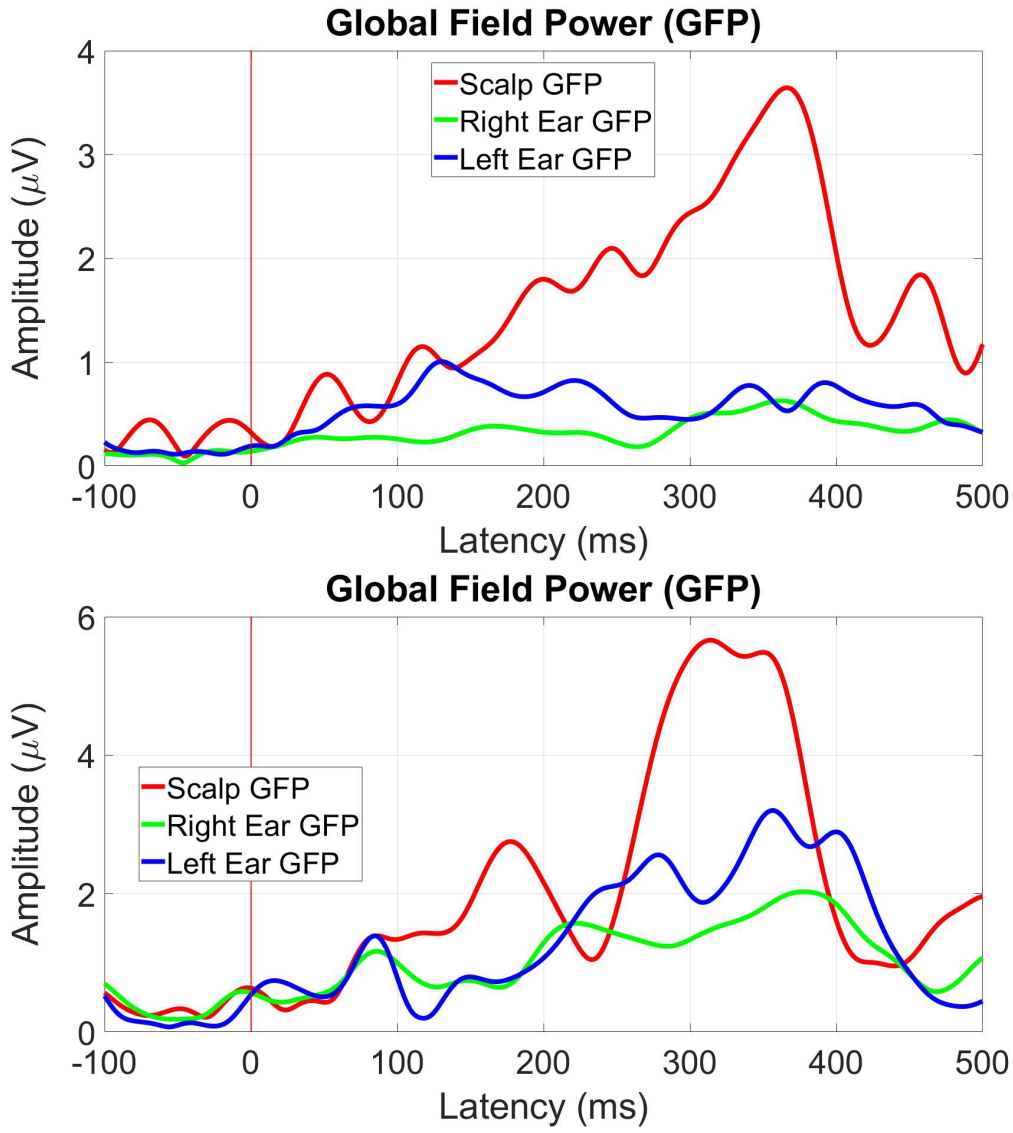

Figure D.16: Global Field Power (GFP) - ER3 referenced for the ear-EEG P300 paradigm, split between scalp, left and right ear electrodes for a wet (n = 5) (top) and dry (n = 1) (bottom) electrode setting

Table D.4: Ear-EEG SSVEP SNR (dB) for a Cz, T8, and ER3 references across scalp, left ear, and right ear (ordered top to bottom) electrodes for wet (n = 5) and dry (n = 1) electrode settings - omitted values were deemed not significant, based on an f-test ($p < 0.05$)

	C3	**C4**	**T7**	**T8**	**Fz**	**Cz**	**Pz**	**Oz**
					Wet Ear-EEG			
Cz	7.5 ± 3.5	-	7.1 ± 3.1	5.6 ± 3.1	7.0 ± 3.7	X	12.1 ± 3.1	8.9 ± 3.2
					Dry Ear-EEG			
Cz	-	-	-	-	-	X	6.8 ± 2.7	10.3 ± 3.0

	EL1	**EL2**	**EL3**	**EL4**	**EL5**	**EL6**	**EL7**	**EL8**
					Wet Ear-EEG			
Cz	6.0 ± 2.3	5.5 ± 2.5	6.5 ± 3.3	6.3 ± 2.4	7.1 ± 3.5	7.0 ± 3.7	7.0 ± 3.8	7.0 ± 3.8
T8	3.7 ± 1.6	3.9 ± 1.9	4.1 ± 2.6	4.1 ± 1.7	5.0 ± 2.9	4.9 ± 2.9	5.0 ± 3.0	4.9 ± 3.0
ER3	-	-	-	-	-	-	-	-
					Dry Ear-EEG			
Cz	X	4.6 ± 2.6	X	4.5 ± 2.3	5.2 ± 2.5	5.1 ± 2.7	5.0 ± 2.7	4.9 ± 2.7
T8	X	4.8 ± 2.1	X	4.3 ± 1.8	5.4 ± 2.0	5.2 ± 2.2	5.1 ± 2.2	4.7 ± 2.2
ER3	X	-	X	-	-	-	-	-

	ER1	**ER2**	**ER3**	**ER4**	**ER5**	**ER6**	**ER7**	**ER8**
					Wet Ear-EEG			
Cz	6.3 ± 3.8	6.7 ± 3.9	6.5 ± 3.7	6.5 ± 3.8	6.5 ± 3.9	6.5 ± 3.9	6.5 ± 3.9	6.4 ± 3.9
T8	5.5 ± 2.8	5.7 ± 3.1	5.7 ± 2.8	5.9 ± 3.1	5.9 ± 3.2	5.9 ± 3.2	5.9 ± 3.3	5.9 ± 3.1
ER3	-	-	X	-	-	-	-	-
					Dry Ear-EEG			
Cz	-	-	-	-	5.0 ± 2.6	4.7 ± 2.7	-	-
T8	-	-	4.5 ± 2.0	-	6.6 ± 2.1	6.4 ± 2.2	5.6 ± 2.4	5.1 ± 2.5
ER3	-	-	X	-	-	-	-	-

Table D.5: Ear-EEG Alpha Modulation (dB) for a Cz, T8, and ER3 references across scalp, left ear, and right ear (ordered top to bottom) electrodes for wet (n = 5) and dry (n = 1) electrode settings - omitted values were deemed not significant, based on an t-test ($p < 0.05$)

	C3	**C4**	**T7**	**T8**	**Fz**	**Cz**	**Pz**	**Oz**
				Wet Ear-EEG				
Cz	2.6 ± 2.8	3.0 ± 3.2	3.0 ± 2.5	3.4 ± 3.0	2.4 ± 3.0	X	4.2 ± 2.1	6.7 ± 1.8
				Dry Ear-EEG				
Cz	1.4 ± 2.7	2.3 ± 2.4	1.2 ± 3.4	1.9 ± 3.0	1.6 ± 2.6	X	2.7 ± 4.2	2.6 ± 4.5

	EL1	**EL2**	**EL3**	**EL4**	**EL5**	**EL6**	**EL7**	**EL8**
				Wet Ear-EEG				
Cz	5.1 ± 1.7	6.4 ± 2.2	2.8 ± 4.0	5.2 ± 1.6	3.1 ± 2.6	2.8 ± 2.9	3.4 ± 2.8	3.2 ± 2.8
T8	3.3 ± 1.6	3.7 ± 1.9	2.2 ± 4.1	3.2 ± 1.6	2.4 ± 2.8	1.9 ± 3.2	2.7 ± 2.8	2.5 ± 2.9
ER3	2.1 ± 1.6	2.1 ± 1.9	1.5 ± 4.3	1.9 ± 1.	1.3 ± 2.8	0.9 ± 3.2	1.8 ± 2.6	1.8 ± 2.6
				Dry Ear-EEG				
Cz	X	1.3 ± 3.2	X	1.0 ± 3.2	1.1 ± 3.1	1.4 ± 3.3	1.5 ± 3.4	1.4 ± 3.4
T8	X	-	X	-	-	-	-	-
ER3	X	-	X	-	-	-	-	-

	ER1	**ER2**	**ER3**	**ER4**	**ER5**	**ER6**	**ER7**	**ER8**
				Wet Ear-EEG				
Cz	3.9 ± 3.3	3.7 ± 3.1	3.9 ± 2.9	3.9 ± 3.0	3.9 ± 3.0	3.7 ± 3.0	3.8 ± 3.1	3.7 ± 3.1
T8	2.9 ± 2.8	2.9 ± 2.9	3.1 ± 2.6	3.2 ± 2.9	3.3 ± 2.9	3.2 ± 3.0	3.3 ± 3.0	3.1 ± 3.0
ER3	-	-	X	1.5 ± 3.2	0.7 ± 2.5	1.1 ± 2.4	0.9 ± 2.0	2.0 ± 2.0
				Dry Ear-EEG				
Cz	0.8 ± 2.2	1.3 ± 2.5	1.6 ± 2.8	-	2.1 ± 2.5	2.1 ± 2.9	2.0 ± 2.9	1.9 ± 2.9
T8	0.6 ± 2.0	0.8 ± 2.5	1.0 ± 2.6	-	0.9 ± 2.7	1.0 ± 3.0	-	-
ER3	-	-	X	-	-	-	-	-

Table D.6: EOG Blinks (hard/soft) ratios for a Cz, T8, and ER3 references across all scalp, left ear, and right ear electrodes for wet (n = 5) and dry (n = 1) electrode settings

	C3	**C4**	**T7**	**T8**	**Fz**	**Cz**	**Pz**	**Oz**
				Wet Ear-EEG				
Cz	2.0	2.1	2.8	2.4	2.4	X	1.9	1.7
				Dry Ear-EEG				
Cz	1.4	1.6	2.0	1.0	1.6	X	1.4	1.6

	EL1	**EL2**	**EL3**	**EL4**	**EL5**	**EL6**	**EL7**	**EL8**
				Wet Ear-EEG				
Cz	2.4	2.7	2.2	2.3	2.2	1.9	2.2	2.2
T8	2.6	2.9	2.4	2.4	2.2	1.8	2.3	2.2
ER3	3.2	3.3	2.8	2.8	2.3	1.9	1.9	2.4
				Dry Ear-EEG				
Cz	X	1.7	X	1.9	1.7	2.0	1.8	1.8
T8	X	2.1	X	2.1	2.0	2.1	2.0	2.1
ER3	X	1.6	X	1.6	1.5	1.9	1.5	1.5

	ER1	**ER2**	**ER3**	**ER4**	**ER5**	**ER6**	**ER7**	**ER8**
				Wet Ear				
Cz	2.2	3.2	2.1	2.2	2.0	2.1	2.2	2.0
T8	2.5	3.3	2.4	2.5	2.4	2.2	2.4	2.1
ER3	2.5	4.1	X	2.1	2.9	2.6	3.1	3.0
				Dry Ear				
Cz	1.4	1.6	1.6	2.7	1.5	1.4	1.4	1.4
T8	1.8	2.1	1.8	3.0	1.9	1.7	1.8	1.8
ER3	1.3	1.1	X	4.0	1.2	1.0	1.1	1.0

E

Silicone and Carbon Fiber Ear-EEG Phantom Results

Table E.1: Silicone and carbon fiber (CF) measured impedances (kohm) - values above 50khom are displayed as 50+, meaning very poor or no contact at all

	EL3	**EL4**	**EL5**	**EL6**	**El7**	**EL8**	**ER3**	**ER4**	**ER5**	**ER6**	**ER7**	**ER8**
Day 1 - Dry	50+	6	6	6	50+	50+	50+	4	4	6	50+	50+
Day 1 - Wet	11	4	5	5	50+	50+	40	5	5	50+	50+	50+
Day 2 - Dry	50+	50+	50+	50+	50+	50+	50+	50+	50+	50+	50+	50+
Day 2 - Wet	15	4	5	27	50+	14	29	4	21	50+	50+	50+

Table E.2: Silicone and carbon fiber (CF) measured noise floor RMS (µVrms)

	EL3	**EL4**	**EL5**	**EL6**	**El7**	**EL8**	**ER3**	**ER4**	**ER5**	**ER6**	**ER7**	**ER8**
Day 1 - Dry	-	2.0	1190.8	-	1344.7	877.6	-	-	-	-	-	-
Day 1 - Wet	4.8	9.5	6.8	8.8	6.7	689.3	1.0	20.6	15.6	25.1	517.1	6.5
Day 2 - Dry	94.4	88.0	87.4	88.0	551.1	18.5	32.2	166.8	166.9	165.7	776.3	106.4
Day 2 - Wet	3.3	0.5	2.9	0.5	112.5	11.2	6.5	28.3	27.9	129.6	429.0	23.2

Table E.3: Silicone and carbon fiber (CF) measured Alpha Simulation SNR (dB) - omitted values were deemed not significant, based on an f-test

	EL3	**EL4**	**EL5**	**EL6**	**El7**	**EL8**
Day 1 - Dry	-	20.7 ± 6.8	12.4 ± 2.2	-	6.3 ± 0.9	7.2 ± 1.0
Day 1 - Wet	9.3 ± 2.0	16.3 ± 2.2	19.1 ± 3.2	19.3 ± 3.4	0.4 ± 0.0	11.2 ± 2.6
Day 2 - Dry	-	6.9 ± 2.0	12.6 ± 2.3	10.5 ± 2.1	-	5.6 ± 0.5
Day 2 - Wet	7.2 ± 1.4	20.8 ± 6.0	18.9 ± 2.9	20.8 ± 7.3	-	2.0 ± 0.4

	ER3	**ER4**	**ER5**	**ER6**	**ER7**	**ER8**
Day 1 - Dry	-	-	-	-	-	-
Day 1 - Wet	-	17.1 ± 1.8	16.3 ± 1.6	19.3 ± 2.8	13.2 ± 2.6	1.2 ± 0.2
Day 2 - Dry	9.3 ± 2.6	14.3 ± 2.8	14.5 ± 2.8	14.4 ± 2.8	10.4 ± 3.1	3.0 ± 0.9
Day 2 - Wet	19.9 ± 2.9	22.6 ± 4.8	22.6 ± 5.1	17.2 ± 2.0	12.2 ± 2.0	18.6 ± 2.4

F

Other Images

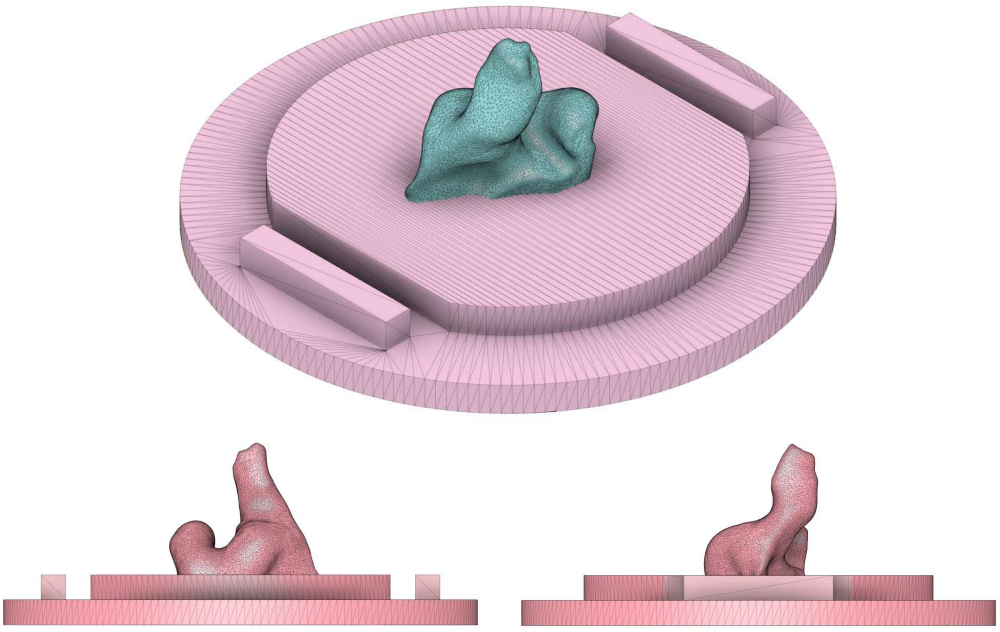

Figure F.1: **Top** - Example of a left ear scan being centered and orientated with the phantom's lid mesh **Bottom** - Different views of the alignment and depth of the ear mesh and a lid mesh into a single rendered object

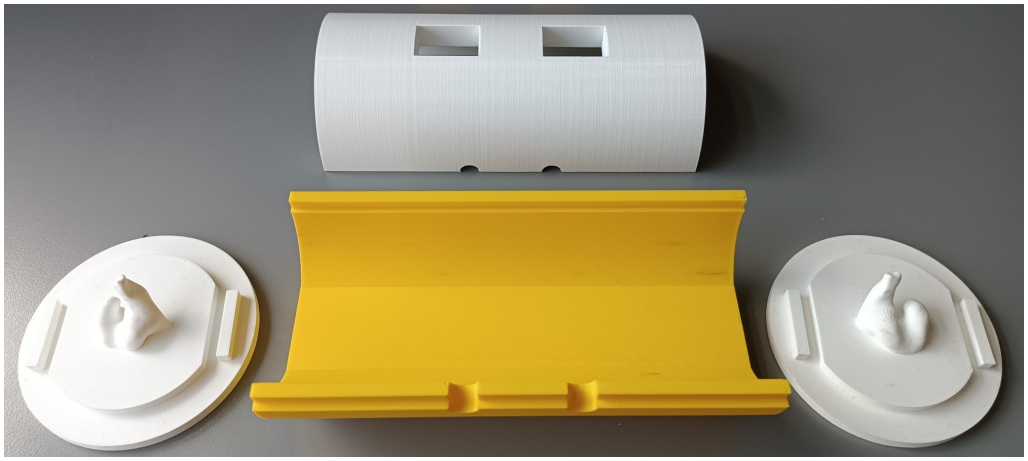

Figure F.2: Dissembled ear-EEG phantom - bottom half (in yellow), top half (in white, similar to yellow), and two lids with a left and right ear imprint from one of the subjects

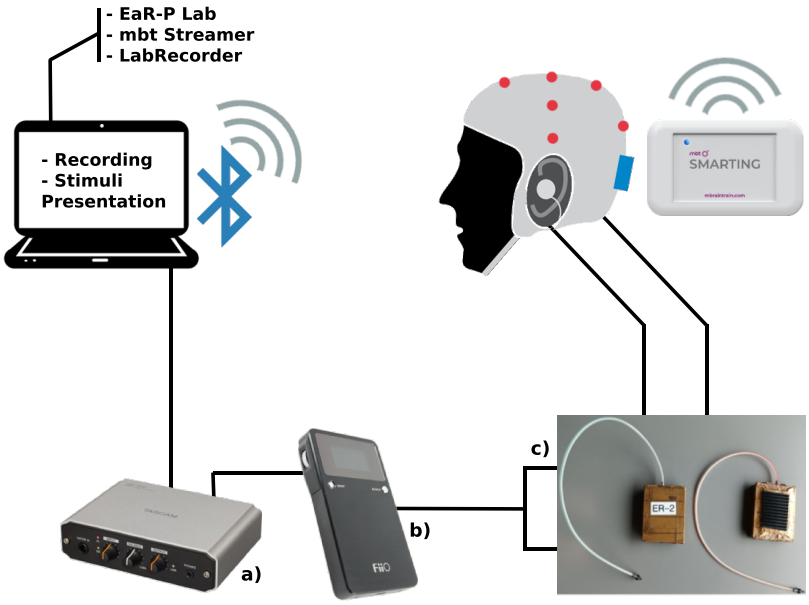

Figure F.3: EEG acquisition setup schematic and equipment - **a)** USB Audio Interface TASCAM US-100 **b)** - Digital-Analog Converter (DAC) Amplifier FiiO Alpen 2 **c)** - ER2 Etymotic tubal insert research grade earphones

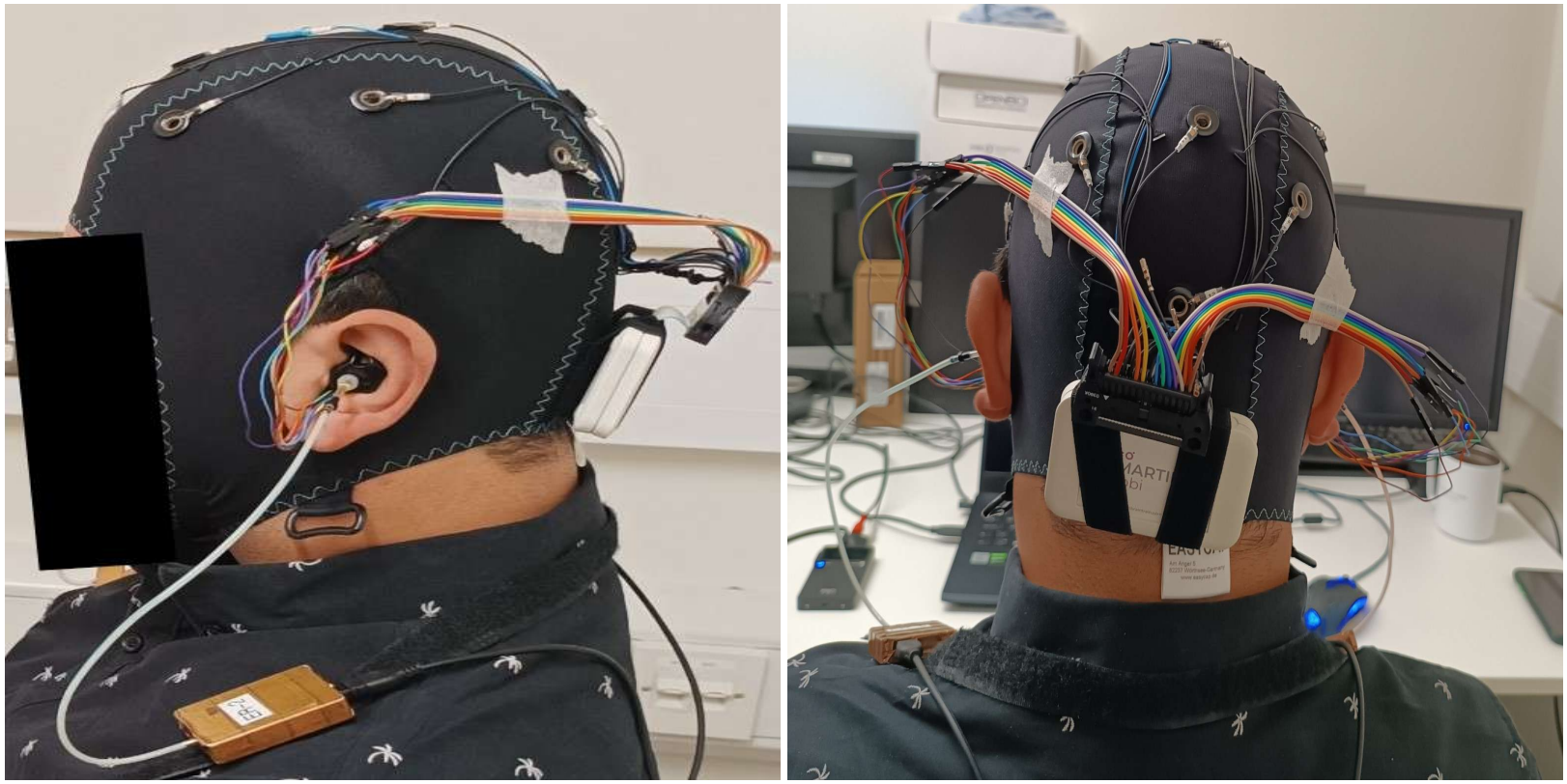

Figure F.4: Ear-EEG head setup - side (left) and posterior (right) views

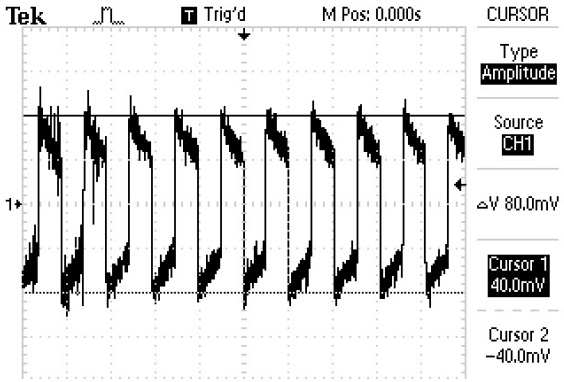

Figure F.5: Exemplary peak-to-peak amplitude integrity measurement for BG - Day 1